IOWA STATE UNIVERSITY
Digital Repository

Graduate Theses and Dissertations

Iowa State University Capstones, Theses and Dissertations

2017

Performance-based design prodedure for a novel semi-active cladding connection applied to blast mitigation

Sijia Lu
Iowa State University

Follow this and additional works at: https://lib.dr.iastate.edu/etd

 Part of the Civil Engineering Commons

Recommended Citation
Lu, Sijia, "Performance-based design prodedure for a novel semi-active cladding connection applied to blast mitigation" (2017). *Graduate Theses and Dissertations*. 16171.
https://lib.dr.iastate.edu/etd/16171

This Thesis is brought to you for free and open access by the Iowa State University Capstones, Theses and Dissertations at Iowa State University Digital Repository. It has been accepted for inclusion in Graduate Theses and Dissertations by an authorized administrator of Iowa State University Digital Repository. For more information, please contact digirep@iastate.edu.

Performance-based design procedure for a novel semi-active cladding connection applied to blast mitigation

by

Sijia Lu

A thesis submitted to the graduate faculty

in partial fulfillment of the requirements for the degree of

MASTER OF SCIENCE

Major: Civil Engineering (Structure Engineering)

Program of Study Committee:
Simon Laflamme, Major Professor
Sri Sritharan
Robert Whitehead

The student author, whose presentation of the scholarship herein was approved by the program of study committee, is solely responsible for the content of this thesis. The Graduate College will ensure this thesis is globally accessible and will not permit alterations after a degree is conferred.

Iowa State University

Ames, Iowa

2017

Copyright © Sijia Lu, 2017. All rights reserved.

TABLE OF CONTENTS

LIST OF FIGURES

Page

LIST OF TABLES

Page

ACKNOWLEDGMENTS

With my deepest gratitude and appreciation, I would like to thank my major professor, Dr. Simon Laflamme for his continuous help and support throughout academic study at Iowa State University. I especially thank him for his brilliant ability to successfully manage my research work. His guidance and persistent help this thesis would not have been possible. I also appreciate Dr. Rob Whitehead, and Dr. Sri Sritharan be willing to be my committee members. I have special thanks to Professor. Whitehead for his rigorous and technical advice and guidance of cladding construction.

In addition, I am especially thankful to Liang Cao for his programing assistance and thesis organization suggestions. Without his patient and help on my research work, my completion of my thesis could not be accomplished. I would like to thank Irvin Pinto for the language advice. Also thanks to Gongyong Qiang for his hard work on checking my calculations. I extend my thanks to Dr. Ricles, Dr. Spence Quiel and Elif Ecem Bas from Lehigh University for their help with the numerical model.

This thesis is based upon work supported by the National Science Foundation under Grant No. 1493497. Their support is gratefully acknowledged. Any opinions, findings and conclusions or recommendations expressed in this material are those of the authors and do not necessarily reflect the views of the National Science Foundation.

I also want to thank my uncle Aaron Tan and my parents for their financial and moral support during my entire college life. Their patience and understanding give me a huge encouragement and support.

At last, I am appreciating that I study in Iowa State University with these two years' academic experience.

ABSTRACT

Cladding systems are conventionally designed to provide buildings with environmental protection against wind, temperature, humidity, moisture, etc. Recently, researchers have proposed to leverage these systems to provide additional protection against manmade (e.g., bombs) and natural (e.g., earthquakes, hurricanes) hazards. This can be achieved, for example, by redesigning the connection cladding-structure to provide energy dissipation capabilities. While promising, these strategies are typically effective against single types of hazards. Here, we propose to utilize a novel semi-active damping system connecting cladding to the structure. This system is based on a variable friction mechanism. By varying the normal force applied on the friction plates through a system of moving toggles, it is possible to mitigate vibrations over a wide frequency range, therefore making it useful to mitigate different types of hazards, or multi-hazards. In a passive mode, i.e. unactuated, the device is designed to provide very high stiffness and friction resistance to provide blast mitigation capabilities.

The objective of this thesis is to enable a holistic integration of such device within the structural design process by developing performance-based design procedures. The study will focus on the passive mode of the device, which will provide a stepping stone for the development of performance-based design procedures for its semi-active, i.e. actuated, capabilities. The proposed performance-based design procedure consists of: 1) determining the design performance criteria, including the blast properties and allowable distance cladding-structure; 2) selecting design properties for the cladding connection, including stiffness and damping; and 3) designing the impact rubber located between the structure and the cladding in order to prevent the cladding from impacting the structure.

In this work, we first describe the novel semi-active device in the context of cladding systems designed for blast resistance. It is followed by a description of the proposed performance-based design procedure, which includes the derivation of different models to simply the derivation of key equations. These equations are then used to provide design guidance. The proposed design procedures are verified and validated on a single degree-of-freedom model, on a two degree-of-freedoms model, and on a realistic four stories structure. Results show that the design methodology can be applied for the semi-active connection utilized in a passive mode against blast load.

CHAPTER 1. INTRODUCTION

1.1 Motivation

Buildings and other civil infrastructures are designed, constructed, and maintained to provide significant service and benefits to the communities. In order to guarantee daily operability and public safety, the resistance to extreme loads and building serviceability must be maintained. Earthquake, wind, explosion, and some ambient forces can provoke different level damages on the buildings, and may lead to collapses, in particular for high-impulse earthquakes, hurricanes, tornadoes, and blasts. More frequent events like wind-induced vibration can lead to discomfort and frequent inoperability. Depending on the geographical location, the design demand for buildings varies. Buildings are designed to resist possible hazards through the selection of an appropriate structural configuration, with appropriately sized components, damping systems and added non-structural elements for additional protection such as against blast [74]. It must be noted, however, that recent advances in materials and construction methods have enabled lighter and more flexible structures, whereas natural and man-made hazards may result in larger motions [1].

A method to increase structural performance vis-a-vis service and extreme loads is termed performance-based design (PBD) [1]. This approach can be used to restrict motion of facilities and infrastructures from various excitations by designing the structural stiffness and appropriate damping system for a given mass system to a prescribed performance [1, 2]. Sometimes, various excitation inputs need to be considered individually or combined, for which a multi-hazards design procedure is prescribed and necessitates the utilization of high-performance control systems (HPCSs)due to the limitations of passive systems [3, 4, 5].

Similar to passive systems, HPCS leverage inertial or differential motion between components to dissipate vibrations. One of these components is structural cladding, which constitutes the building envelope. Cladding is conventionally designed to provide environmental protection including wind, temperature, humidity, moisture, etc. [6]. Also, heavyweight cladding systems can be used to contribute to lateral stiffness and add a significant inertia [7]. Typically, cladding systems are connected from the edge to the structural frame using tie-back and bearing supports connections (discussed in details in Section 2.4.1). Such connections are generally passive, in the sense that they are not designed to mitigate wind and seismic loads. Passive cladding connections for energy dissipation have been proposed, in particular for earthquake mitigation, whereas the cladding is used as a tuned mass damper [8]. Other studies [7, 8, 9] demonstrated advantages of ductile connections in reducing inter-story floor drifts.

The design of cladding connections plays a critical role in the interaction between cladding and supporting frame, because the cladding system can non-negligibly affect the dynamics of the structure. For conventional cladding connections, the objective is to minimize the interaction between the cladding and the structural frame for high lateral loads such as one produced by a seismic event. This is a strength-based approach. An alternative is to allow component movement and leverage the motion to dissipate energy from the lateral load [73]. This is a motion- or performance-based approach.

In this research, a novel semi-active friction mechanism is to connect cladding elements to the structural system for multi-hazard mitigation is investigated. The mechanism, described in what follows, is a semi-active friction device capable of varying friction through the variation of a normal force applied from an actuator.

1.2 Novel semi-active cladding connection

The novel semi-active mechanism is schematized in Figure 1.1 (a). It consists of sliding friction plates subjected to a normal force produced by an actuator applied via a toggle system. An impact rubber is mounted between the cladding and structure (Figure 1.1 (a)) to mitigate pounding of the cladding onto the structure. This device can be mounted between floor slabs and external friction plates can provide mechanical restraints on different applications. It is also designed to provide damping based on a decentralized scheme, where each cladding element (Figure 1.1 (b)) is damped individually between each floor. Other configurations can be used. For example, top and bottom connections to the cladding could be semi-active, while the middle connections could be conventional gravity connectors. In this research, it is assumed that the semi-active cladding connection only transfers lateral forces. The gravity load is transferred from the cladding panel to the structural frame through a gravity connection (e.g., bearing support).

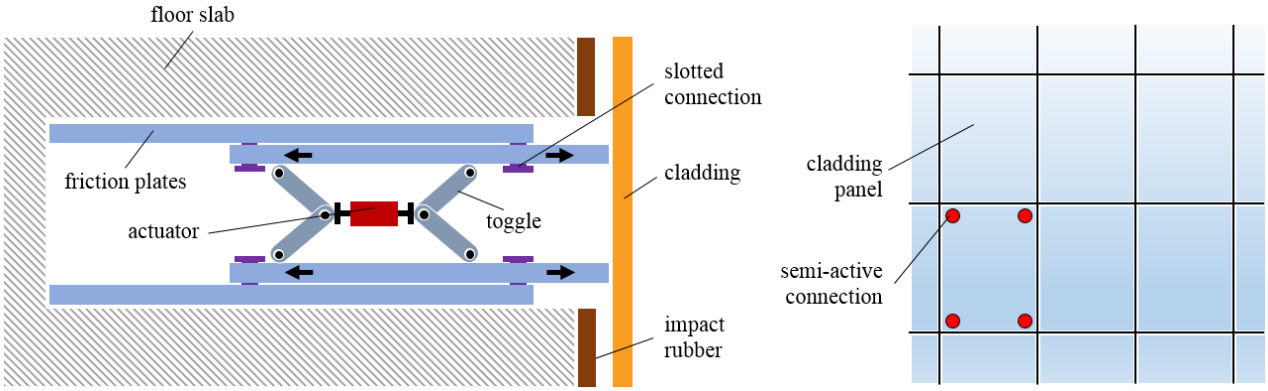

Figure 1.1 Semi-active device integrated in (a) floor slab (top view); (b) building facade (elevation view); and (c) floor slab (lateral view)

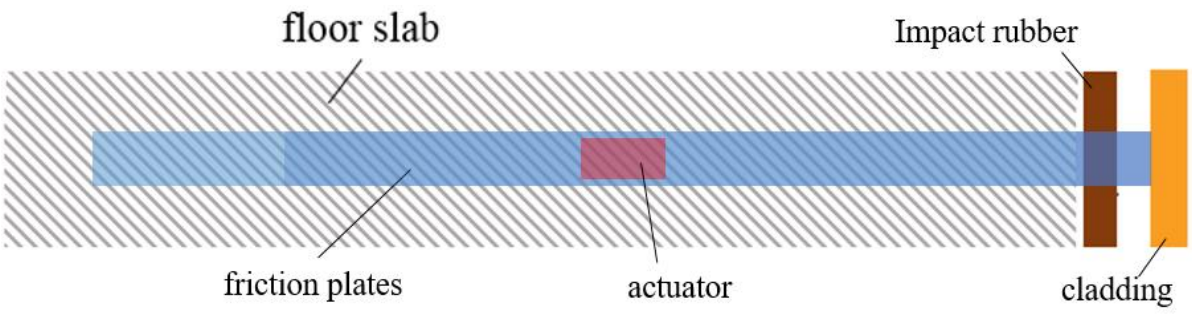

(c)

Figure 1.1 (continued)

The variation in toggles' geometries provide the variation in the normal force. Four damping configurations are possible:

- Toggles locked daily operations. Both toggles are pushed vertically, resulting in a locking of the device in high friction mode. This is the passive mode, as no power is required to maintain the toggles in the locked position. This high state of friction is sufficient to avoid slippage of the connection during moderate-to-high loads, and the cladding system performs like any conventional cladding system.
- Toggles locked, blast load. The passive mode is designed for blast load mitigation. Assuming that the cladding resists the blast force, the impact force will be higher than the static friction, resulting in slippage of the connection, therefore dissipating blast energy through friction. No feedback control is required during blast.
- Toggles unlocked, varied by the actuator. The device behaves as a variable friction damper. This particular configuration can be used to control inter-story drift to limit damage to cladding (e.g. under extreme wind or seismic events).
- Toggles are retracted. The friction plates are fully disengaged and the resistance provided by the connection is minimal. This configuration is also passive, as no power input is

necessary once the toggles are retracted. This configuration can be used to limit acceleration transfer to floors.

The friction interfaces consist of a metal-free brake and clutch lining. Steel plates are used to minimize wear at the friction interface. The nonmetallic pad is used due to its high temperature resistance, high friction, and generally excellent wear resistance. The pad supplier's specification sheet lists a maximum coefficient of friction of 0.47 and an operating temperature up to 480◦C. While its wear rate is not provided, the wear rate of a nonmetallic pad made of phenolic resin and glass fiber was reported to be $2{:}5 \times 10^5$ mm^3(N·m) under sliding speeds below 7 m/s. Note that the device's application in civil structure is considered to be of high intensity over infrequent short periods of time due to the nature of mitigated excitation, whereas it is hypothesized that the choice of friction material would be adequate. A possible alternative to the metal-free brake and clutch lining pad is a high-strength brake and clutch lining (also termed semimetallic woven strip) pad, which is rated with a maximum friction coefficient 160 of 0.51 and an operating temperature up to 500◦C. Also, cast-iron on cast-iron could be considered in the event that clutch lining would pose long-term durability issues.

Structural components are typically designed to resist blast loads through rigid components. Instead, the semi-active cladding connection system dissipates energy through sliding provoked by a lateral load. In the particular case of a blast event, high reaction forces are transmitted into the semi-active device, which forces are in turn dissipated through heat produced by the sliding of friction plates, resulting in lower reaction forces being transmitted to the structural system. Figure 1.2 illustrates this example.

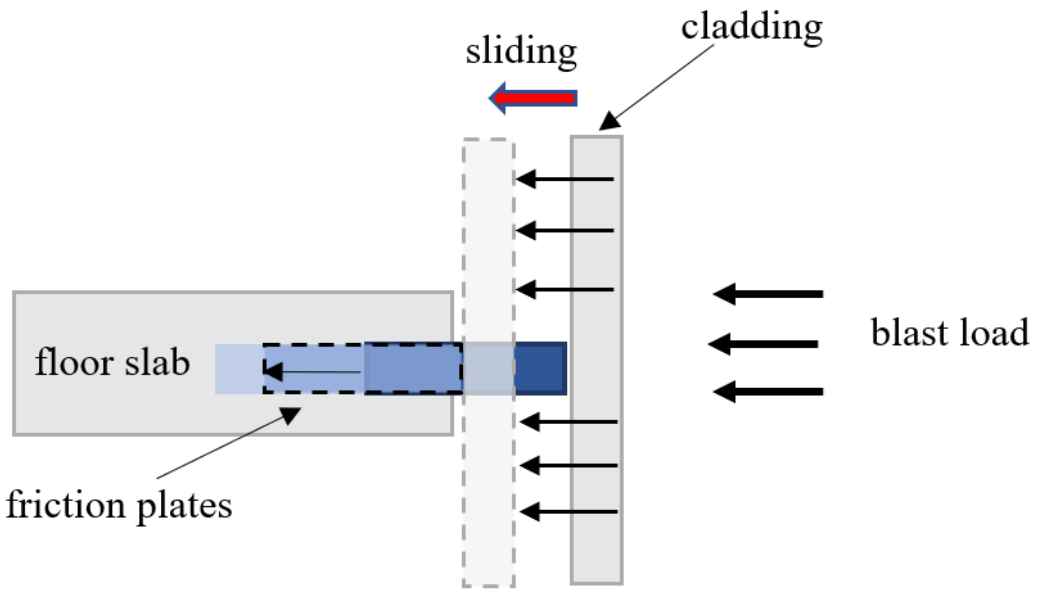

Figure 1.2 Semi-active device exposed to a blast load (lateral view)

1.3 Problem Statements and Objectives

Given the novelty of the semi-active connection, PBD procedures need to be developed to guide and facilitate the holistic integration of these devices within the structural design phase. This study focuses on the design of the device in its passive mode, for which toggles are locked to maintain daily operations. This configuration is engineered for blast resistance. Therefore, the overarching objective of this study is to develop PBD procedures for the passive friction mode of the cladding connection. Note that the design of the device is limited to the selection of its dynamic parameters, including the friction and stiffness elements.

1.4 Contributions

The contributions of this thesis are as follows

- Derived analytical solutions governing the dynamics of the novel cladding connection in its passive mode.
- A PBD procedure enabling the holistic integration of the semi-active connection within the structural design phase for blast mitigation.
- Design tables facilitating the PBD procedure.
- Simulation data supporting the PBD procedure.

These contributions will provide a stepping stone for the future development of PBD procedures for the semi-active utilization of the device.

1.5 Organization of the thesis

This thesis is organized as follows: Chapter 2 reviews recent advances in the design of cladding systems for blast resistance, and includes a discussion on existing cladding connections used against natural and man-made hazards. Chapter 3 presents the mathematical model of the device, and derives the analytical solutions for different states of the semi-active device during a blast event. Chapter 4 presents the proposed PBD procedure, developed based on the analytical solutions from Chapter 3 and numerical simulations. The PBD is verified and validated on simple models. Chapter 5 validates the PBD procedure on a realistic four stories building and discussion of results. Chapter 6 provides conclusions on the research, including a discussion on impacts, limitations, and future work.

CHAPTER 2. LITERATURE REVIEW

2.1 Introduction

The objective of utilizing blast resistance panels or exterior wall is to provide personal safety and reduce structural damage. The blast resistance of cladding panels is provided by their ability to absorb the blast energy. Cladding systems are available in different materials leading to various blast resistance levels, from a thin skin or layer to a stiff pre-cast concrete panel. It what follows, cladding components are reviewed in terms of resistance to blast loads.

2.2 Cladding Materials

The exterior walls and cladding systems of a structure are the direct defense against an explosive threat, and cladding is typically designed to undergo ductile failure when subjected to a blast load for users' safety considerations.

Various materials can be considered in the design of exterior components to provide a given resistance to high pressure loads. Timber is not recommended for blast resistance, because it is too light and fragile. For high pressure loads cladding or curtain wall, materials should have ability to resist blast while reducing the pressure on the structural frame. Of particular interest are blast resistance strategies for government buildings. For instance, in the United States, all new U.S. embassies must be constructed by using cast-in-place concrete [11]. Precast concrete cladding can be used to provide additional blast resistance to government buildings [16]. For the gap distance design between cladding and structure frame, the Building Construction Book [14] indicates that the Precast/Prestressed Concrete (PCI) recommends a minimum horizontal clearance of 2 in between precast panels or brick veneer and building's frame. A James F. Battin

U.S. Courthouse located in Billings, Mont has approximately 5 in between cladding side and frame edge [16].

2.2.1 Precast concrete (PC)

Precast claddings are the most widely use of precast concrete for building envelopes [13]. Precast concrete (PC) cladding find a wide range of applications, and are often used in mid- to high-rise hospitals, apartment buildings, hotels, parking garages, and office buildings [14]. These panels need to be designed for a ductile response. Typically, these panels can have as much as 75 percent additional reinforcement by increasing the thickness of panels, but such reinforcement needs to be limited to ensure yielding of the materials before brittle failure. For example, reference [11] recommends that reinforcement bars be spaced no greater than the thickness of the panel in order to increase ductility and reduce chance of flying concrete fragments.

Key design decisions in PC panels include their size, shape, and function, and come in the form of wall panels, spandrel panels, spandrel plus infill panels, and so on [14]. A 28-day concrete strength is recommended when the panels are removed from the form since to achieve design strength, for which a 5000 psi resistance is commonly obtained in the case of PC curtain wall. The relatively high strength provides a greater durability and better resistance to loads, building movements, and thermal, creep and shrinkage effects. PC panels also provide improved in-service performance and greater protection from rainwater penetration. The panel thickness is governed by the erection or handling stresses rather than the stresses caused by in-service loads. Considering some surface treatment, such as abrasive blasting and acid etching, the total thickness of a PC wall panel minimally 5 in. A thicker panel can provide a better resistance to water leakage, higher fire protection, and greater capacity for heat-storage [14].

The connection of PC wall panel or cladding to the main building structure is the most critical part in PC wall panel design. Typically, there are two types of connections in each panel: gravity load connection (also referred to bearing supports located close to the columns) and lateral load connection (also referred to tiebacks, two or more per panel). These two types of connections are described in what follows.

Bearing supports are mostly used for floor to floor panels in the form of steel tube sections, embedded steel plates, or welded steel connections, as shown in Figure 2.1. One part of the steel tube is embedded in the panel, and the cantilevered part is connected to the edge of the spandrel beam. In the erection process, leveling shims or bolts are used under the bearing supports, and the bearing supports are welded to the bearing plate, which is typically embedded in the spandrel beam.

Typically, the tieback is used to resist lateral loads (winds or earthquake) on the panel, and tiebacks can allow panel movements horizontally. In this thesis, the proposed device replaces conventional horizontal connection (tieback) to resist lateral forces under blast loads. The bearing support to transfer gravity load is placed in the lower middle of one panel with appropriate clearance to allow for the device installation. Figure 2.2 shows the layout of proposed connectors and gravity support.

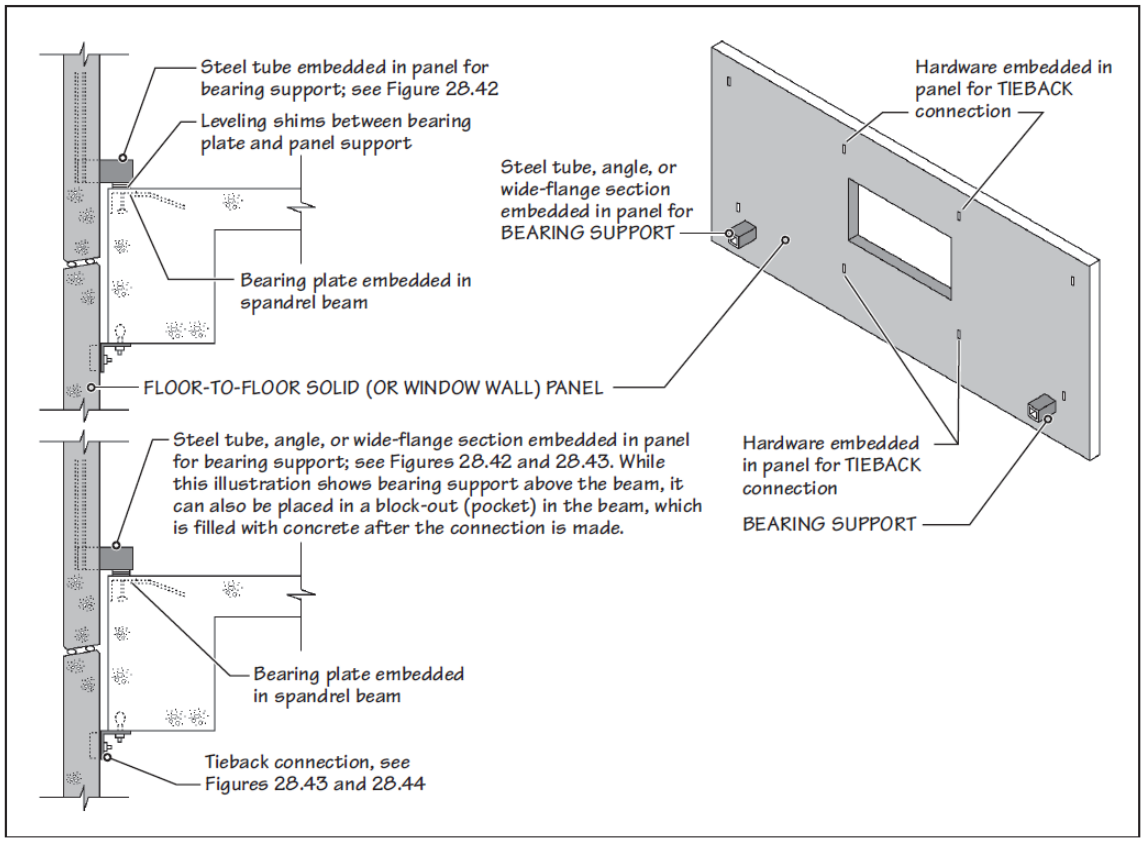

Figure 2.1 Details on bearing supports and tieback, Mehta, Madan, Walter Scarborough, and Diane Armpriest [14].

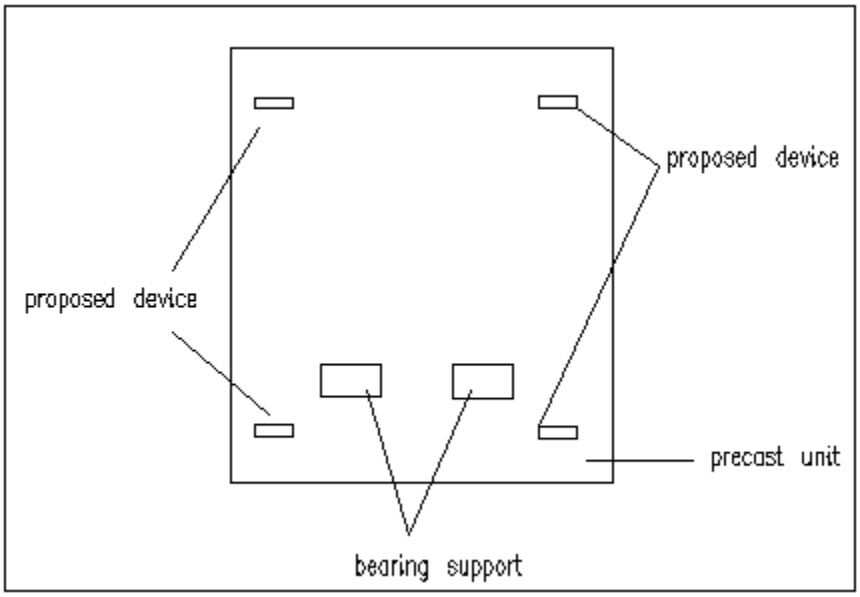

Figure 2.2 Layout of the proposed device and bearing support

2.2.2 Glazing

Glazing is common used in architectural applications for daylights and ventilation [66]. Several studies have focused on the performance of glazing or windows versus blast loads. See references [14, 28, 66, 67, 68, 69] for instance.

To ensure safety, a blast-resistant glazing component is designed to remain within its frame following failure while eliminating any falling or flying glass shards [69]. Table 2.1 lists the performance level requirements for glazing systems. In government design criteria, a blast mitigation window can be designed to sustain between 4 psi to 40 psi pressures [11].

Table 2.1 Performance Conditions for Windows [11]

Performance condition	**Protection Level**	**Hazard Level**	**Description of Window Glazing**
1	Safe	None	Glazing does not break. No visible damage to glazing or frame.
2	Very High	None	Glazing cracks but is retained by the frame. During or very small fragments near still or not floor acceptable.
3a	High	Very Low	Glass cracks. Fragments enter space and land on floor nor further than 3 meters (3.3 feet) from window
3b	High	Low	Glazing cracks. Fragments enter space and on floor no further than 3 meters (10 feet) from the window.
4	Medium	Medium	Glazing cracks. Fragments enter and land on floor and impact a vertical witness panel at a distance of no more than 3 m (10 feet) from the window at a height no greater than 2 feet above the floor.
5	Low	High	Glazing cracks and window system fails catastrophically. Fragments enter space impacting a vertical witness panel at a distance of no more than 3 m (10 feet) from the window at a height greater than 0.6 m (2 feet) above the floor.

2.3 Design of cladding panels for blast resistance

Flying debris following a blast are a significant cause of injuries and fatalities. Cladding systems being the first line of defense versus a blast load, they must be designed wisely, including the selection of the cladding materials and its connections. Heavier claddings and very stiff connections are not prescribed, as they may cause premature failure of the system [11, 17]. Lighter, more ductile systems should be preferred [11]. After considering static forces, a dynamic analysis should be conducted to account for the impulsive nature of the blast (high amplitude load over a short duration). Columns, spandrels and walls can be modeled using a single degree-of-freedom (SDOF) approach to establish governing equations, and a finite element (FE) is typically used for validation.

2.3.1 Blast effects

Blast damage can be ranked by analyzing the damaged area, materials and numbers of casualties and injures. Reference [21] provides a brief description of minor, moderate, and major damage level. In the minor damage level, the structural elements of buildings (e.g., windows, doors, curtain walls, and ceilings) would not be damaged. Fatalities are not expected, but injures may occur. In the moderate damage level, the structural failure only occurs on structural beams, slabs, and non-bearing walls, and can be repaired. Injures and some fatalities are expected. In the major level, primary structural components (columns or girds) are damaged. Extensive fatalities are expected. Table 2.2 lists different damage types as a function of the blast's incident overpressure.

Table 2.2 Typical damage type of blast pressure [18, 19, 20, 21]

Damage	Incident Overpressure (psi)
Typical window	0.15-0.22
Minor damage to some buildings	0.5-1.1
Panels of sheet metal buckled	1.1-1.8
Failure of concrete block walls	1.8-2.9
Collapse of wood-framed buildings	Over 5.0
Serious damage to steel-framed buildings	4-7
Severe damage to reinforced concrete structures	6-9
Probable total destruction of most buildings	10-12

2.3.2 Cladding connections for blast resistance

Precast cladding connections

Precast cladding relies on mechanical connectors that may be easily damaged during a blast [63]. For a panel to absorb blast energy and provide ductility, it must develop its full plastic flexure capacity. The failure mode should be not splitting, spalling or pulling out of the concrete. The connections are required to design for at least 20% more capacity than the member's bending and shear capacity. Also, steel-to-steel connections are required to be designed such that the weld is not the weakest element [63]. The capacity of a panel to deform significantly and absorb energy depends on the ability of its connections to maintain integrity during the response to a blast. Both bolted and welded connections are known to perform well under blast loads [63]. An example of typical connections between precast panel and structural frame under blast load is shown in Figure 2.3. Figure 2.3 (a) shows the load bearing connection, which is designed to transfer the weight of cladding panels to building structure. Figure 2.3 (b) shows restraint connection, which are designed to hold cladding panels back to the structure and transfer horizontal forces [83]. The proposed device is to replace those connections to resist lateral loads,

while bearing supports are used to transfer gravity loads. Figure 2.4 shows different types of bearing supports on precast concrete cladding panel [63]. Figure 2.5 shows the proposed connections between panels and slab.

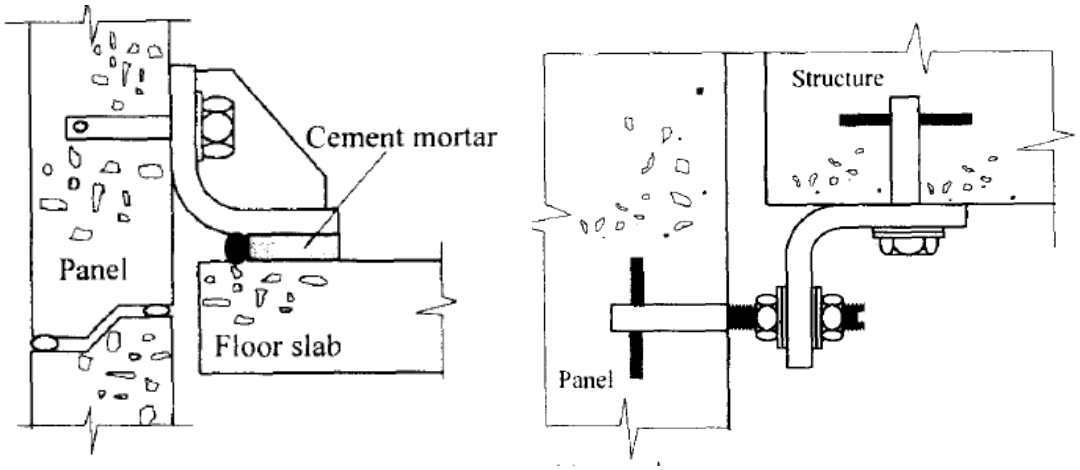

(a) (b)

Figure 2.3 Typical connections for cladding panels: (a) typical load bearing connection, (b) typical restraint connection [83]

Glazing cladding connections

Glazing is prone to failure during a blast event. For this reason, glazing is limited to 15% of the façade for embassies. This number increases to40% for commercial buildings. Glazing, frames, and connections must be analyzed at the system level for quantifying their response to a blast. The cladding panels must be able to resist the dynamic reaction from a failing window [63]. Figure 2.6 shows a typical section of a frame and a blast window. The inner frame includes a frame angle and glazing stop. The inner frame is designed to allow replacement of the glazing. The outer frame is fabricated from plates, channels, or angles to satisfy architectural requirements.

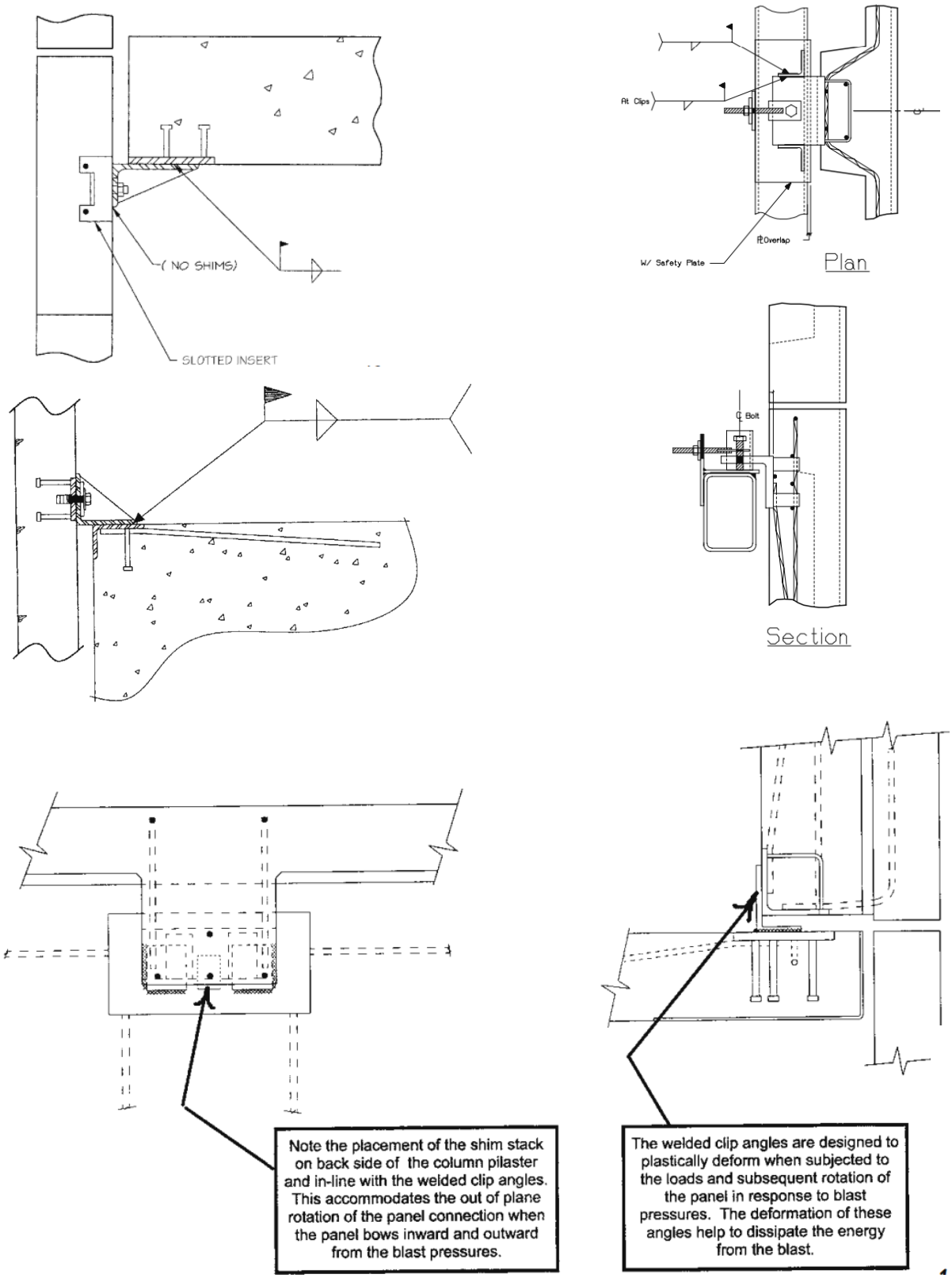

Figure 2.4 Bearing connections [63]

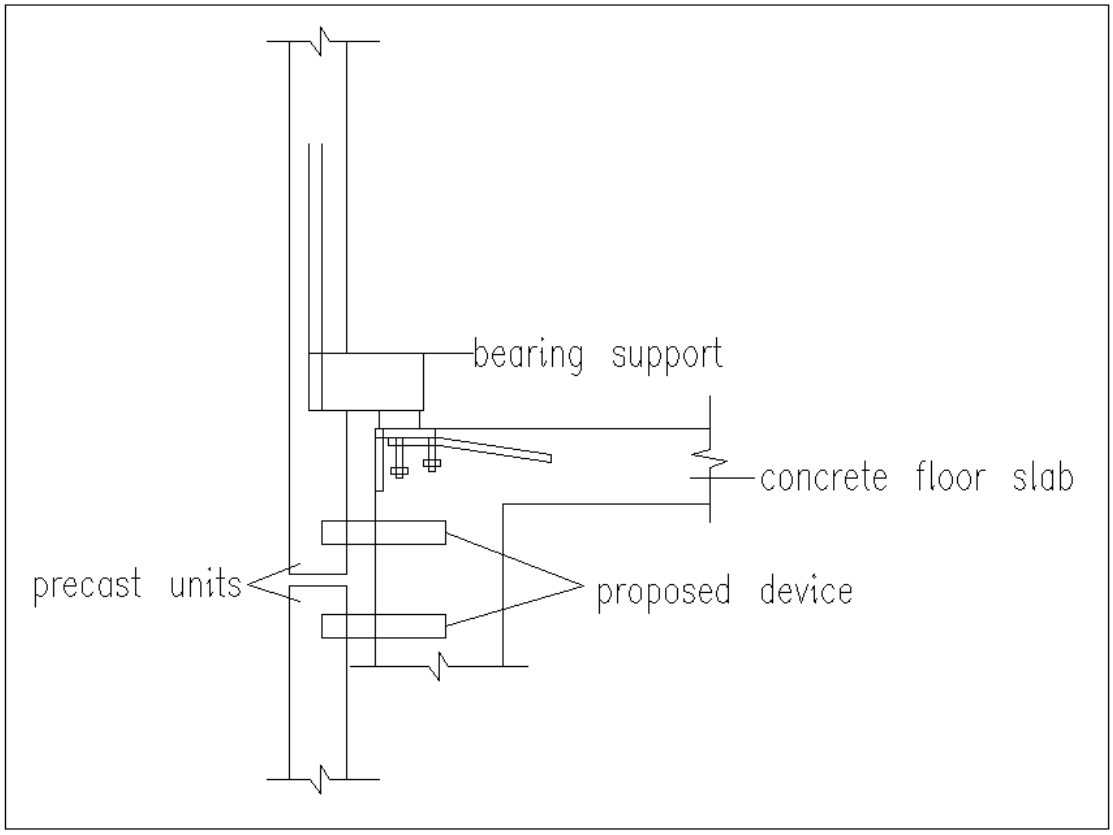

Figure 2.5 Bearing support and proposed device for precast panel

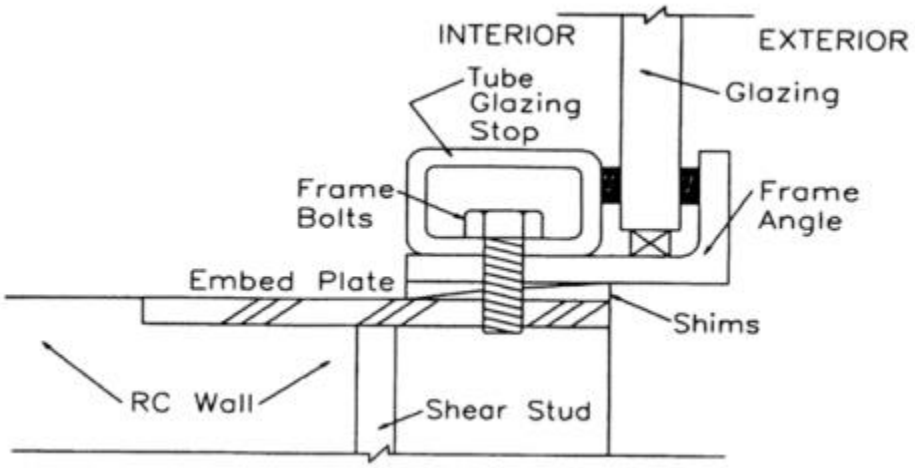

Figure 2.6 Generic blast window glazing and frame detail [80]

2.3.3 Examples of cladding systems

There exists several examples of exterior wall and other claddings designed for blast mitigation. For example, blast panels from Fyfe Co. LLC can resist design pressure from 5 psi to 30 psi, and the maximum impulse can reach to 300 psi-msec. The typical panel dimensions are 10 feet wide and 12 ft tall with 7.4 in thickness [52]. A tested blast-resistant panel is exhibited in Figure 2.7. Figure 2.7(a) indicates that this brand blast panel is easy to install and be finished with any type of materials. Figure (b) shows the panel in a tested tube which is survived high pressures with limited deformations. Figure 2.8 illustrates the performance of the Tyfo panel to a blast, compared with an unreinforced panel, demonstrating its blast resistance.

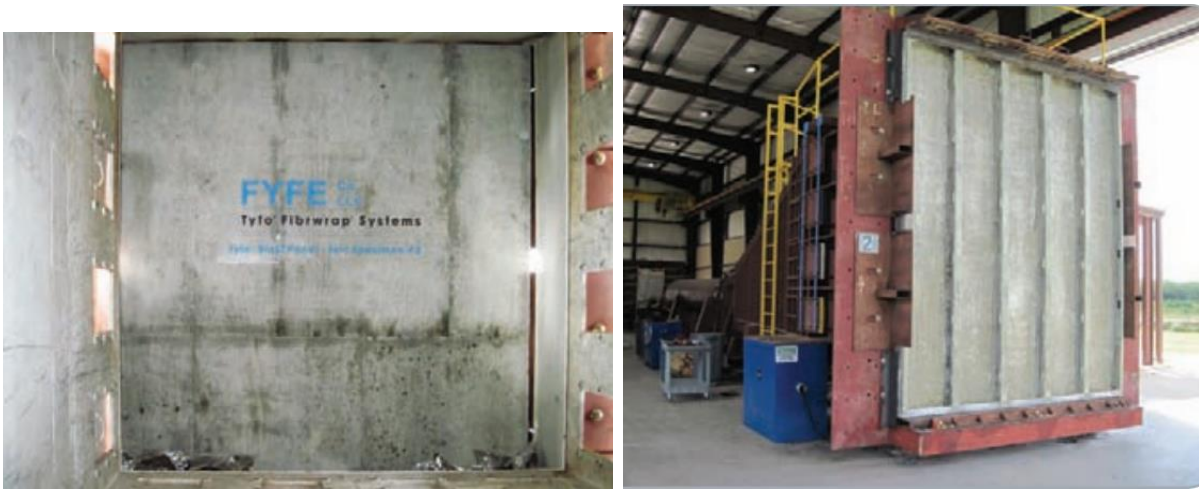

(a) (b)

Figure 2.7 Blast Panels of Fyfe Co. in its tested specimen (a) interior, and (b) exterior [52]

Figure 2.8 Blast Panels of Fyfe Co. in the conditions of two panels after explosive blast [52]

Sizes can be varied for the different project requirements. Stromberg has developed a type of blast mitigation cladding by using glass fiber-reinforced concrete, which can exceed 10 psi peak pressure in their laboratory settings [53]. Stromberg GFRC clients includes US Pentagon, US Navy, US Army Corp of Engineers, hospitals and embassies. A ProTek passive fire and blast protection panels manufactured by Solent Composites is bolted to a secondary steel structure, It provides high performance structures for different demands, such as energy, aerospace, defense, construction, automotive and marine [54]. Figure 2.9 shows its appearance and panel connection details. This kind of cladding is lightweight and relies on a bolted connection as its high strength composite materials which cannot be welded. This panel is designed to resist a two-hour jet fire test with a 0.3 kg/s gas release, and blast test up to 1.5 bar (22 psi).

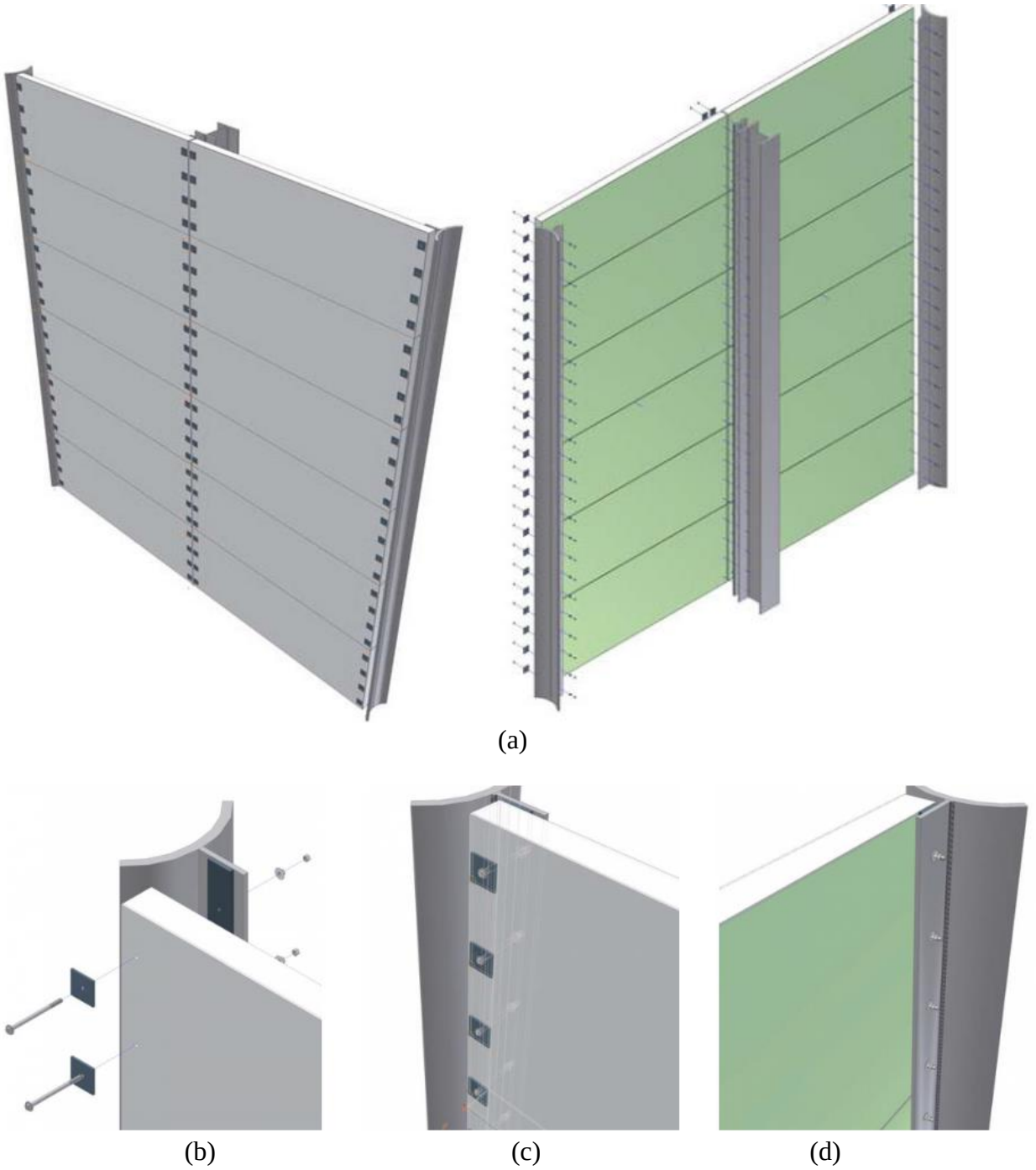

Figure 2.9 ProTek Cladding panel connection details (a) general view, (b) tubular showing exploded view of bolts and gasket seal, (c) tubular showing bolts and gasket seal assembled (d) non-harard side of panel, (e) relastic view of non-harzard side for fire and Blast wall, (f) hazard side of panel at strccutral member showing bolts and gasket seal, (g) non-hazard side at surcutural member and tubular [53]

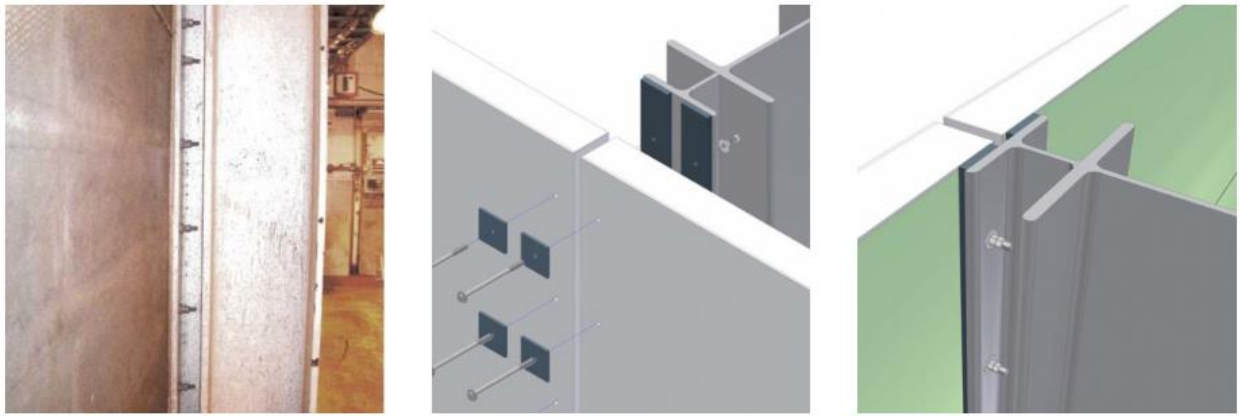

(e) (f) (g)

Figure 2.9 (continued)

The Van Dam Blast relief cladding is utilized on external offshore platforms, onshore Refinary's, Living Quarters, and control buildings. This type of cladding is a fully bolted and lightweight wall system, and it can withstand blast overpressure of 0.725psi (0.05 bar) in 20 ms [55]. A brief panel connection details are shown in Figure 2.10.

WAUSAU (window and wall Systems Company) provide modern blast-mitigation assemblies with its flexibility and energy absorption capability. According to GSA ISC Security Design Criteria and Department of Defense UFC 4-010-01 [56], 2250I-BHM windows and 8000-BHM curtain walls can be used for blast hazard mitigation, and the blast performance can exceed to 4 psi, 28 psi-msec impulse, and 10 psi and 89 psi-msec impulse, respectively [57]. Figure 2.11 expresses the process of window in the different phase under blast load. Table 2.3 summarizes these available products for blast resistance.

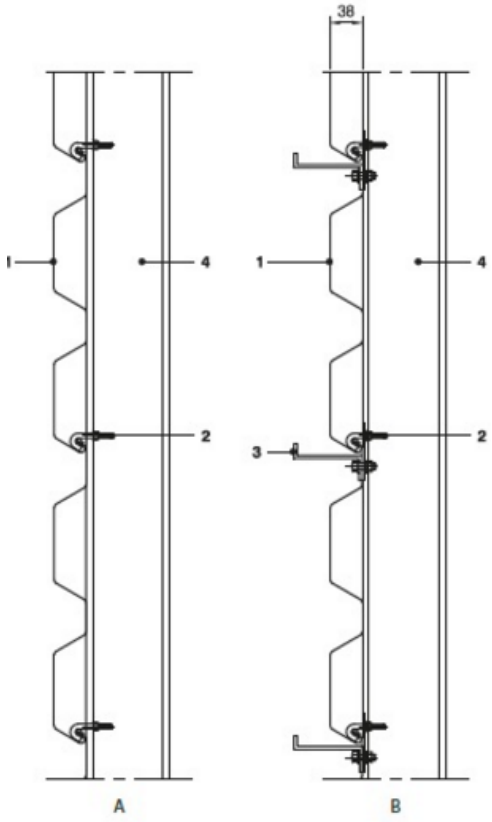

Figure 2.10 Brief blast relief cladding and its connections

(a) (b) (c)

Figure 2.11 Window for blast hazard mitigation (a) before the test, (b) during the test (at peak positive pressure), (c) after the test [57]

Table 2.3 Available cladding products for blast resistance

Cladding System	**Designed Blast Overpressure**
Tyfo Fibrwrap Blast Panels [52]	5-30 psi , 80 to 300psi-msec impluse
Stromberg GFRC Blast Cladding [53]	10 psi, 89 psi-msec impluse
ProTek Fire &Blast Cladding [54]	22 psi (1.5 bar)
The Van Dam Blast Relife Cladding [55]	0.72 psi(0.05 bar) within in 20ms
2250I-BHM windows [57]	4psi, 28psi-msec impluse
8000-BHM Curtain wall [57]	10psi, 89 psi-msec impulse

The blast resistance capability of the entire building should also be considered. In the late 1990's, steel reinforced concrete was the only option for blast protection. Now steel-fabricated and factory manufactured blast resistant buildings can be a good option for live safety and equipment protection. Compared with concrete construction, steel constructions perform very well under dynamic loads as it has a high level of ductility and energy absorption capacity [58]. Table 2.4 list various building types and their performance versus blast.

Table 2.4 Building types and their performance under blast [58]

Building Type	**Peak side-on Overpressure**	**Consequences**
Wood-framed trailer	1 psi	Roof and walls collapse
Unreinforced masonry building (bearing walls)	1.5 psi	Complete collapse
Pre-engineered steel building	2.5 psi	Frame stands, but cladding and interior walls are destroyed
Steel-fabricated, blast resistant building	> 25 psi	Per design basis (can be no damage or client's stated limit)

CHAPTER 3. METHODOLOGY

3.1 Idealization of the structure-cladding system

The dynamics of the structure-cladding interaction is nonlinear given the presence of a friction element and an impact bumper (nonlinear stiffness), and the time-varying nature of a blast load. Some simplifications are conducted in order to facilitate the derivation of analytical solutions, which will be used to estimate transfer functions enabling PBD. The analytical solutions will be derived for the first half-cycle displacement response of the cladding following a blast load, which corresponds to the maximum displacement of the cladding and highest possible impact force on the building. This section discusses the simplified models used for the derivation of these solutions.

3.1.1 SDOF

The structure-cladding interaction is studied both in a single-degree-of-freedom (SDOF) and a two degree-of-freedom (2DOF) configuration. The SDOF configuration is utilized to derive analytical solutions for PBD procedures. In this model, the structure is taken as fixed, based on the assumption that the dynamics of the structure itself can be negligible during the first half-cycle displacement of the cladding [22]. Figure 3.1 (a) shows the SDOF representation of the cladding and its connection. The cladding of mass m_c is connected to the structure via a stiffness element k_c, a viscous element c_c, and a friction element f_c. An impact rubber of length l_r is installed at a distance $l_c - l_r$ from the cladding, where l_c is the total distance separating the cladding from the structure. The rubber is modeled as a nonlinear stiffness element k_r. The blast load is represented by a time series $p(t)$.

The 2DOF configuration, represented in Figure 3.1 (b), is used for validating the design methodology or a more realistic dynamics. In this representation, the cladding is connected to the structure of mass m_s, connected to its based by a stiffness element k_s and a viscous element c_s.

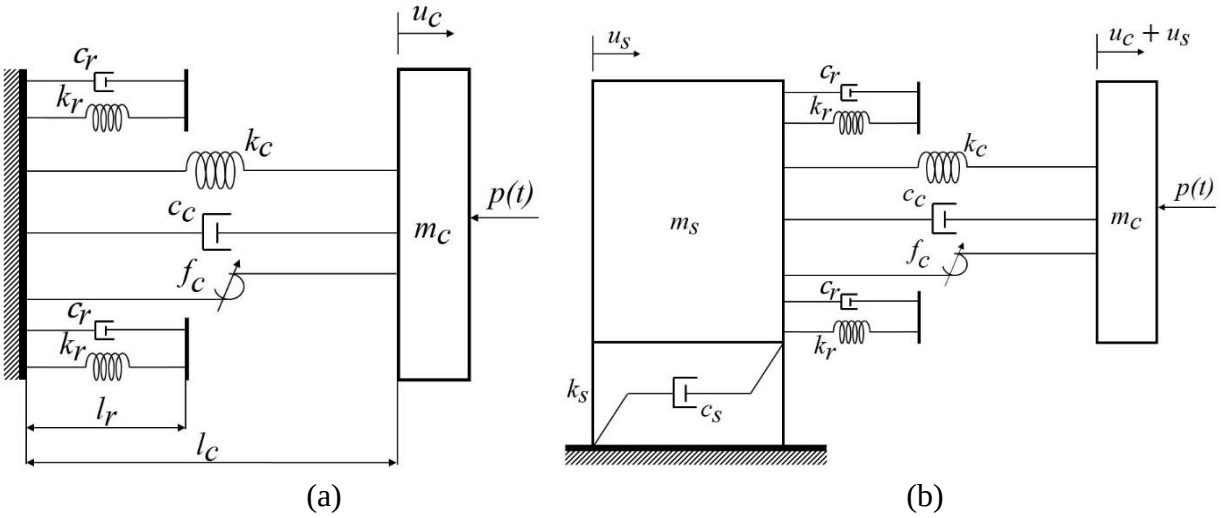

Figure 3.1 (a) (SDOF) representation (b) (2DOF) representation

3.2 Idealization of blast load

3.2.1 A brief introduction of a blast load (phenomenon)

A blast produces a high-amplitude, high-impulse fast and unexpected energy wave. Generally, there are two different types of explosions: physical and chemical explosions. As the reaction progresses, the explosive materials characterized as physical states of solids and liquids can be changed to very high dense, temperature and pressure gases [23, 24, 25]. This high velocity and power will cause a shock wave when it reaches equilibrium in the surrounding air.

The high temperature gases produced by the detonation of high explosive can reach a temperature of 3000-4000 ℃ and the pressure can go up to 300 kbar. Since the blast load is a sudden release of energy, the power of the blast will drop as time passes. The explosion produced expands at a very high velocity at the very beginning with high energy which will

produce a shock wave [25]. The shock waves are formed by highly compressed air, and it acts rapidly from the source at supersonic velocity. Each explosion energy has different effects. The first third of the energy is a major reason for the high exploding process, and the other two thirds of the energy will release the products which mix in the air and burn very slowly. In the whole process, the high speed expansion of hot gasses will give rise to several compression waves which are shock wave, and each peak pressure in one wave will decrease with time rapidly.

3.2.2 Triangular model of blast load

A typical blast pressure wave is shown in Fig.3.2 [23]. At the beginning of the explosion, the air pressure suddenly rapid up to the peak pressure σ_{max}. The pressure delays to normal pressure during time t_d (positive phase) and drops to the negative pressure σ_{min} before the pressure returns to normal at time $t_{blast} = t_d + t_n$ (negative phase). The positive phase means that the shock wave pressure is larger than the atmospheric pressure, likewise if the wave pressure is smaller than atmosphere pressure, the pressure is in the negative phase [23, 25, 26, 27].

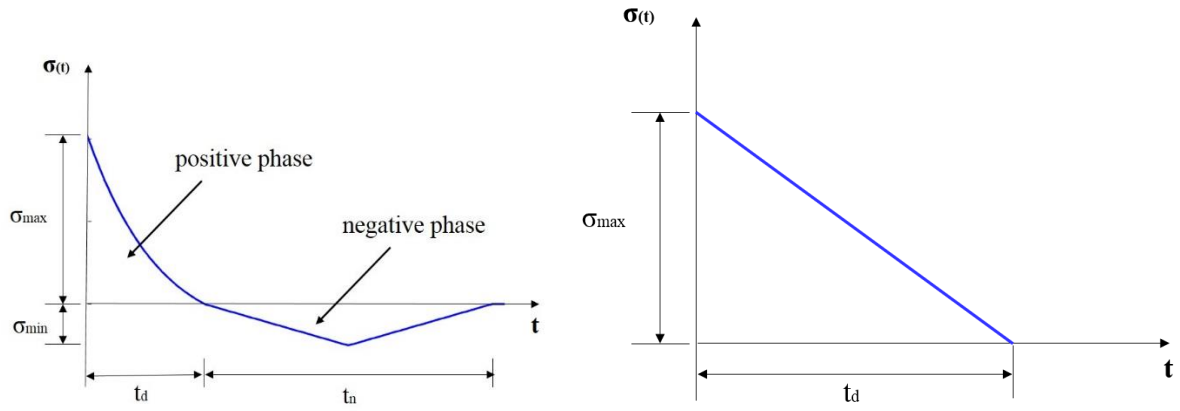

Figure 3.2 Time history curve for air blast wave pressure: (a) typical model (b) idealization model

The simplify the blast load, it is assumed that $\sigma_{min} \approx 0$ and $t_d \ll t_{blast}$, that the positive phase can be approximated by a linearly function. This idealization, shown in Figure 3.4 [28], is used to create the blast load time series:

$$p(t) = \begin{cases} F_m\left(1 - \frac{t}{t_d}\right), & 0 < t < t_d \\ 0, & t > t_d \end{cases} \quad (1)$$

where $F_m = A_c\sigma_{max}$ is the amplitude or maximum value of the blast load and A_c is the area of the cladding.

The blast load reflected impulse I is the area under the triangular distribution force-time curve, the equation is shown as follows:

$$I = \frac{1}{2}F_m t_d \quad (2)$$

3.2.3 Blast design considerations

Typical blast loads can be estimated at the design stage following design handbooks or other relevant sources. The U.S. Department of Defense, Department of State, and General Services Administration have developed specific antimerism requirements for embassy, military, and federal building respectively. Table 3.1 provides recommendations for private facilities [31]. The blast pressure can also be obtained considering the types of explosive, distance from the building R, the mass of explosive charge W, c and the maximum quantities of explosives in different vehicles, as listed in Table 3.2.

Table 3.1 Recommended antiterrorism design criteria [31]

Tactic	Parameter	Estimated Likelihood of Terrorist Attach				
		Low	**Medium**	**High**	**Very High**	**Measurement of Standoff Distance R**
Vehicle Bomb	Vehicle Size * (lbs. GVW)	4,000	4,000	5,000	12,000	Controlled Perimeter, Vehicle barrier, or unsecured parking/road
	Charge Size W(lbs. TNT)	50	100	500	2,000	
Placed Bomb	Charge Size W(lbs. TNT)	0	2	100	100	Unobstructed space or unsecured parking/road
Standoff Weapon	Charge Size W(lbs. TNT)	2	2	50	50	Neighboring structure

Table 3.2 Estimated quantities of explosives in various vehicles (in kg)

Vehicle	Charge Mass W (kg)
compact car truck	115
trunk of a large car	230
closed van	680
closed truck	2270
truck with a trailer	13610
truck with two trailers	27220

The value of maximum pressure can be found by using TNT equivalents (the equivalent weight of the explosive in TNT is W) and the standoff distance, R, which is the distance from the cladding surface to the center of a spherical explosion. The minimum standoff distance for inhabited buildings of conventional construction is provided by Chapter 2.3.2.1 in ASCE/SEI 59-11 [30, 71]. The blast should be scaled when calculating a blast load. Two shock waves might be similar at same scaled distances with different size when there two explosive charges will be in a similar geometry or they have the same explosive [23]. The scaled distance Z (m per kg TNT

equivalent) can be determined using Eq. (3a). For every point of interest, the standoff distance R_h with its height can be calculated by using Eq. (3b). The positive time duration period in the positive phse can be determined by Eq. (3c) [64, 65]. The peak overpressure in kPa from equivalent TNT with scaled distance can be expressed by Eq. 3(d) [23, 32]:

$$Z = \frac{R}{W^{1/3}} \tag{3a}$$

$$R_h = (R^2 + h^2)^{\frac{1}{2}} \tag{3b}$$

$$t_{blast} = W^{\frac{1}{3}} 10^{-2.75+0.27log(Z)} \tag{3c}$$

$$\sigma_{max} = \frac{1772}{Z^3} - \frac{114}{Z^2} + \frac{108}{Z} \tag{3d}$$

Also there are some other ways to provide a direct and quick way for predicting blast loads. A figure from U.S. Air force, shown in Figure 3.3, installation force protection guide. Another way is to use a software product. For example, AT Blast [72], can help to calculate blast load parameters includes shock front velocity, time of arrival, pressure, impulse, and its duration time.

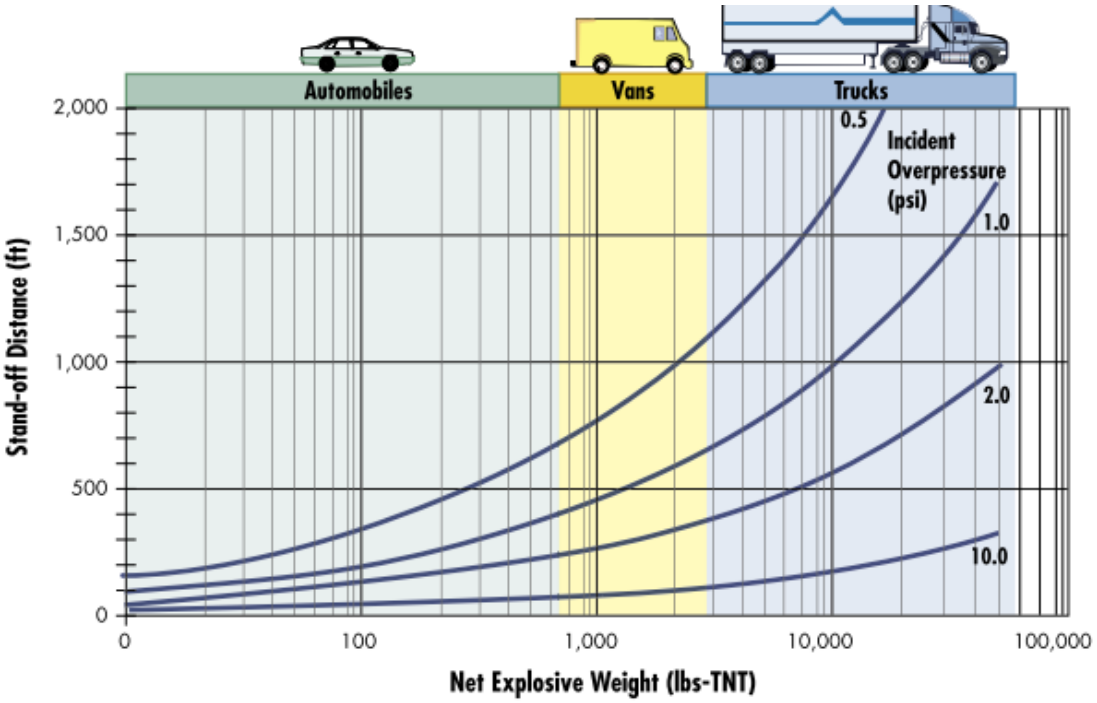

Figure 3.3 Incident overpressure measured in pounds (-TNT) per square inch [34]

3.3 Idealization of rubber bumper

Most buildings usually experience large horizontal relative displacements in strong earthquakes. In some regions, the limiting distance between buildings and deformations between their stories will cause structural pounding between adjacent buildings. Pounding and unseating damage mitigation on structural buildings or bridges elements such as deck, spans, or piers have been investigated in a lot of research under many seismic excitations [23 35 36 37 38]. Rubber bumpers can be used effectively as a shock absorption to mitigate the pounding effects and unseating problems on multi-span bridges by ground motion. For buildings, a rubber bumper is provided at one end of the structure wall so that they can resist further relative displacement which exceeds the original gap [35]. Although earthquake excitation is different from blast loading, and they are two different fundamental physical phenomena, seismic control methods concentrates on dissipating energy and controlling the deflections safely, and blast loading can also be controlled on energy dissipations by using rubber bumpers [37]. Since the behavior of rubber bumper is nonlinear subjected to a quick impact force, there is sparse literature of a right impact model to describe rubber bumpers sufficiently. P.C.Polycarpou etl. (2012) provides a new nonlinear inelastic force-based impact model to represent the behavior of rubber under an impact force [35].

Generally, there are five different types of forces, compression, tension, torsion and shear. Rubber can dissipate both shear and compression forces while shearing forces causes from ground motion and compression forces causes from blast load. Different rubber will have different capacities, it is up to the designer to choose an appropriate type of rubber, and one of the purposes of this project is to give a reasonable design procedure to choose the size (thickness) of the rubber.

3.3.1 Impact model for the rubber bumper

One of the method used is the using force-based method, also called penalty method. This method uses the stiffness of the contact spring and impact velocity to get the contact forces which are applied to the structure [36]. There are two different types of impact models mentioned by Petros K. [36]. The two kind of viscoelastic impact model can be considered under the impact force are the linear viscoelastic impact model and the nonlinear viscoelastic impact model.

(a) Linear viscoelastic impact model

The linear viscoelastic impact model, also known as Kelvin-Voigt Model is one of the most commonly used model for structure collision. The configuration considers one linear impact spring and a viscous impact dashpot in parallel. Petros K [36] also provides the impact force at time t is provided by

$$F_r(t) = k_r u_r(t) + c_r \dot{u}_r(t) \tag{4}$$

where k_r is the stiffness of the linear impact spring, $u_r(t)$ is the interpenetration depth of the indentation, c_r is the impact damping coefficient, and $\dot{u}_r(t)$ is the relative velocity between the pounding at time t. The impact damping coefficient in viscoelastic impact models is shown as a function of the coefficient of restitution (COR) and the masses m_1 and m_2 of two pounding bodies.

$$c_r = 2\xi_{imp}\sqrt{k_r \frac{(m_1 m_2)}{m_1 + m_2}} \tag{5a}$$

$$\xi_{imp} = -\frac{\ln(COR)}{\sqrt{\pi^2 + (\ln(COR))^2}} \tag{5b}$$

ξ_{imp} is the impact damping ratio ($0 < \xi_{imp} < 1$). The COR above is the ratio of the relative velocities between the pounding bodies before and after impact ($0 \leq COR \leq 1$) [13].

(b) Non-linear viscoelastic impact model

Hertz's model is one of the most commonly model used in impact structure by using a non-linear impact spring. This model is assumed that the impact force increases exponentially with the indentation depth. An exponent of 1.5 is commonly used. Some researchers [35, 36, 37] used the configuration with a non-linear damper parallel to the non-linear spring during the approach phase by impact force. The impact force during the approach phase equals [39, 40]

$$F_r(t) = k_r u(t)^{1.5} + c_r \dot{u}_r(t) \tag{6a}$$

And during the restitution phase, the impact force equals

$$F_r(t) = k_r u_r(t)^{1.5} \tag{6b}$$

The impact-damping coefficient is shown in the following formula in terms of the impact damping ratio and the interpenetration depth, $u(t)$ [36, 41].

$$c_r(t) = 2\xi_r \sqrt{k_r \sqrt{u_r(t)} \frac{(m_1 m_2)}{m_1 + m_2}} \tag{7a}$$

The impact damping coefficient will change with time and with respect to the indentation. According to Jankowski [40], the formula of impact-damping ratio, ξ_{imp} is shown as follows,

$$\xi_{imp} = \frac{9\sqrt{5}}{2} \frac{1 - COR^2}{COR(COR(9\pi - 16) + 16)} \tag{7b}$$

(c) Hertz damp model

One limitation of the Herts model is that it cannot represent the energy dissipated during contact. A non-linear damper is used in the conjunction with the Hertz spring [42]. Most of this model is used for robotics and multi body systems, and the uses and effects are neglected in the structural design [42]. The exponent for this model, n, is determined by the material. The impact force can be expressed as

$$F_r(t) = k_{imp} u_r(t)^n + c_r \dot{u}_r(t) \tag{8}$$

The non-linear damping coefficient is shown as follows [18]:

$$c_r = \xi_{imp} u_r^n \tag{9a}$$

The loss of energy during the impact to the energy dissipated by pamper, an expression can be shown as follows:

$$\xi_{imp} = -\frac{3k_{imp}(1 - \mathrm{COR}^2)}{4\dot{u}_r} \tag{9b}$$

3.3.2 Behavior of rubber under impact loading

According to the observation from the relevant experiments and the stress-strain curves from both static and dynamic tests, the behavior of the linear impact models during impact force is not ideal. The use of a nonlinear impact models is deemed more appropriate for simulating a rubber bumper [35]. From the observations of the relevant impact test model in Fig. 3.4 (c), (d) and (e), the impact force increases exponentially with the indentation during the approach phase of impact.

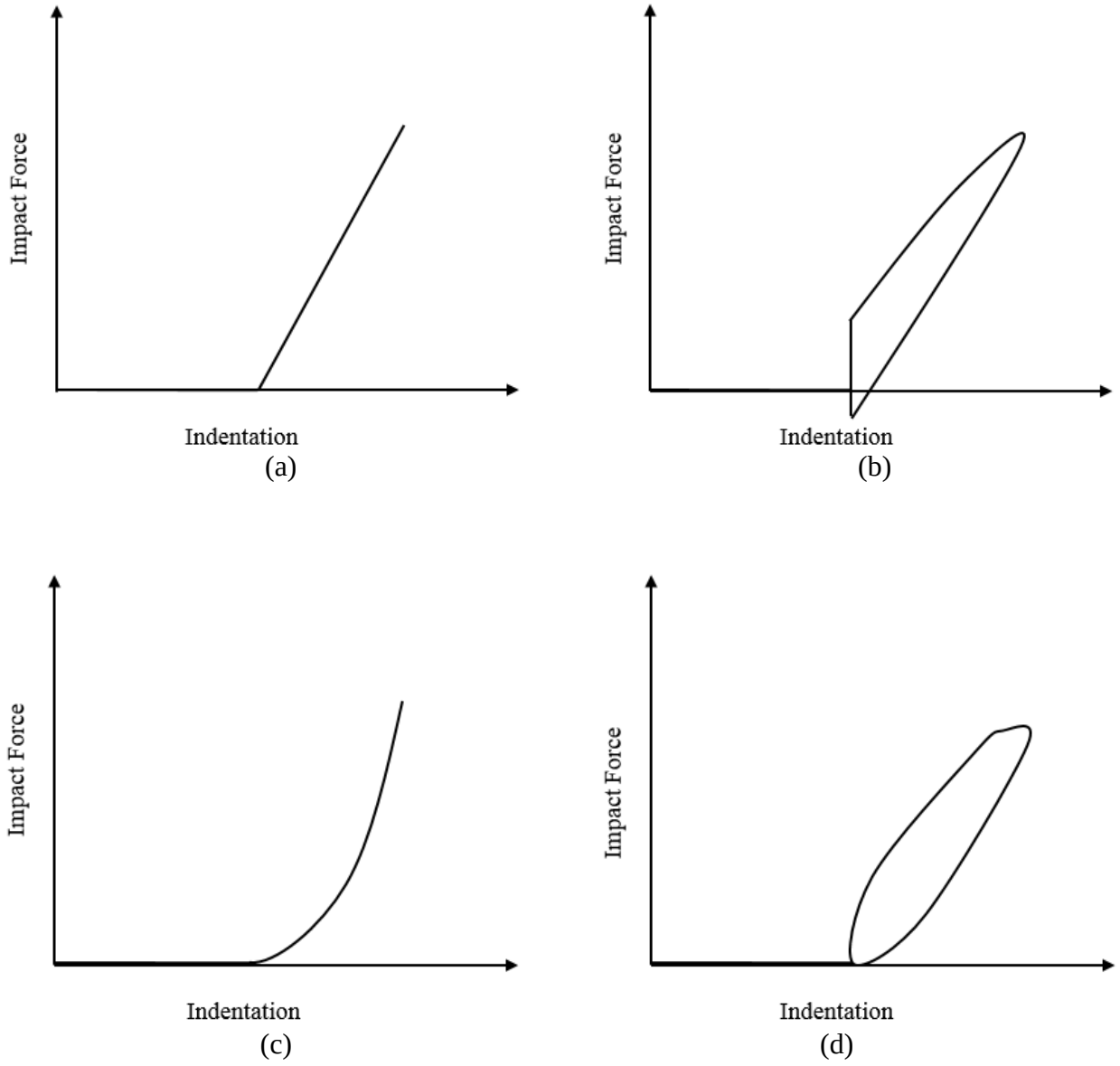

Figure 3.4 Impact Force-Indentation relationship for various impact models:(a) Linear spring element; (b) Linear viscoelastic impact Model (Kelvin Model); (c) Hertz spring Model; (d) Hertz nonlinear viscoelastic model; and (e) Hertz Damp model [35,36,42]

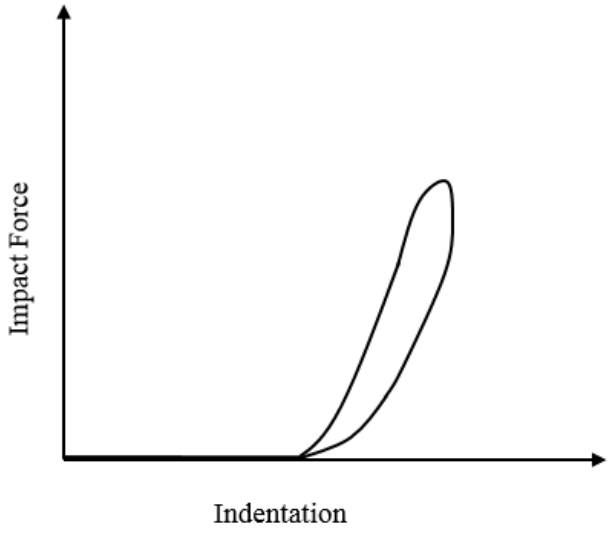

(e)

Figure 3.4 (continued)

From reported experimental results, the curve of the impact force is very close to the profile of the stress-strain curves [35]. The dissipation of kinetic energy during impact is formed by a hysteresis loop of approach phase curve to the restitution phase curve in Fig 3.5(a).

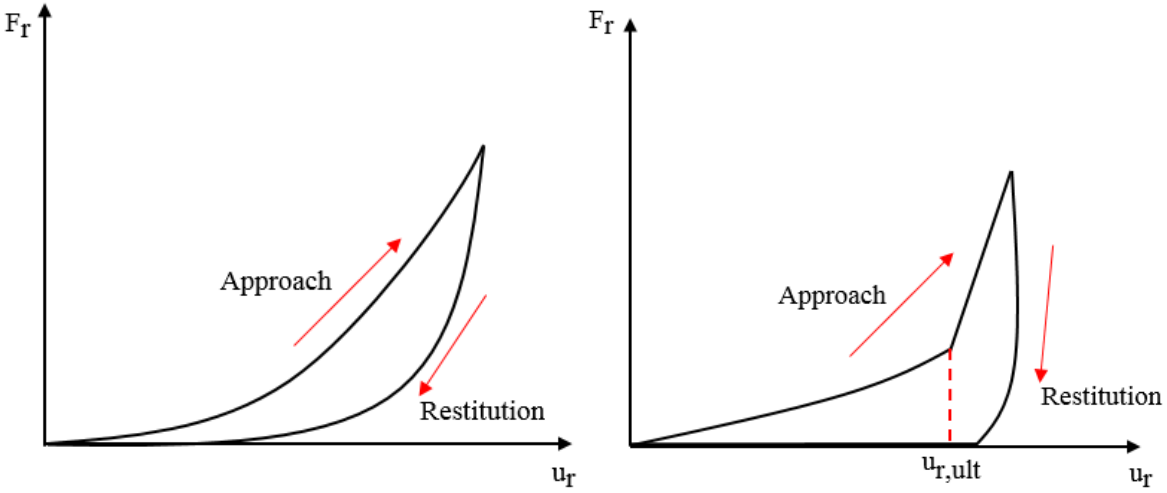

(a) (b)

Figure 3.5 The nonlinear impact model, (a) rubber behavior when $u_{r,max} < u_{r,ult}$; (b) rubber behavior when $u_{r,max} > u_{r,ult}$

The model assumed from [35] providing the impact force at a certain indentation during the approaching phase is expressed as follows:

$$F_r = \begin{cases} k_r u_r^n & u_r < u_{r,u;t} \\ k_r u_{r,ult}{}^n + k_{r,y}\left(u_r - u_{r,ult}\right) & u_r > u_{r,ult} \end{cases} \quad when\ \dot{u}_r > 0 \tag{10a}$$

This equation considers the ultimate compression stain of the materials in the approach phase. Specifically,$u_{r,ult}$ corresponds to the ultimate compression capacity of the rubber bumper. $k_{r,y}$, a linear post-yield stiffness, is used when the rubber indentation reaches a certain critical value is over the ultimate indentation distance.

During the restitution phase, the impact force is expressed as:

$$F_r = k_r u_r^n (1 + c_r \dot{u}_r) \qquad when\ \dot{u}_r < 0 \tag{10b}$$

Each point over the indentation, u_r describes the force derivation with respect to time. The impact stiffness k_r of a specific rubber bumper can be expressed as

$$k_r = \beta \frac{(K_r A)}{l_r^n} \tag{11a}$$

where β is a strain rate-dependent coefficient, A is the contact area of the bumper, l_r is the bumper thickness, and K_r is the material's stiffness. Respectively, n>1 is the impact exponent, and A and l_r denotes the size of the rubber and the parameters K_r and l_r^n are determined by the material characteristics.

The following equation can determine c_{imp} of the material

$$m_{eff} = \frac{m_1 m_2}{m_1 + m_2} \tag{11b}$$

where m_2 and m_1 are the total mass of the two-colliding structure.

There are three ways to calculate the impact damping coefficient c_r. The following expression indicate the evaluation of the appropriate value for the impact force. COR here is a value which represents the impact properties of the rubber bumper only.

$$c_r = 1.55 * \frac{1 - COR^2}{COR^{0.7076} * m_{eff}^{0.0025} * v_r^{0.9755}} \tag{12a}$$

where v_r is the impact velocity in the first pounding.

The second impact damping coefficient c_r does not include the two adjacent structure masses. The vulnerability of second way is not accurate, because the restituting relative velocity is COR, smaller than the related velocity during the approach phase. The expression of the impact damping coefficient is shown as

$$c_r = \frac{(1-COR^2)*3}{COR*v_r*2} \tag{12b}$$

Here is another approximation of c_r, which does not include the masses of two adjacent structure. In this case, the damping coefficient is assumed to be the relation between the relative velocity during the restitution and the relative velocity during the approach phase, and is an exponential trend. The expression is

$$c_r = \frac{(1-COR^2)}{v_r 2} \ln^3(COR) / (COR(2 + \ln^2(COR) - 2\ln(COR) - 2) \tag{12c}$$

P.C.Polycarpou (2012) gives an experimental example of the rubber use by impact force. The parameters of impact with rubber bumper is shown in the Table 3.3 [35]

Table 3.3 Impact parameters with the rubber bumper [35]

Property	Value
Exponent, n	2.65
Impact Stiffness (k_r)	0.36 kN/mm$^{2.65}$
Coefficient of restitution(COR)	0.5
Bumper's maximum stain ($u_{r,ult}/l_r$)	0.8
Post-yield impact stiffness	2500 kN/mm
Impact rubber contact area (A)	40mm x 40mm

3.3.3 Equivalent damping system

Solving the nonlinear equation of the impact rubber is a nontrivial task. Therefore, the equivalent damping system approach is used to analyze the system. . With this approach, the impact rubber is sized to provide a given level of damping equivalent to a linear viscous damper. Consider a half cycle response for the cladding system. The hysteresis of the impact rubber (Fig. 3.9) can compared to the hysteresis of a linear viscous damper. The impact rubber can therefore be approximated

$$F = c_{eq}\dot{u}_r \tag{13}$$

where F is the linear viscous damping force, c_{eq} is the equivalent damping coefficient, and $\dot{u}_r$is the velocity of the impact rubber. Assuming a periodic excitation, the response of the equivalent system is written:

$$u_r(t) = \bar{u}_r \sin(\omega t) \tag{14}$$

where $\bar{u}_r$ is the maximum displacement of the impact rubber. Eq. (10) becomes:

$$F = c_{eq}\bar{u}_r\omega \cos(\omega t) \tag{15}$$

The energy dissipation of the linear viscous damping W for this half cycle response using this equivalent damping representation is expressed

$$\begin{aligned} W &= 2\int_0^{\bar{u}_r} k_{eq}u_r \; du_r \\ &= \frac{1}{2}k_{eq}{\bar{u}_r}^2 \end{aligned} \tag{16}$$

In addition, the energy dissipation of the impact rubber can be taken as the area between the approaching and the to the restitution phase curves. According to the Eq. (10), F_r^A represents the impact force when cladding is in the approaching phase, and F_r^R represents the force in restitution phase. Since it is difficult to do the integration when the exponent value is not an

integer, a nearly integer exponent value is Taken.The energy dissipation of the impact rubber is expressed as: The energy dissipation of the impact rubber can expressed by estimated rubber dynamic model:

$$W_r = \int_0^{\bar{u}_r} F_r^A \; du_r$$

$$= \int_0^{\bar{u}_r} k_r u_r^n \; du_r$$

$$= \frac{1}{n+1} k_r \bar{u}_r^{n+1}$$

$$= \frac{1}{3.65} k_r \bar{u}_r^{3.65} \tag{17}$$

where superscripts A and R denote the approach and the restitution phases, respectively. Equating Eq.(16) and Eq.(17) gives

$$k_{eq} = \frac{2}{3.65} k_r \; \bar{u}_r^{1.65} \tag{18}$$

Figure 3.6 show the equivalent energy dissipation concept. The area of red triangle represents the energy dissipation from linear stiffness and the area of black line is the dissipation of rubber energy. In this figure, linear stiffness has same energy dissipation as impact rubber under approach phase.

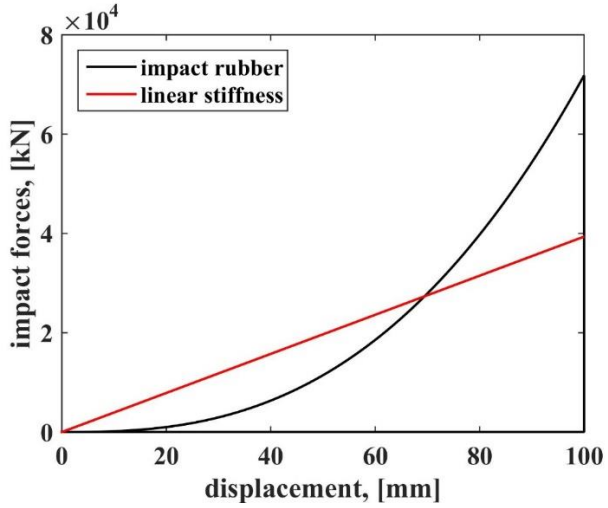

Figure 3.6 Equivalent linear stiffness hysteresis and impact rubber hysteresis (approach phase)

3.4 Idealization of Friction

Friction is the tangential reaction force between two surfaces in contact. Physically, these reaction forces are the results of many different mechanisms which depend on contact geometry and topology. Some experiments show that friction changes depending on various parameters, which include sliding speed, acceleration, critical sliding distance, temperature, normal force, humidity, surface preparation, and material combination [43].

Here, a Coulomb friction model is used to idealize the friction behavior:

$$F_c = f_c \mathrm{sgn}(\dot{u}_c) \tag{19}$$

where f_c is the friction force magnitude produced by the proportional to the normal force, $\dot{u}_c$ is the relative velocity of the moving object, and sgn is the sign can determine the direction of frictions depend on the velocity directions. This equation is plotted in Fig. 3.7.

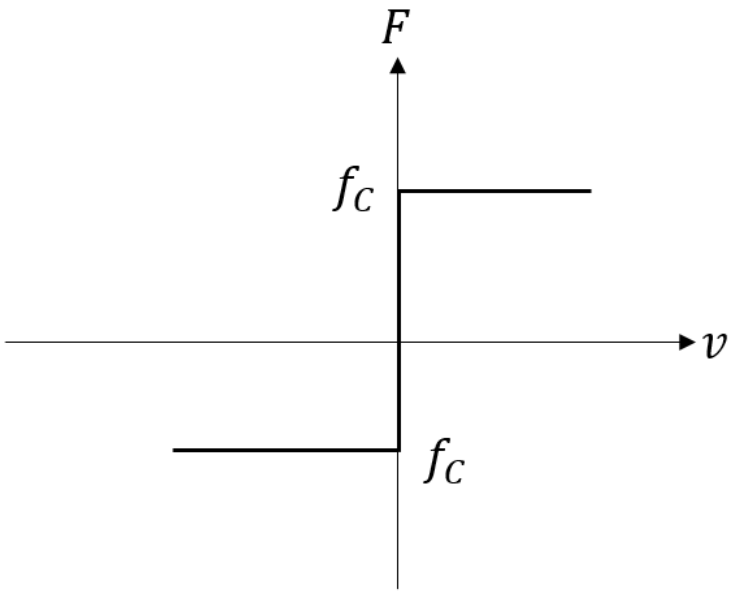

Figure 3.7 Coulomb Friction Model [43]

CHAPTER 4. PBD PROCEDURE

The proposed PBD procedure for connection exposed to a blast load is illustrated in Figure 4.1. It consists of four steps. Step 1 is the selection of the performance criteria, which include the design blast force F_{blast} along with its period t_{blast}, the actual distance between the cladding and the structure l_c, which can be determined based on cladding materials. Step 2 consists of selecting the dynamic parameters of the cladding system based on the performance parameters from Step 1. They include the cladding mass m_c, damping c_c, and stiffness k_c as well as the friction element F_c. The selection of $m_c,\ c_c,\ k_c\ and\ F_c$ will provide a measure of the maximum cladding displacement $u_{c,max}$. Step 3 is the design of the rubber element with its thickness. The magnitude of F_c, f_c can be determined on a small fraction of blast force F_{blast} in Step 2.

In Step 2, if l_c is smaller than $u_{c,max}$, use a minimum rubber thickness and make sure the indentation of rubber is smaller than the rubber thickness. Otherwise, go to Step 3 design the rubber location and thickness, using H2 and H3 to find $u_{r,max}$, check if $u_{r,max}$ is smaller than the rubber thickness the design is complete. If it is no, we have three options to redesign the system until they satisfy the requirements.

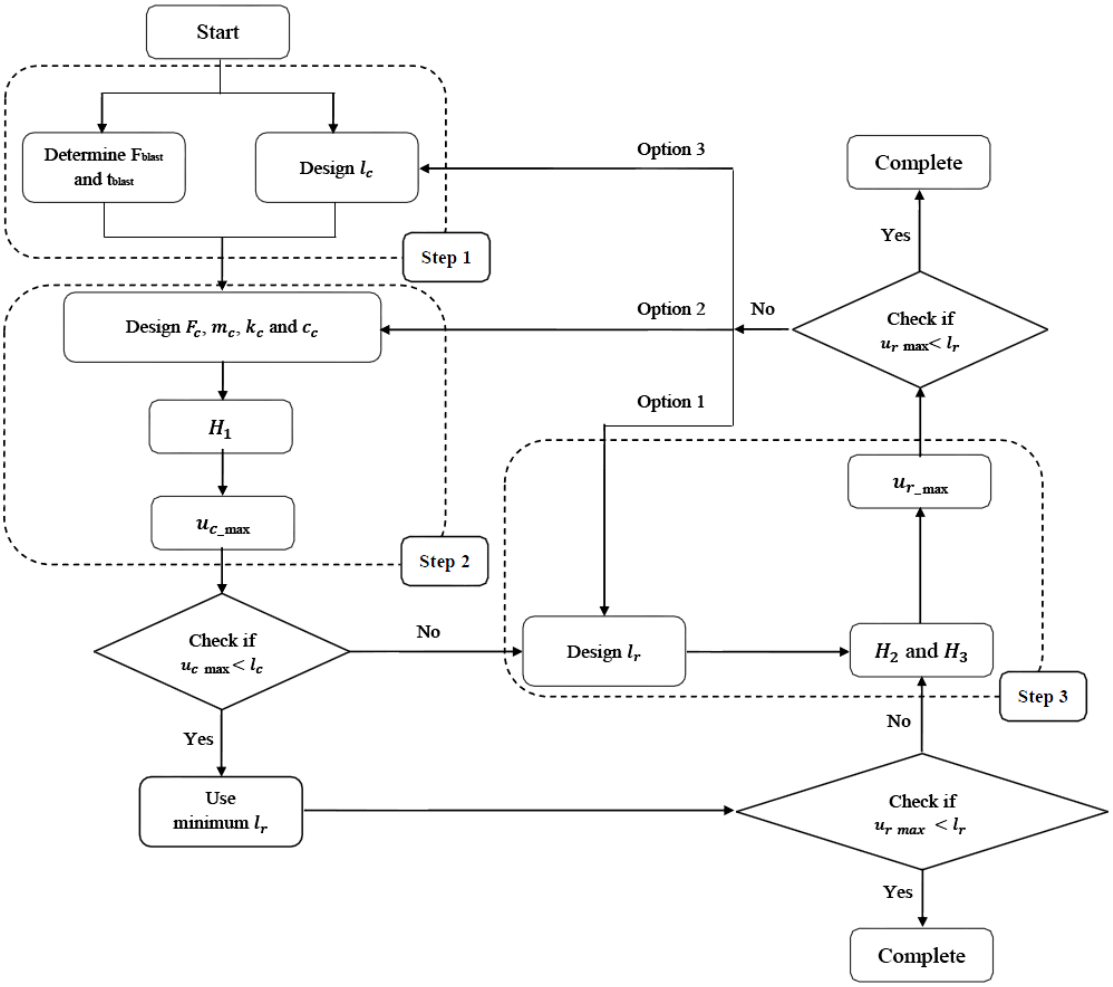

Figure 4.1 Design procedure

4.1 Step 1 Performance Criteria

The first step is to establish parameters that will define the performance requirement of the cladding system. They include design blast load, and the clearance of panels from the structural frame.

4.1.1 Blast design considerations

The mass of the explosive charge W can be estimated depending on antiterrorism design criteria (from Table 3.1) or quantities of explosives in various vehicles (from Table 3.2). The

explosive weights used in designing buildings requirements should be based on potential bomb locations. The standoff distance R for conventional constructions should be determined. The minimum standoff distance for inhabited buildings of conventional construction is provided in Table 4.1 [57]. The maximum blast pressure in kPa from equivalent TNT are based on scaled distance Z from Eq. 3. The design blast force F_{blast} can be taken as $A_c\sigma_{max}$, where A_c is the area of entire cladding, and t_{blast} the period of the blast excitation, which can be determined using Eq. (3b).

Table 4.1 Standoff distance for new and existing buildings [57]

Building Category	Distance to	Minimum Standoff Distance
• Billeting and High Occupancy Family Housing • Primary Gathering Building • Inhabited Building	Controlled Perimeter or Parking and Roadways without a Controlled Perimeter	20ft (6m)
	Parking and Roadways with a Controlled Perimeter	13ft (4m)
	Trash Containers	13ft (4m)

Generally, cladding panels are separated from the structure (using connectors), which separation is termed connection space, l_c (see section 2.2.1). There is no required maximum clearance between the cladding and the structural frame. The spacing needs to accommodate the cladding connection system, drainage, air movement, vapor diffusion, and insulation pad [14, 44, 51]. As an example, a cladding system described in [44] that uses tapered connectors requires a minimum spacing tolerance of 15 cm (6 in).

4.2 Step 2 Cladding and Friction parameters

The second step in the design is to select the dynamic parameters of the cladding and the friction capacity of the friction element. Let m_c denote the mass of cladding and k_c, the stiffness of cladding system. For simplicity, the damping of the cladding c_c is assumed to have a negligible effect on the system's performance against blast, and is ignored. The strength of the assumption will be discussed later.

Consider a SDOF representation of the cladding system subjected to a blast load:

$$m_c\ddot{u}_c + c_c\dot{u}_c + k_c u_c + F_c = F_m\left(1 - \frac{t}{t_{blast}}\right) \qquad 0 \le t \le t_{blast} \tag{20a}$$

$$m_c\ddot{u}_c + c_c\dot{u}_c + k_c u_c = -F_c \qquad t \ge t_{blast} \tag{20b}$$

where F_m is the amplitude or maximum value of the blast load, and t_{blast} is the blast duration, with the friction force F_c approximated using the Coulomb model discussed above:

$$F_c = f_c \mathrm{sgn}(\dot{u}_c) \tag{21}$$

Here, because only the first quarter cycle of the response is considered, we take $F_c = -f_c$. Eq. 20(a) and (b) can be used to characterize the dynamics of the cladding system before it collides with the impact rubber. Assuming that the first quarter cycle response time $T/4 \gg t_{blast}$, Eq. 20(a) is solved to find the initial conditions $u_c(t_{blast})$ and $\dot{u}_c(t_{blast})$ by solving Eq. 20(b).

The solution of Eq. (20a) can be derived by using Duhamel's integral as follows:

$$u_c(t) = \frac{1}{m\omega_d}\int_0^\tau \{[F_m\left(1 - \frac{\tau}{t_{blast}}\right) + f_c] * e^{-\xi\omega_n(t-\tau)}\sin[\omega_d(t-\tau)]\}\ d\tau \tag{22}$$

The final solution after integration by parts is expressed as follow:

$$u_c(t) = e^{-\xi\omega_n t}\left[\left(u_0 + \frac{f_c sgn(\dot{u}_c)}{k_c}\right)\cos\omega_d t + \frac{\dot{u}_0 + \left(u_0 + \frac{f_c sgn(\dot{u}_c)}{k_c}\right)\xi\omega_n}{\omega_d}\sin\omega_d t\right] - \frac{f_c sgn(\dot{u}_c)}{k_c}$$

$$+\frac{F_m}{k_c}\left[1-e^{-\xi\omega_n t}\left(\frac{\xi}{\sqrt{1-\xi^2}}\sin\omega_d t+\cos\omega_d t\right)\right]$$
$$-\frac{F_m}{k_c t_{blast}}\left[t-\frac{2\xi}{\omega_n}+\frac{e^{-\xi\omega_n t}}{\omega_n}\left(2\xi\cos\omega_d t+\frac{2\xi^2-1}{\sqrt{1-\xi^2}}\sin\omega_d t\right)\right]$$
$$0\le t\le t_{blast} \quad (23)$$

and velocity is expressed:

$$\dot{u}_c(t)=e^{-\xi\omega_n t}\left[(\dot{u}_0)cos\omega_d t-\left(\frac{(u_0+\frac{f_c sgn(\dot{u}_c)}{k_c})\omega_n+\xi\dot{u}_0}{\sqrt{1-\xi^2}}\right)sin\omega_d t\right]$$
$$+\frac{F_m}{k_c}\left[e^{-\xi\omega_n t}\left(\frac{1}{\sqrt{1-\xi^2}}\omega_n\sin\omega_d t\right)\right]$$
$$-\frac{F_m}{k_c t_{blast}}\left[1-e^{-\xi\omega_n t}\left(\cos\omega_d t+\frac{\xi}{\sqrt{1-\xi^2}}\sin\omega_d t\right)\right]$$
$$0\le t\le t_{blast} \quad (24)$$

When $t=t_{blast}$, and substitute to Eq. 23 and Eq. 24, the results of $u_c(t_{blast})$ and $\dot{u}_c(t_{blast})$ are used as initial condition for Eq. 20(b).

Eq. 20(b) can be solved using the summation of a homogenous solution u_h and a particular solution u_p with

$$u_h(t)=e^{-\xi\omega_n t}(Acos\omega_d t+Bsin\omega_d t) \quad (25)$$

and

$$u_p(t)=-\frac{f_c sgn(\dot{u}_c)}{k}$$

giving

$$u_c(t)=e^{-\xi\omega_n t}(Acos\omega_d t+Bsin\omega_d t)-\frac{f_c sgn(\dot{u}_c)}{k}$$

for which

$$u_c(t)=e^{-\xi\omega_n t}\left[\left(u_c(t_{blast})+\frac{F_c sgn(\dot{u}_c)}{k_c}\right)\cos\omega_d t\right.$$
$$\left.+\frac{\dot{u}_c(t_{blast})+\left(u_c(t_{blast})+\frac{F_c sgn(\dot{u}_c)}{k_c}\right)\xi\omega_n}{\omega_d}\sin\omega_d t\right]-\frac{f_c sgn(\dot{u}_c)}{k_c}$$
$$t\ge t_{blast} \quad (26)$$

is a solution.

Then, Eq. 26 is used to find the maximum displacement. A critical point, t_1 can be used to calculate maximum displacement in Eq. 26. Derivative Eq. 26, and giving

$$\dot{u}_c(t) = e^{-\xi\omega_n t}\left[(\dot{u}_c(t_{blast}))cos\omega_d t - \left(\frac{(u_c(t_{blast}) + \frac{f_c sgn(\dot{u}_c)}{k_c})\omega_n + \xi\dot{u}_c(t_{blast})}{\sqrt{1-\xi^2}}\right)sin\omega_d t\right] \quad t \geq t_{blast} \tag{27}$$

Set Eq. 27 equal to zero, and the result of t in first cycle can infer to the maximum value of u_c, $u_{c,max}$. The expression of result t and $u_{c,max}$ are shown:

$$t_1 = \frac{actan\left(\frac{\dot{u}_c(t_{blast})\sqrt{1-\xi^2}}{\left(u_c(t_{blast})+\frac{f_c sgn(\dot{u}_c)}{k_c}\right)\omega n + \xi\dot{u}_c(t_{blast})}\right)}{\omega_d} \tag{28}$$

$$u_{c\_max} = u_c(t_1) = e^{-\xi\omega_n t_1} * \frac{-\sqrt{\left(\left(u_c(t_{blast})+\frac{f_c sgn(\dot{u}_c)}{k_c}\right)^2\omega_d^2 + \left(\dot{u}_c(t_{blast}) + \left(u_c(t_{blast})+\frac{f_c sgn(\dot{u}_c)}{k_c}\right)\xi\omega_n\right)^2\right)}}{\omega_d} + \frac{f_c}{k_c} \tag{29}$$

A unitless transfer function H_1 is created to facilitate the design procedure:

$$H_1 = \frac{u_{c\_max}}{F_m/k_c} = \frac{u_{c\_max}}{u_{st}} \tag{30}$$

where $u_{st} = \frac{F_m}{k_c}$ is the static displacement from a constant load equal to F_m. Figure 4.2 are plots of H_1 as a function of the ratio t_{blast}/T_n for different friction capacity ratio f_c/F_m and structural damping ratio ξ.

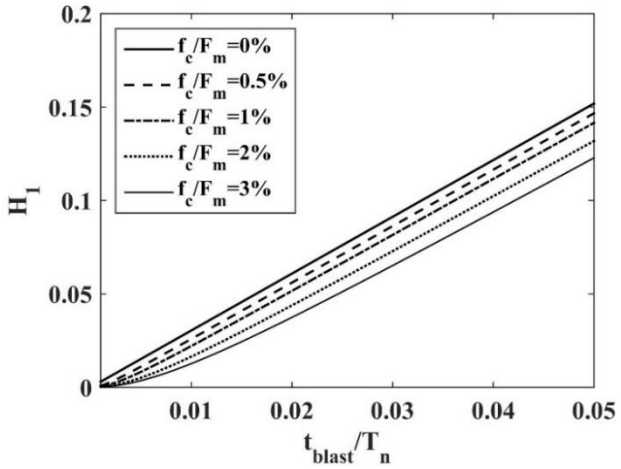

(a)

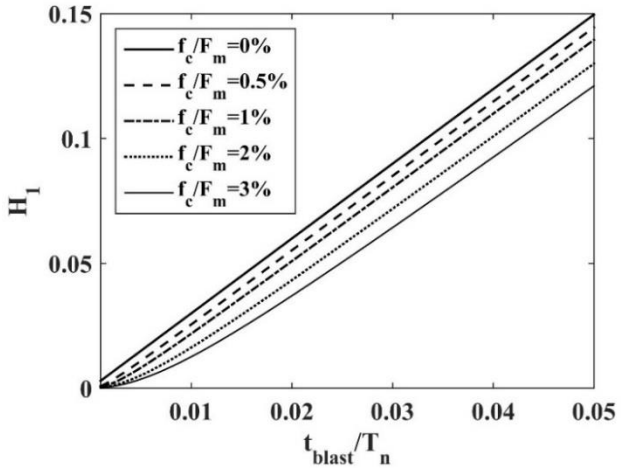

(b)

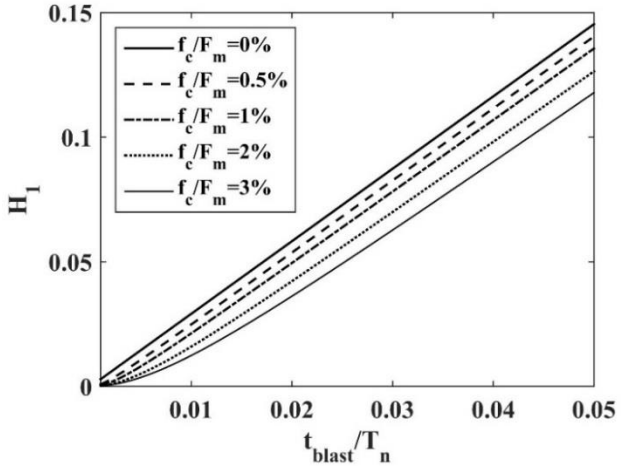

(c)

Figure 4.2 H_1 function: (a) $\xi = 0.02$, (b) $\xi = 0.03$, (c) $\xi = 0.05$, (d) $\xi = 0.1$

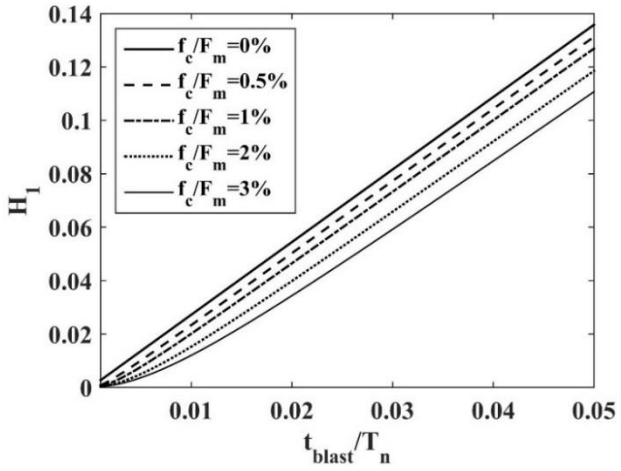

(d)

Figure 4.2 (continued)

The maximum displacement of cladding u_{c_max} can be calculated by Eq. 30. If u_{c_max} <l_c, a minimum thickness of rubber will be sufficient. Otherwise, Step 3 is required. After that, if u_{c_max} <$l_c - l_r$, the design can be completed.

4.3 Step 3 Impact rubber parameters

If $u_{c\_max} > (l_c - l_r)$ or u_{c_max} >l_c, the cladding will collide with the impact rubber. This length determine the location of rubber bumper and following impulse on the structure connected to the rubber, $I_{structure}$. The location of rubber, $(l_c - l_r)$ is determine as a fraction of the static deformation F_m/k_c, therefore a ratio $\rho_{space} = \frac{l_c - l_r}{F_m/k_c}$, is used as varying rubber location. In this case, the initial conditions will be transferred to the structural system, and one could design the connection to minimize the impulse transfer to the structure. A second transfer function H_2 is taken as:

$$H_2 = \frac{I_{structure}}{I_{blast}} = \frac{m_c \dot{u}_c(t_{rubber})}{\frac{1}{2} F_{blast} t_{blast}} \tag{31}$$

where $\dot{u}_c(t_{rubber})$ is the solution of the time derivative of Eq. 27

When ρ_{space} is selected, $l_c - l_r$ can be determined as $\rho_{space} * F_m/k_c$, the time t_{rubber} can be figure out from Eq.27. So that the impulse velocity at a selected rubber position can be:

$$\dot{u}_c(t_{rubber}) = e^{-\xi\omega_n t_{rubber}} \left[(\dot{u}_c(t_{blast}))cos\omega_d t_{rubber} - \left(\frac{\left(u_c(t_{blast}) - \frac{f_c}{k_c}\right)\omega_n + \xi\dot{u}_c(t_{blast})}{\sqrt{1-\xi^2}} \right) sin\omega_d t_{rubber} \right] \tag{32}$$

Figure 4.3 are plots of H_2 as a function of the ratio t_{blast}/T_n for different friction capacity ratio f_c/F_m and a different rubber location ratio $\rho_{space} = \frac{l_r - l_r}{u_{st}}$.

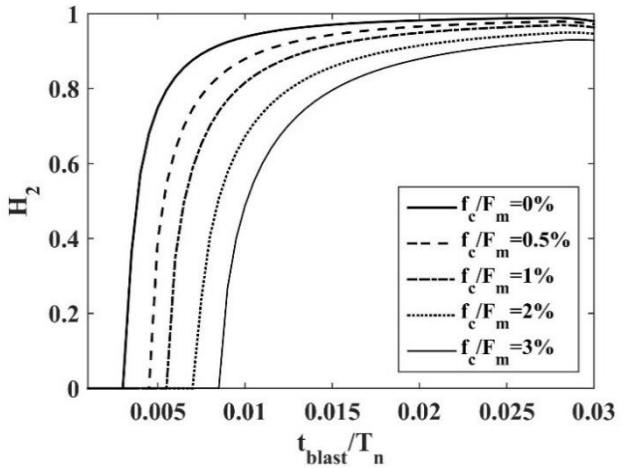

(a)

Figure 4.3 H_2 functions with structural damping $\xi = 2\%$ and $\rho_{space} = \frac{l_c - l_r}{u_{st}}$: (a) $\rho_{space} = 1\%$, (b) $\rho_{space} = 2\%$, (c) $\rho_{space} = 3\%$, (d) $\rho_{space} = 4\%$, (e) $\rho_{space} = 5\%$, (f) $\rho_{space} = 6\%$

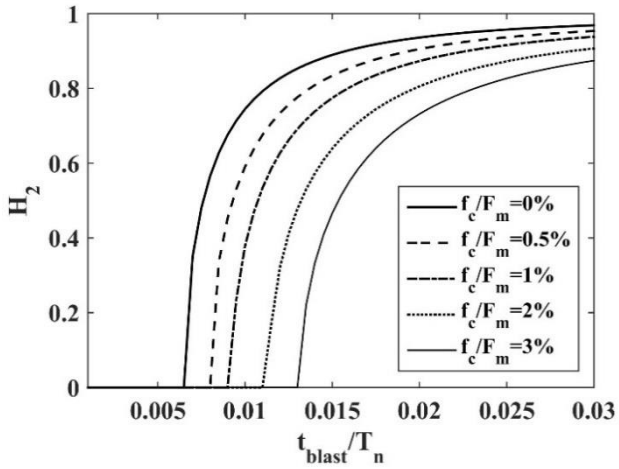

(b)

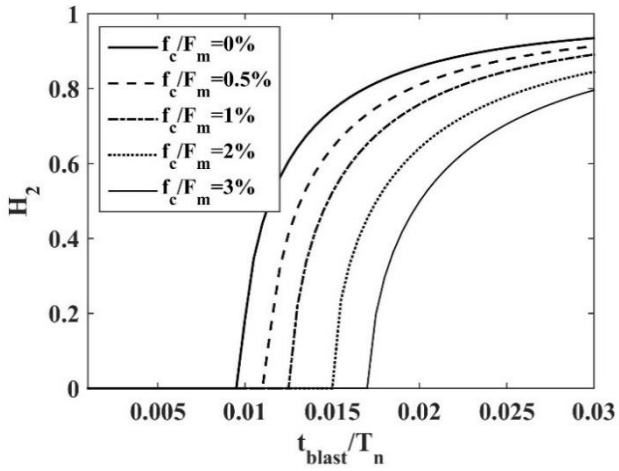

(c)

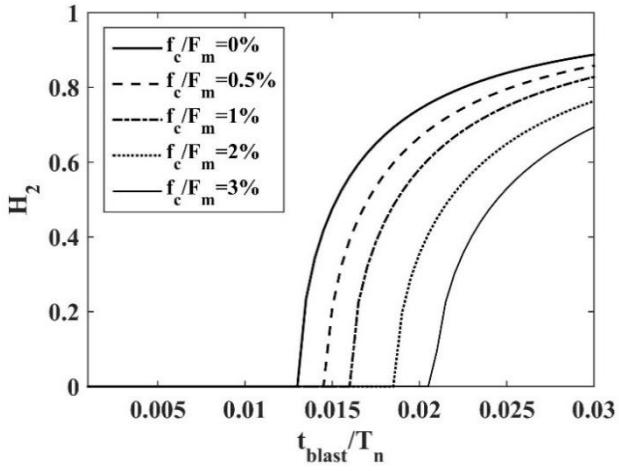

(d)

Figure 4.3 (continued)

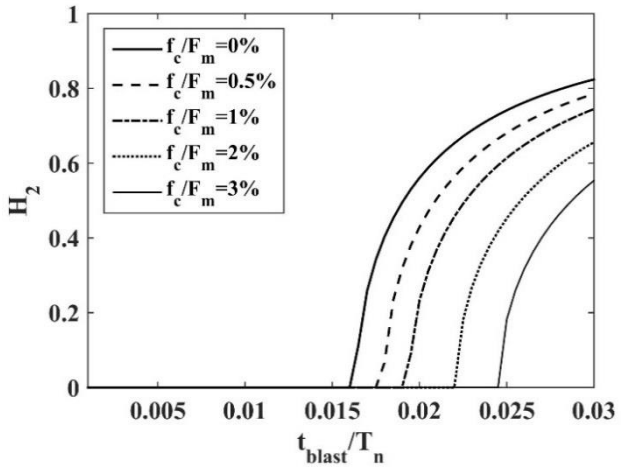

(e)

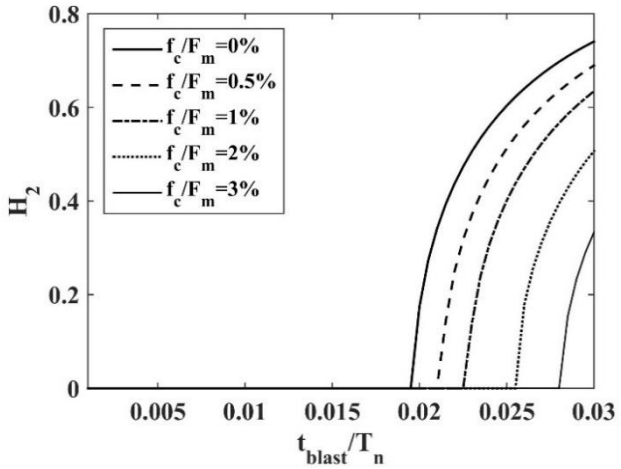

(f)

Figure 4.3 (continued)

The impact rubber is sized to provide a given level of damping. As discussed in section 3.3., the rubber dynamic model should be used in terms of equivalent viscous damping to provide a more convenient mathematical form [1]. The entire dynamics model included impact rubber and friction is expressed:

$$m_c\ddot{u}_c + c_c\dot{u}_c + k_c u_c + F_r = -F_c \tag{33a}$$

where t should be larger than the blast time, since the explosive blast in mostly just remains in milliseconds. In this design procedure, impact rubber is applied to use for the redundant vibration after blast loads.

Since the equivalent damping system, Eq. 10(a) has a same value with Eq. 18, Eq .33(a) can be modified to:

$$m_c\ddot{u}_c + (c_c + c_{eq})\dot{u}_c + k_c u_c = -F_c \tag{33b}$$

In this case, cladding starts from rubber, so cladding deformation is the same as the rubber indentation. A new dynamic equation can be shown:

$$m_c\ddot{u}_r + c_c\dot{u}_r + (k_c + k_{eq})u_r = -F_c \tag{34}$$

where u_r is the rubber indentation, initial value of u_r and $\dot{u}_r$ include: (1) $u_r(0) = 0$, assumes cladding movement starts from the edge of rubber bumper. (2) $\dot{u}_r(0) = \dot{u}_c(t_{rubber})$, assumse the velocity from the edge of rubber bumper is the cladding velocity when cladding impacts the rubber (from Eq. 32). The solution of rubber indentation is similar to Eq. 26 with similar derivation. The only change is damping ratio and damped frequency. ξ_r is the new damping ratio, and the ω_{new} is the new damped frequency, expression are shown:

$$\omega_{new} = \sqrt{\frac{k_c + k_{eq}}{m_c}} \tag{35}$$

$$\xi_r = \frac{c_c}{2\omega_{new} m_c} \tag{36}$$

and solution of rubber indentation giving

$$u_r(t) = e^{-\xi_r \omega_{new} t}\left[\left(u_r(0) + \frac{f_c + k_c|u_c(t_{rubber})|}{k_c}\mathrm{sgn}(\dot{u}_r)\right)\cos\omega_{dr}t + \frac{\dot{u}_c(t_{rubber}) + \left(u_r(0) + \frac{f_c + k_c|u_c(t_{rubber})|}{k_c}\mathrm{sgn}(\dot{u}_r)\right)\xi_r\omega_n}{\omega_{dr}}\sin\omega_{dr}t\right] - \frac{f_c + k_c|u_c(t_{rubber})|}{k_c}\mathrm{sgn}(\dot{u}_r) \quad (37)$$

velocity of impact rubber giving:

$$\dot{u}_r(t) = e^{-\xi_r\omega_n t}\left[\dot{u}_c(t_{rubber})\cos\omega_{dr}t - \left(\frac{(u_r(0) + \frac{f_c + k_c|u_c(t_{rubber})|}{k_c}\mathrm{sgn}(\dot{u}_r))\omega_n + \xi_r\dot{u}_c(t_{rubber})}{\sqrt{1-\xi_r^2}}\right)\sin\omega_{dr}t\right] \quad (38)$$

where t here is a new time line corresponding to cladding touching the rubber. Similar to Step 2, we set Eq. 38 equal to zero, and the result of t in after first cycle will produce the maximum value of u_r, u_{r_max}. The expressions for t and u_{r_max} are:

$$t_2 = \frac{actan\left(\frac{\dot{u}_c(t_{rubber})\sqrt{1-\xi_r^2}}{\left(u_r(0)+\frac{f_c+k_c|u_c(t_{rubber})|}{k_c}sgn(\dot{u}_r)\right)\omega n + \xi_r\dot{u}_c(t_{rubber})}\right)}{\omega_{dr}} \quad (39)$$

$$u_{r\_max} = u_r(t_2) = -\frac{f_c+k_c|u_c(t_{rubber})|}{k_c}\mathrm{sgn}(\dot{u}_r) + e^{-\xi_r\omega_{new}t_2}\frac{-\sqrt{\left(\left(\frac{f_c+k_c|u_c(t_{rubber})|}{k_c}\mathrm{sgn}(\dot{u}_r)\right)^2\omega_{dr}^2 + \left(\dot{u}_c(t_{rubber}) + \left(u_r(0)+\frac{f_c+k_c|u_c(t_{rubber})|}{k_c}\mathrm{sgn}(\dot{u}_r)\right)\xi_r\omega_{new}\right)^2\right)}}{\omega_{dr}} \quad (40)$$

$$H_3 = \frac{u_{r\_max}}{F_m/k_c} = \frac{u_{r\_max}}{u_{st}} \quad (41)$$

where $u_{st} = \frac{F_m}{k_c}$ is the static deformation. According to the given value from Step 1 and the parameters selected from H_2, H_3 value can be found in Figure 4.5 for a different t_{blast}/T_n condition. If the rubber indentation calculated using Eq. 37 is smaller than the rubber thicknessl_r, the design is successful. Otherwise, we go back to select the rubber thickness in Step 3 or redesign those prime parameters (m_c, k_c, c_c, f_c) in Step 2. Rubber thickness directly affects the impact stiffness of rubber k_r and equivalent damping coefficientc_{eq}. Eq. 11(a) provides that the rubber impact stiffness is varied by the rubber size (bumper contact area and bumper thickness). According to the Table 2.2, the material stiffness K_r can be taken as $3.58\frac{kN}{mm^2}$ ($\beta = 2$) or$2.86 * 10^{-3}\frac{kN}{mm^2}$ ($\beta = 2.5$). This way, the material stiffness with its strain rate-dependent coefficient β can be calculated by substituting the values in Table 2.2 and Eq. 11(a). After the material properties K_r and exponent n are obtained, the impact rubber stiffness k_r of any rubber bumper with similar material and given dimensions can be calculated using Eq. 11(a). Figure 4.4 plots the response from different impact rubber stiffness of variable dimensions.

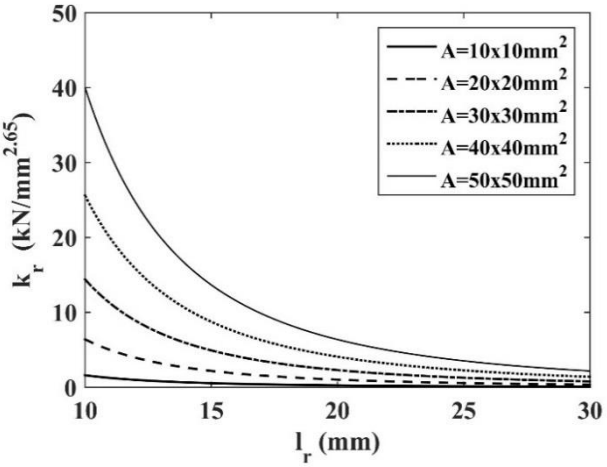

(a)

Figure 4.4 Impact rubber stiffness with different thickness using the same rubber material: (a) $l_r = 10 - 30mm$, (b) $l_r = 30 - 60mm$, (c) $l_r = 60 - 100mm$

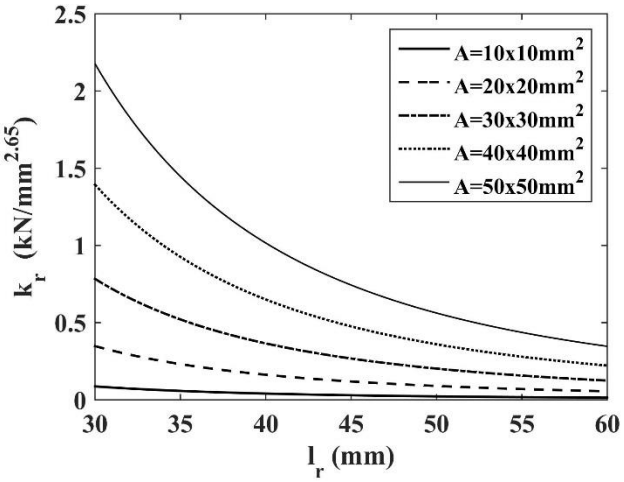

(b)

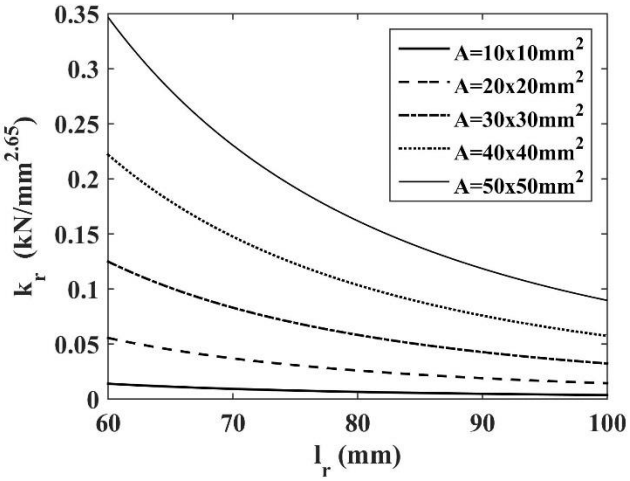

(c)

Figure 4.4 (continued)

The H_3 function is a dimensionless ratio of rubber indentation over static deformation. The rubber impact stiffness k_r can be calculated using the rubber thickness and dimension or taken from Figure 4.4. The friction ratio f_c/F_m can be determined using the H_1 function (see Figure 4.2). The rubber location ratio $(l_c - l_r)/u_{st}$ can be determined by the H_2 function (see Figure 4.3). Figure 4.5 are plots of H_3 functions for $\xi = 2\%$ and $(l_c - l_r)/u_{st} = 1\%$ under variable friction ratios.

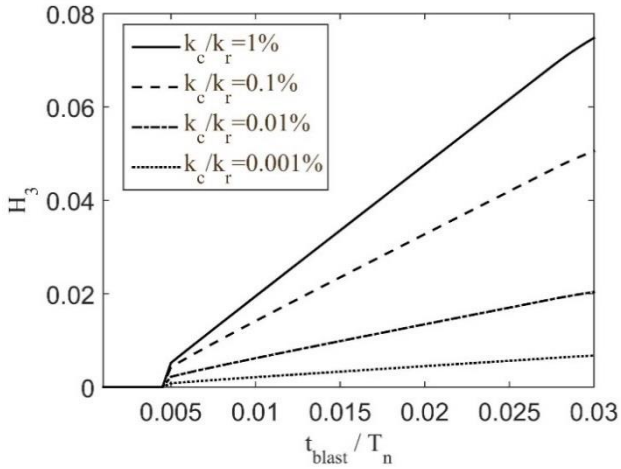

(a)

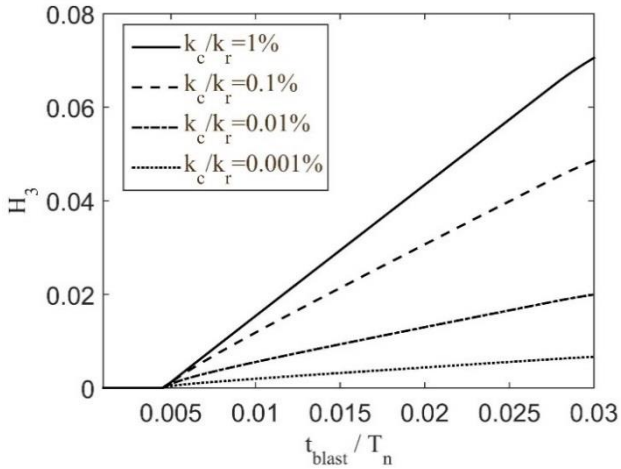

(b)

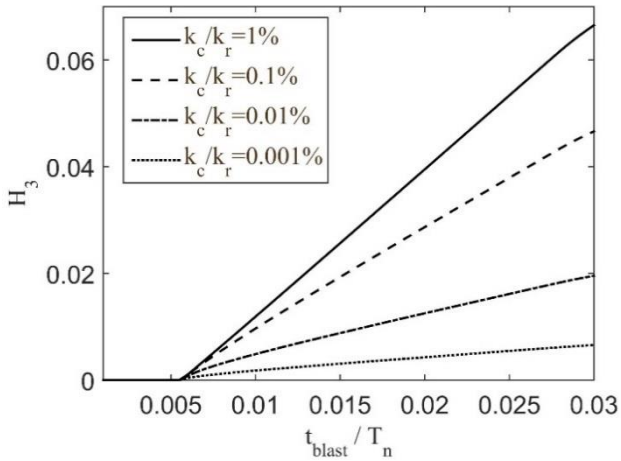

(c)

Figure 4.5 H_3 functions with structural damping $\xi = 2\%$ and assuming $\rho_{space} = 1\%$,: (a) $f_c/F_m = 0\%$, (b) $f_c/F_m = 0.5\%$, (c) $f_c/F_m = 1\%$, (d) $f_c/F_m = 2\%$, (e) $f_c/F_m = 3\%$

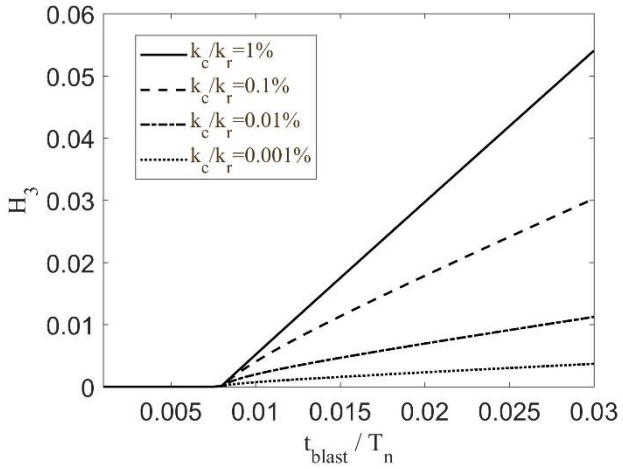

(d)

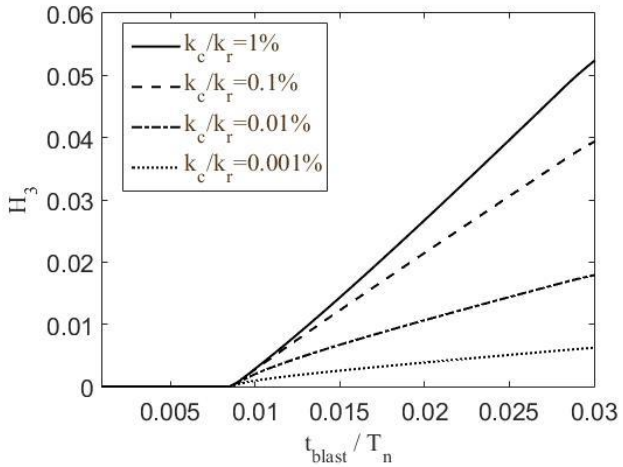

(e)

Figure 4.5 (continued)

CHAPTER 5. NUMERICAL SIMULATIONS ON PROTOTYPE BUILDING

5.1 Brief introduction of the prototype building

5.1.1 Building Design

The proposed PBD design procedure is validated on a prototype building. It is a 4-story symmetric building in both principal directions. The building has 8 bays in the x-direction and 6 bays in the y-direction all spaced at 30 ft. The first floor is 15 ft high and the remaining floors are 13 ft high. Fig 5.1 shows the prototype building plan. This prototype building is designed as a steel frame building. Table 5.1 and Table 5.2 list of the floor gravity loads (ASCE 7-10). The combination loads is calculated by using allowable stress design D+L (ASCE 7-10). In this simulation since only quarter of building is considered, the total weight for each of the first three floor in quarter of building is 4564 kN, and the roof weight is 3122 kN. Table 5.3 provides the steps for calculating the floor mass. A 4 in precast panel is used as cladding. The total weight for each panel is 40 psi. Floor and cladding weights at each level are listed in Table 5.3. The first floor is 15 ft (4.57m) high, and its corresponding cladding mass is 72 kips (320 kN). The rest floors are 13ft (3.96m) high, and their corresponding cladding mass is 62.4 kips 278 kN). A flexibility method is used for finding the stiffness of building, and its damping ratio is taken as 2%.

Figure 5.1 Prototype Building Plan

Table 5.1 Building dead loads (psf)

Type	Weight (typical floor)	Weight (roof)
Floor / Roof Deck	3	3
Floor / Roof Slab	43	0
Roofing Material	0	10
Mechanical Weight	10	10
Ceiling Material	5	5
Floor Finish	2	0
Structural Steel	15	10
Steel Fireproofing	2	2
Building Envelope	0	0
Mechanical Equip. on roof	0	25
TOTAL	**80**	**65**

Table 5.2 Building live load (psf) consideration

Type	Weight (typical floor)	Weight (roof)
Office	50	0
Partitions	15	0
Roof (unreduced)	0	20
TOTAL	**65**	**20**
Live Load Included in Seismic Mass	15	0

Table 5.3 Floor Mass of quarter of building

Level	DL [psf]	LL [psf]	TOTAL [psf]	Area [ft^2]	Floor Weight [kips]	Floor Weight [kN]
1	80	15	95	10800	1026	4564
2	80	15	95	10800	1026	4564
3	80	15	95	10800	1026	4564
Roof	65	0	65	10800	702	3123

Table 5.4 4-story building: contacted cladding weight

Level	Height [ft]	One cladding panel area [ft^2]	One cladding panel weight [kips]	Total cladding panels Weight [kN]
1	15	450	18	80
2	28	390	15.6	69
3	41	390	15.6	69
Roof	54	390	15.6	69

5.1.2 Model assumption

The configuration of this 4-story building with cladding and cladding connection is schematized in Figure 5.2. The circle-cross sign represents the damping device which includes a spring element, a dashpot element, a friction element, and two rubber bumpers. Blast detonates at the ground level and affects 12 degree-of-freedoms (DOFs). There are 4 DOFs at each floor of main structure, and 8 DOFs at the cladding elements. The 12 DOFs representation is illustrated in Figure 5.2, which contains one translational DOF at each floor, and two translational DOFs

per cladding element. Each cladding panel is modeled as a rigid bar of masses m_5 to m_8 (see Table 5.4). m_1 to m_4 represents the mass of each floor (see Table 5.3). The first cladding element spanning between ground level and the first floor has the first semi-active connection directly attached to the ground. For blast load distribution, since the blast load reduces rapidly with the height of the building [25], the blast pressure will decrease by increasing r_h. The distribution of blast load in Figure 5.2 provides eight different load at each cladding node. To simplify the problem, we set adjacent blast loads as equal (e.g., P2=P3, P4=P5, P6=P7). In this study, only the positive phase parameters of blast at the front of the structure will be considered.

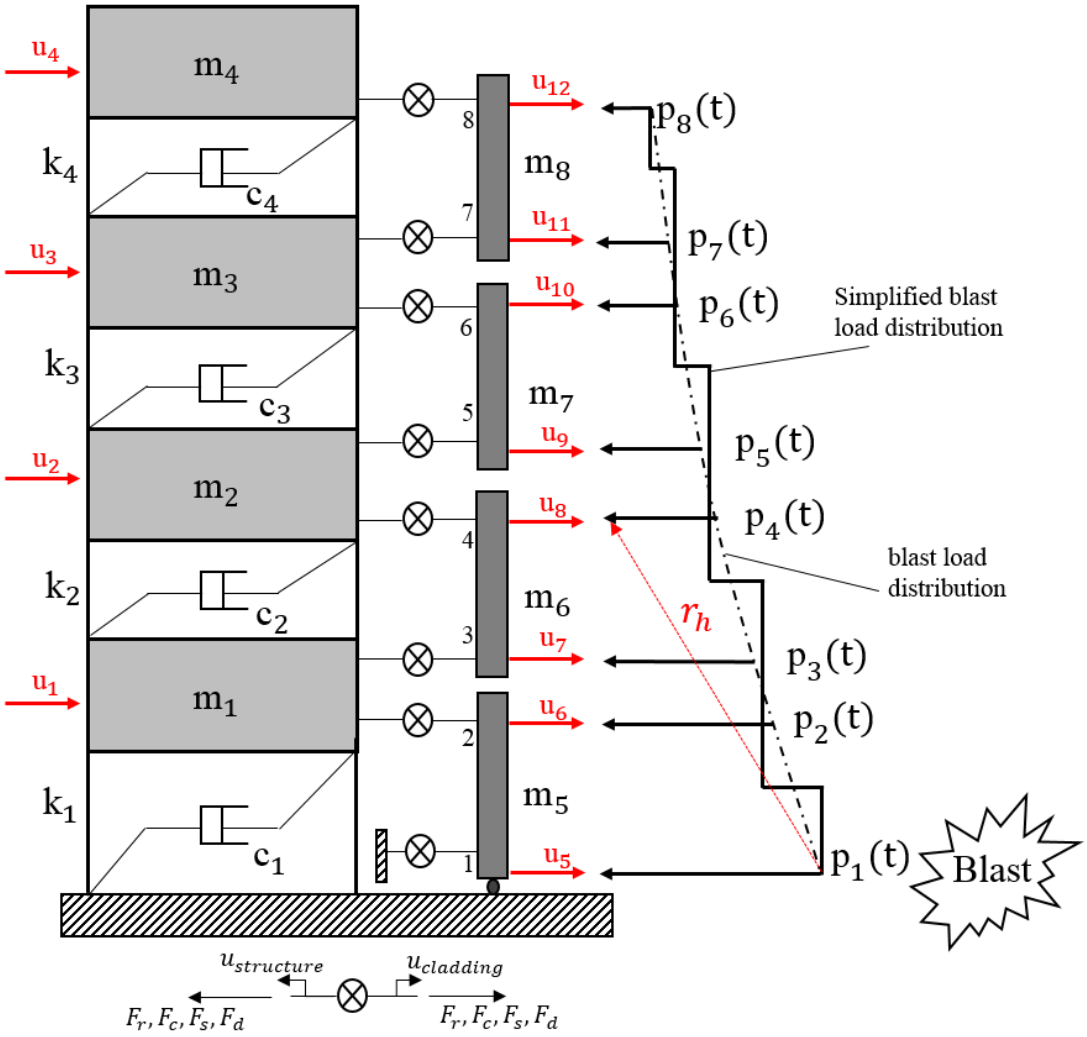

Figure 5.2 Model of prototype building

5.2 Performance based design example

Step 1

A simulated blast load at the ground floor was selected from the Oklahoma bombing event in 1995 when an explosive weight of 1814 kg TNT was detonated at a standoff distance of 4.5 m [23, 25, 46, 47], due to the availability of the time series of the blast load. The model parameter values from this existing blast bombing was scaled in order to provide a blast load below the design capacity of the cladding element (no sudden failure of the cladding system). The standoff distance was changed to 15 m, with a reduced TNT weight 100kg of TNT. The design blast parameters are listed in Table 5.5. The distribution of peak pressure is used for MDOF in each level which is shown in Table 5.6.

Table 5.5 Blast Estimation

Parameter	Value
charge size (kg-TNT)	100
Peak Pressure (kPa)	75.01
R (standoff) (m)	15
t_blast (ms)	11.33

Table 5.6 Explosive pressure in each floor

Floor number	Height (m)	R_h (m)	t_{blast} (s)	Peak Pressure (kPa)
0	0	15	0.0113	75.01
1	4.57	15.68	0.0115	67.94
2	8.53	17.26	0.0118	55.29
3	12.50	19.53	0.0122	43.04
5	16.46	22.27	0.0126	33.60

Step 2

In Step 2, the cladding masses, stiffnesses, damping ratios, and friction are determined using Figure 4.2. The cladding mass is designed from a 4 in thickness and cladding load is 40 psf. Using t_{blast} and F_m from Step 1, the natural period and friction can be obtain from H_1.

Dimensionless ratio in H_1 design

- Cladding damping ratio ξ: 2%
- Blast duration ratio t_{blast}/T_n: 2%
- Friction capacity ratio f_c/F_m: 1%
- H_1: 0.055

Step 3

In Step 3, a rubber bumper is added using Figure 4.4.

Dimensionless ratio in H_2 and H_3 design:

- Rubber location ratio $(l_c - l_r)/u_{st}$: 5%
- Impact rubber dynamic ratio k_c/k_r: 0.001%
- H_2: 0.9
- H_3: 0.004

5.3 Validation of the SDOF approximation

For validating the PBD procedure, which is based on an SDOF approximation, the performance of the designed cladding connection is numerically simulated using the state space method [1]. The expression of second-order equation of motion is

$$M\ddot{u} + C\dot{u} + Ku = F_{blast} - F_c - F_r$$

where F_c is the friction force, and F_r is the rubber resistant force, $M, C, and\ K$ are the mass, damping and stiffness matrices, respectively.

In order to solve the problem conveniently, the formula should be reduce an order, the new form is expressed:

$$\ddot{u} + \frac{C}{M}\dot{u} + \frac{K}{M}u = 0$$

$$\frac{du}{dt} = \dot{u}$$

$$\frac{d\dot{u}}{dt} = -\frac{C}{M}\dot{u} - \frac{K}{M}u + \frac{1}{M}F_{blast} - \frac{1}{M}F_c - \frac{1}{M}F_r$$

using the notation X as the state vector to express the equation.

$$X = \begin{bmatrix} u \\ \dot{u} \end{bmatrix}$$

$$\frac{dX}{dt} = \dot{X} = AX + B_f F_c + B_f F_{rubber} + B_p F_{blast}$$

where

$$A = \begin{bmatrix} 0 & 1 \\ -\frac{K}{M} & -\frac{C}{M} \end{bmatrix}$$

$$\dot{X} = AX$$

The general solution of state space is expressed as [1]:

$$X_{i+1} = e^{A*dt} X_i + A^{-1}(e^{A*dt} - I) * (B_f F_{c_i} + B_f F_{rubber_i} + B_p F_{blast_i}) \quad (46)$$

Validation on a 2DOF system

Before validating the PBD procedure on the prototype building, we first validate on a 2DOF representation where the cladding is attached to the structure (Fig. 3.1(b)). The validity if the assumption is investigated through the comparison of transfer function obtained from the PBD procedure and from numerical simulations. In what follows, the PBD transfer functions H_i $(i = 1, 2, 3)$ are compared against the transfer functions of 2DOF H_i^* obtained numerically. Relative error gives an indication of how good a results is relative to the 2DOF results by using a performance metric $\widetilde{H}_i$:

$$\widetilde{H}_i = \left| \frac{H_i - H_i^*}{H_i^*} \right| \quad \text{for i=1,2,3} \quad (47)$$

Figure 5.3 (a) shows transform function H_1 and H_1^* conducted by analytical solution and numerical method with a blast duration ratio t_{blast}/T_n for different friction capacity ratios f_c/F_m over the range 0.001 to 0.03. The percent error is performance metric $\widetilde{H}_i \times 100\%$ which is plotted in Figure 5.3(b). The error in H_1 is larger for small ratio t_{blast}/T_n, and converges to zero with increasing t_{blast}/T_n. The magnitude of the error increases when friction ratio increases.

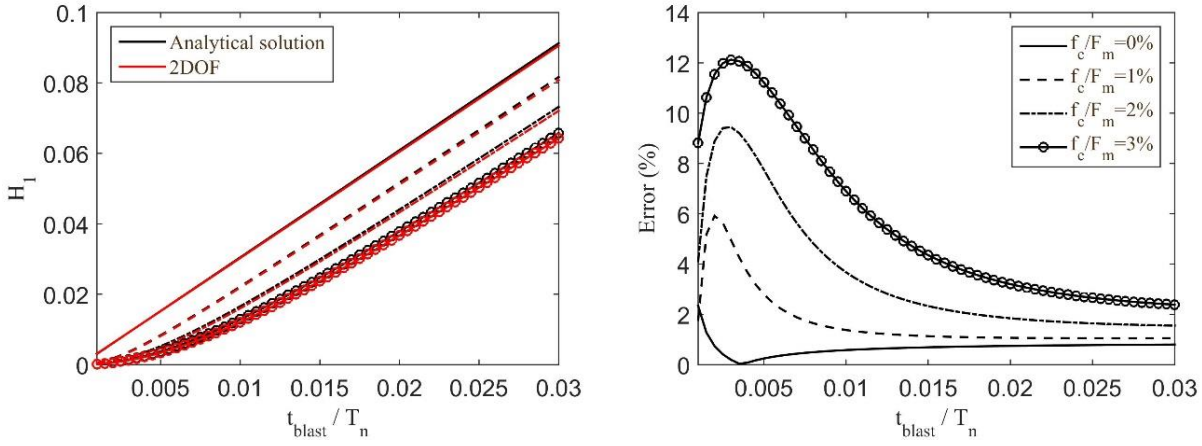

Figure 5.3 H_1 function with structural damping $\xi = 2\%$ (a) H_1 and H_1^*, (b) $\widetilde{H}_1$

In H_1function, the percent error is around 0 to 12.5%There error increases when the friction capacity ratio increases and decreases with increasing blast duration ratio. In the no friction case, the error is less than 2%, but negative, which signifies that a more careful attention is required during the design process due to a possibly under-designed connection.

Transfer function H_2 is validated through the investigation of its fitting performance index $\widetilde{H}_2$ over different values of relative rubber thickness $(l_c - l_r)/u_{st}$. Plots are shown in Figures 5.4-6 for ratio range 1% to 5%, which is a large range of spacing $l_c - l_r$ as u_{st} is relatively large under blast load. A null value H_2 signifies that the cladding does not collide with the structure. The error $\widetilde{H}_2$ is high when H_2 is close to zero, and increase when relative rubber thickness increases. Also, the error converges to zero with increasing blast duration ratio.

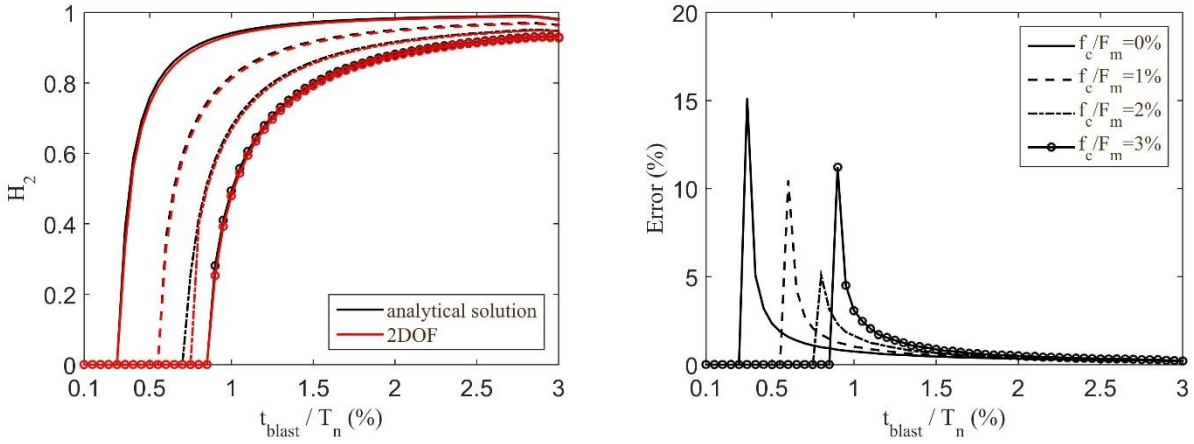

(a) (b)

Figure 5.4 H2 function with structural damping $\xi = 2\%$ and $(l_c - l_r)/u_{st} = 1\%$, (a) H_2 and H_2^*, (b) $\widetilde{H}_2$

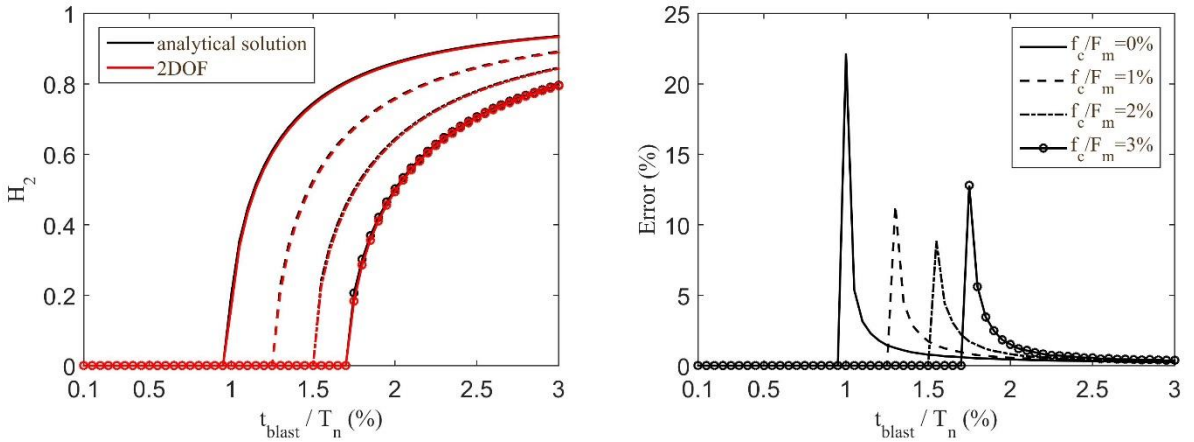

(a) (b)

Figure 5.5 H2 function with structural damping $\xi = 2\%$ and $(l_c - l_r)/u_{st} = 3\%$, (a) H_2 and H_2^*, (b) $\widetilde{H}_2$

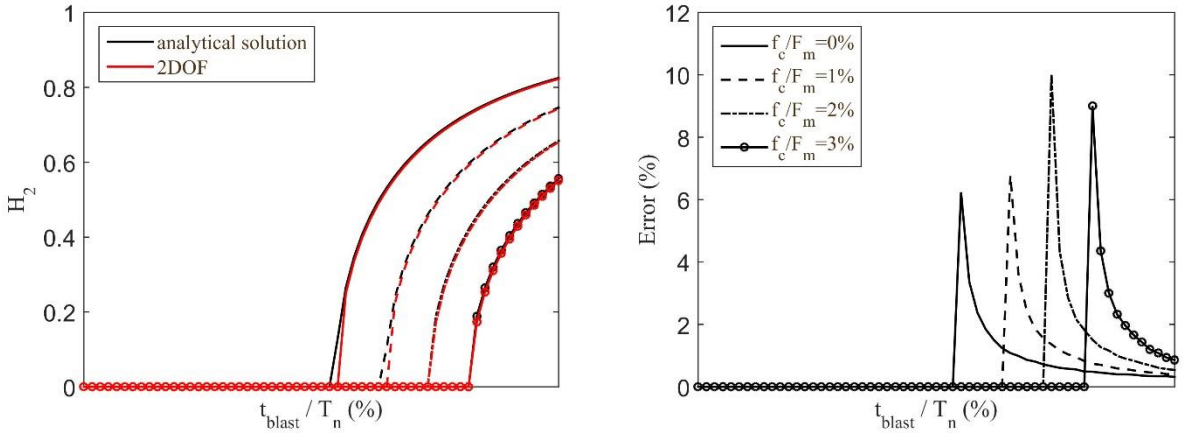

(a) (b)

Figure 5.6 H2 function with structural damping $\xi = 2\%$ and $(l_c - l_r)/u_{st} = 5\%$ (a) H_2 and H_2^*, (b) $\widetilde{H}_2$

The maximum percent error in H_2function peaks at the highest impact and rapidly decreases with increasing blast duration ratio. The zero part can be ignored since there is no pounding between cladding and the structure. Similar to the H_1 function case, a positive error signifies an over-design of the connection, thus an additional factor of safety.

The H_3 function is plotted under different friction capacity ratios f_c/F_m, relative rubber thickness ratios $(l_c - l_r)/u_{st}$ and impact rubber stiffness ratios k_c/k_r in Figures 7 to 9. The error $\widetilde{H}_3$ is high when rubber has smaller deformation when H_3 close to zero. As t_{blast}/T_n increases, the error $\widetilde{H}_3$ drops down rapidly.

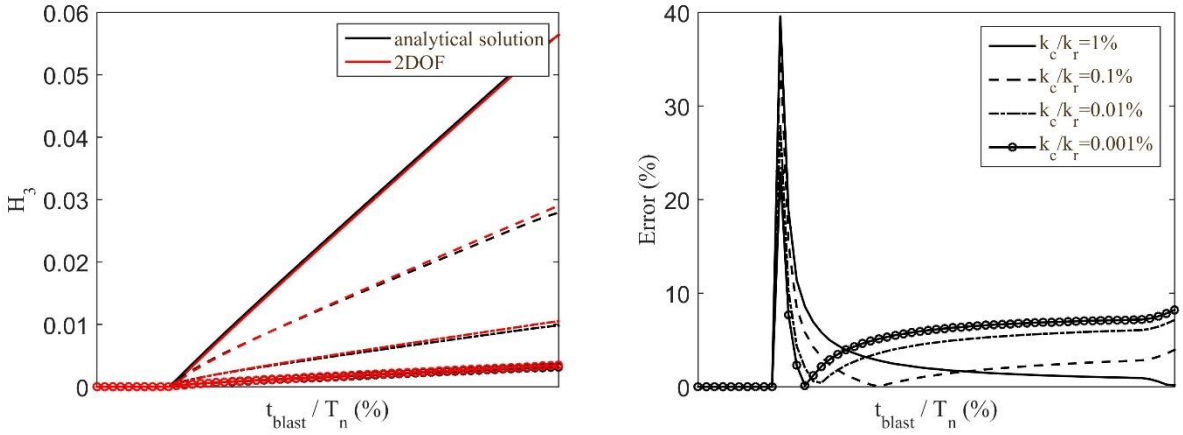

Figure 5.7 H_3 function with structural damping $\xi = 2\%$ $f_c/F_m = 1\%$ and $(l_c - l_r)/u_{st} = 1\%$ (a) H_3 and H_3^*, (b) $\widetilde{H}_3$

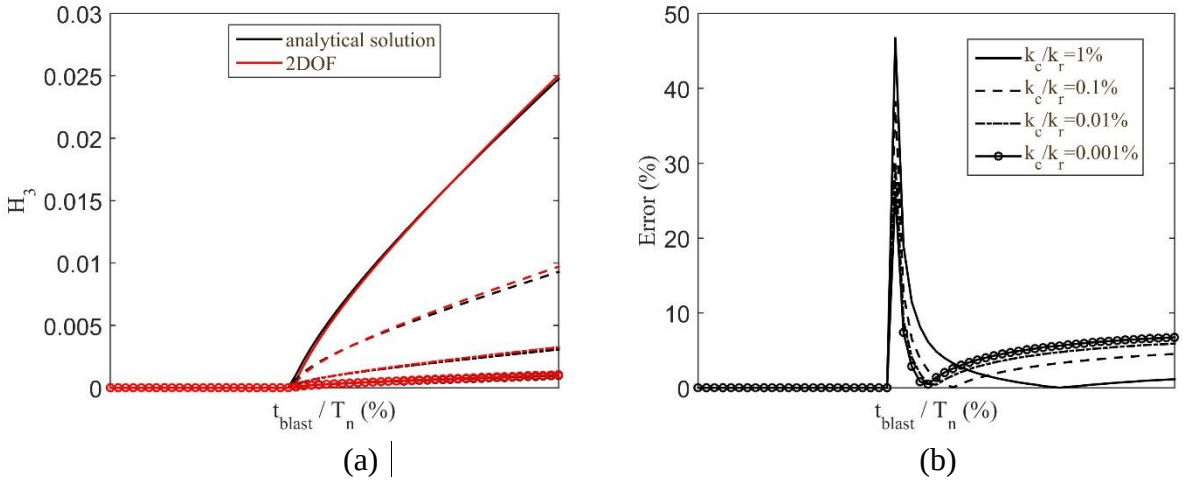

Figure 5.8 H_3 function with structural damping $\xi = 2\%$ $f_c/F_m = 1\%$ and $(l_c - l_r)/u_{st} = 3\%$ (a) H_3 and H_3^*, (b) $\widetilde{H}_3$

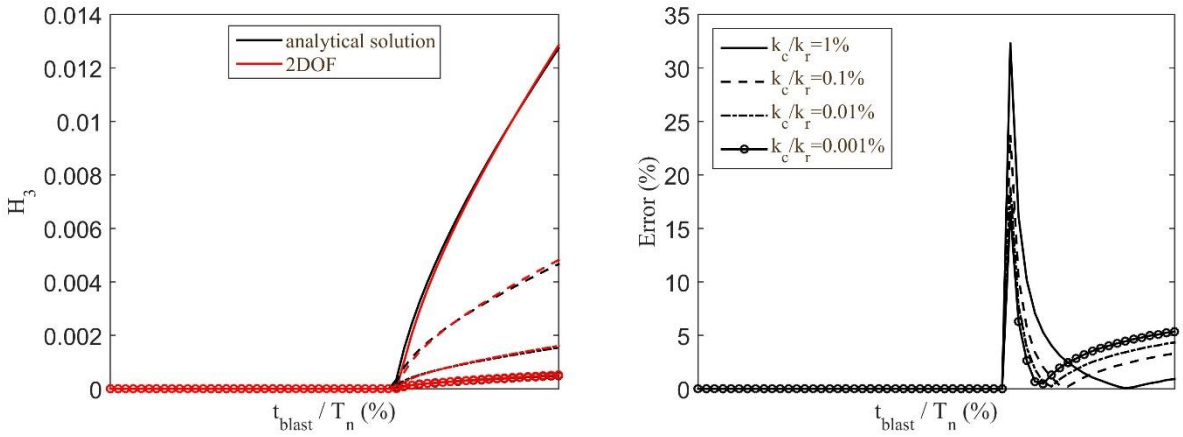

Figure 5.9 H_3 function with structural damping $\xi = 2\%$ $f_c/F_m = 1\%$ and $(l_c - l_r)/u_{st} = 5\%$ (a) H_3 and H_3^*, (b) $\widetilde{H}_3$

The error in H_3function is also highest for the highest impact load and decreases with increasing blast duration ratio, and increase again after it reaches a critical point. The error is always positive, thus leading to an over-design of the connection. Results shown above confirms the applicability of the SDOF approach for designing of the cladding connection, with some limitations where the estimation error on the H functions is high, yet positive. These limitations, which are attributed to unmodeled high nonlinearities, will be reviewed in the next chapter.

5.4 Validation on prototype building

For simplicity, the connection parameters are taken as equal for each floor (which also provides a more realistic design). Table 5.7 shows the blast load deign parameters. where Z and blast period are calculated by Eq. 3 (a) and (c), Table 5.8 shows the cladding connection design for nodes 5 to 12. The mass of each cladding panel m_c is taken as fixed. The assumption of a cladding damping ratio $\xi = 2\%$, a blast duration ratio $t_{blast}/F_m = 2\%$ with a friction capacity ratio $f_c/F_m = 1\%$ yields $H_1 = 0.055$. This H_1 value is used to compute $u_{c,max}$ at each node using Eq. (34). The k_c and c_c can be obtained by $t_{blast}/F_m = 2\%$ and cladding mass m_c. With

these design parameters, all of the nodes remain under the allowable deformation (which is a design assumption) 0.2 m.

.

Table 5.7 Blast load design parameters from Step 1

Determined				
node	**R (m)**	**Z(m/kg)**	**F_m (kN)**	**t_{blast} (ms)**
u_5	15	3.2	6268	11.3
u_6	15.7	3.4	5680	11.5
u_7	15.7	3.4	4924	11.5
u_8	17.2	3.7	4004	11.8
u_9	17.2	3.7	4004	11.8
u_{10}	19.5	4.2	3120	12.1
u_{11}	19.5	4.2	3120	12.1
u_{12}	22.2	4.8	2436	12.6

Table 5.8 Cladding connection design parameters from Step 2

Designed							
node	**m_c (kg)**	**T_n (s)**	**k_c (kN/m)**	**c_c (kN s/m)**	**f_c (kN)**	**$\|u_{st}\|$(m)**	**$\|u_{c,max}\|$ (m)**
u_5	16330	0.57	2019	12	63	3.10	0.16
u_6	16330	0.58	1950	12	57	2.91	0.15
u_7	14152	0.58	1690	10	49	2.91	0.15
u_8	14152	0.59	1605	10	40	2.49	0.13
u_9	14152	0.59	1605	10	40	2.49	0.13
u_{10}	14152	0.61	1526	10	31	2.04	0.11
u_{11}	14152	0.61	1526	10	31	2.04	0.11
u_{12}	14152	0.63	1408	10	24	1.73	0.09

The assumed cladding-structure spacing $l_c = 0.15$ m and the rubber thickness l_r are taken as constant throughout the height of the structure. The design of l_r is conducted based on the blast load on the first floor, which represents the worst case scenario. An initial rubber thickness is selected using $(l_c - l_r)/u_{st} = 1\%$, yielding $l_r = 0.14$ m. Assuming an ultimate compressive capacity of 0.8 [35], the ultimate displacement of rubber bumper is taken as, $u_{r,ult} = 0.8\, l_r = 0.008$ m. The value $H_2 = 0.9$ is obtained from Figure 4.3 (a) using the design parameters from Step 2 ($t_{blast}/F_m = 2\%,\ f_c/F_m = 1\%$), which results in $u_{c,max} = 0.161$ m .

This value is larger than the cladding –structure spacing l_c, the cladding will collide with the structure, requiring design Step 3 to be conducted. Therefore, H_3 needs to be less than $u_{r,ult}/u_{st} = 0.047$. Using Figure 4.5(c), a value of $k_c/k_r = 0.001\%$, $H_3 = 0.004$ can satisfy the requirement. The maximum rubber deflection is $u_{r,max} =$ 0.012 m. since the maximum deformation of rubber is less than the design rubber thickness l_r, the design can be complete. Table 5.9 expresses the design parameter for each node design.

Table 5.9 Rubber connection design parameters from Step 3

Designed		
node	k_r **(N/m$^{2.65}$)**	$\lvert u_{r,max} \rvert$**(m)**
u_5	2.02E+11	0.012
u_6	1.95E+11	0.011
u_7	1.69E+11	0.011
u_8	1.6E+11	0.010
u_9	1.6E+11	0.010
u_{10}	1.53E+11	0.008
u_{11}	1.53E+11	0.008
u_{12}	1.41E+11	0.007

Simulation results

The results from the simulated structure is compared with the design results from the proposed PBD procedure. First, a comparison of the time series inter-story displacements at the each floor are plotted in Figure 5.10 to demonstrated the mitigation capabilities of the cladding system. Results in red show the inter-story displacement using the proposed cladding connection, termed “controlled”. Results in dashed-black show the inter-story displacement using a stiff connection, termed “uncontrolled”. The time series response of the relative cladding deformation at each node is plotted in Figure 5.11, and the impact rubber indentation in its peak deformation are shown as lollipop plots in Figure 5.12.

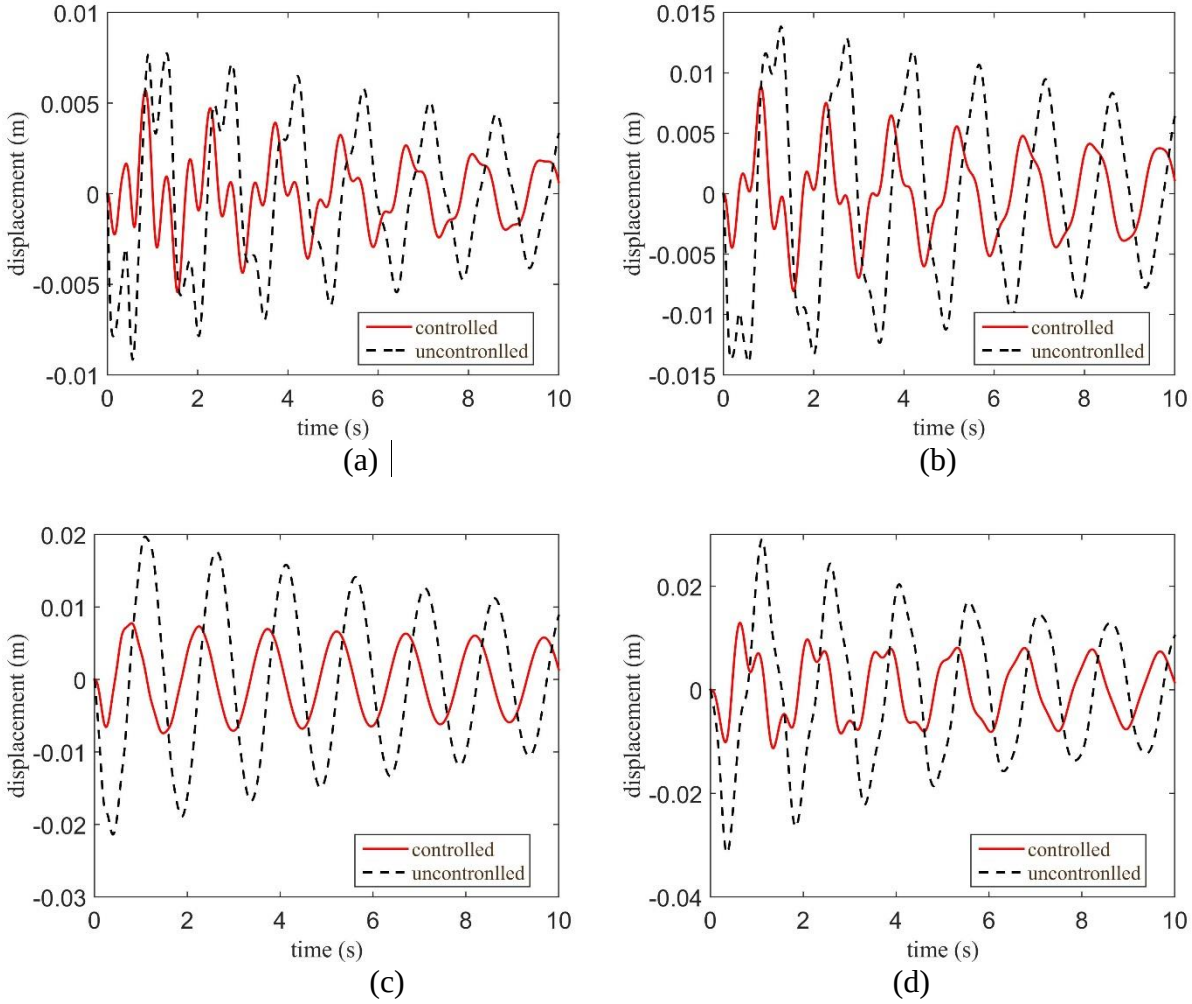

Figure 5.10 Comparison of displacement response at (a) first floor (b) second floor (c) third floor (d) fourth floor

The comparison of structure under multi-functional cladding connections and conventional cladding connections in Figure 5.10 demonstrate the significant mitigation capabilities of the proposed connection. The displacement can be reduced by approximately 67% at all floors.

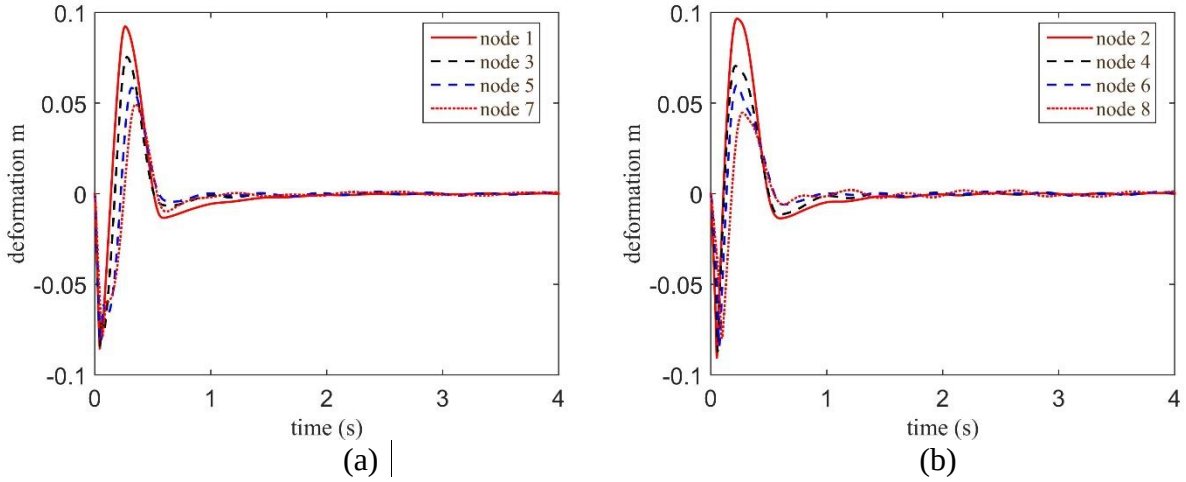

Figure 5.11 Relative cladding displacement in controlled building at (a) node 1, 3, 5, and 7, (b) at node 2, 4, 6, and 8

In the Figure 5.11, the cladding displacement is in the range ± 0.1 m, which is less than the determined cladding-structure spacing 0.15m, the cladding response converges to zero after the first cycle in the each connection node.

Figure 5.12 shows the impact rubber indentation. Results from nodes 1 and 2 demonstrate that the peak value of indentation always occurs in the first cycle under blast excitation, and it is the worst case scenario. The maximum indentation of rubber is 0.02325 m, and the designed rubber thickness is 0.14m. The indentation is very much smaller than the rubber thickness, confirming the design procedure.

The displacement of structure at each floor and the displacement of cladding at each floor are separately plotted in Figure 5.13. Results show that the cladding and structure converge to zero after multiple vibrations, and that there is no pounding between the cladding and the structure.

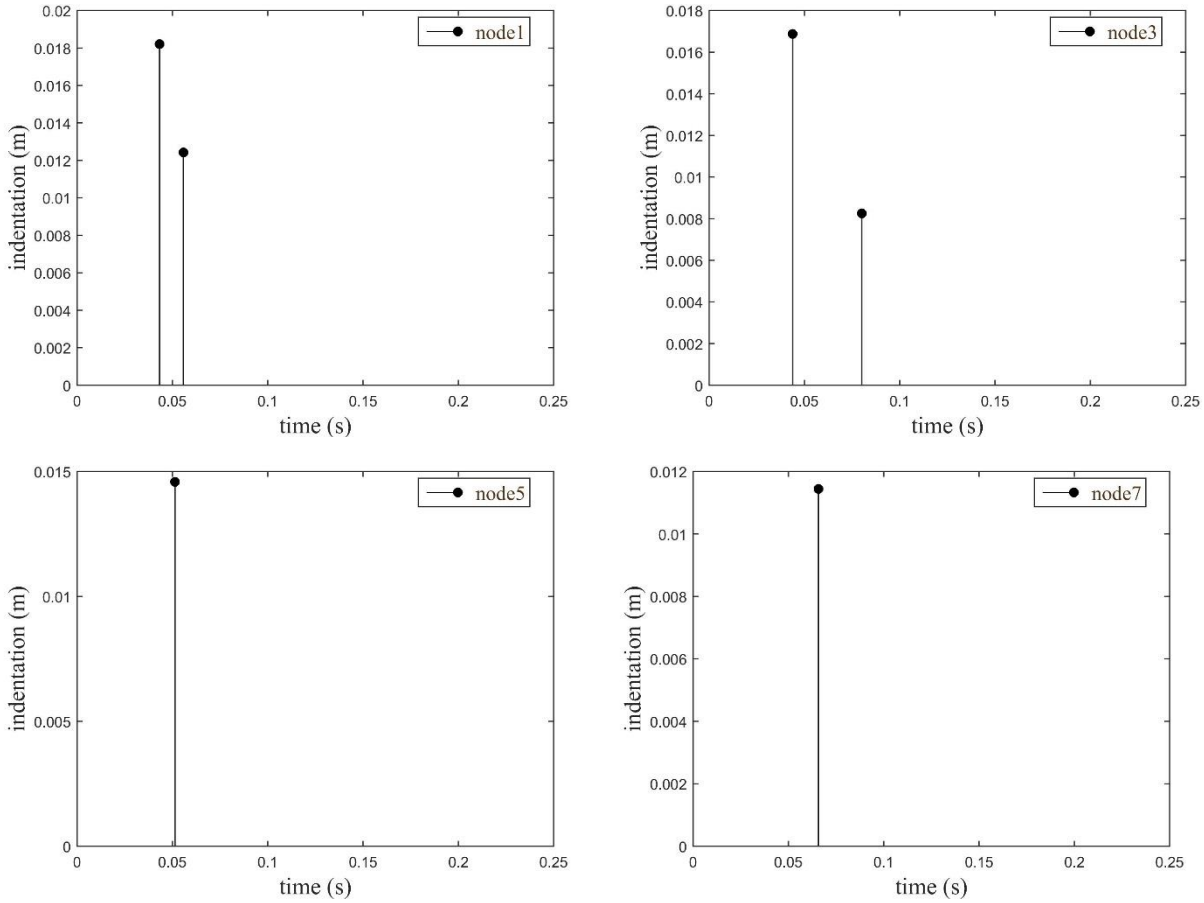

(a)

Figure 5.12 Impact rubber indentation at (a) odd node numbers, (b) even node numbers

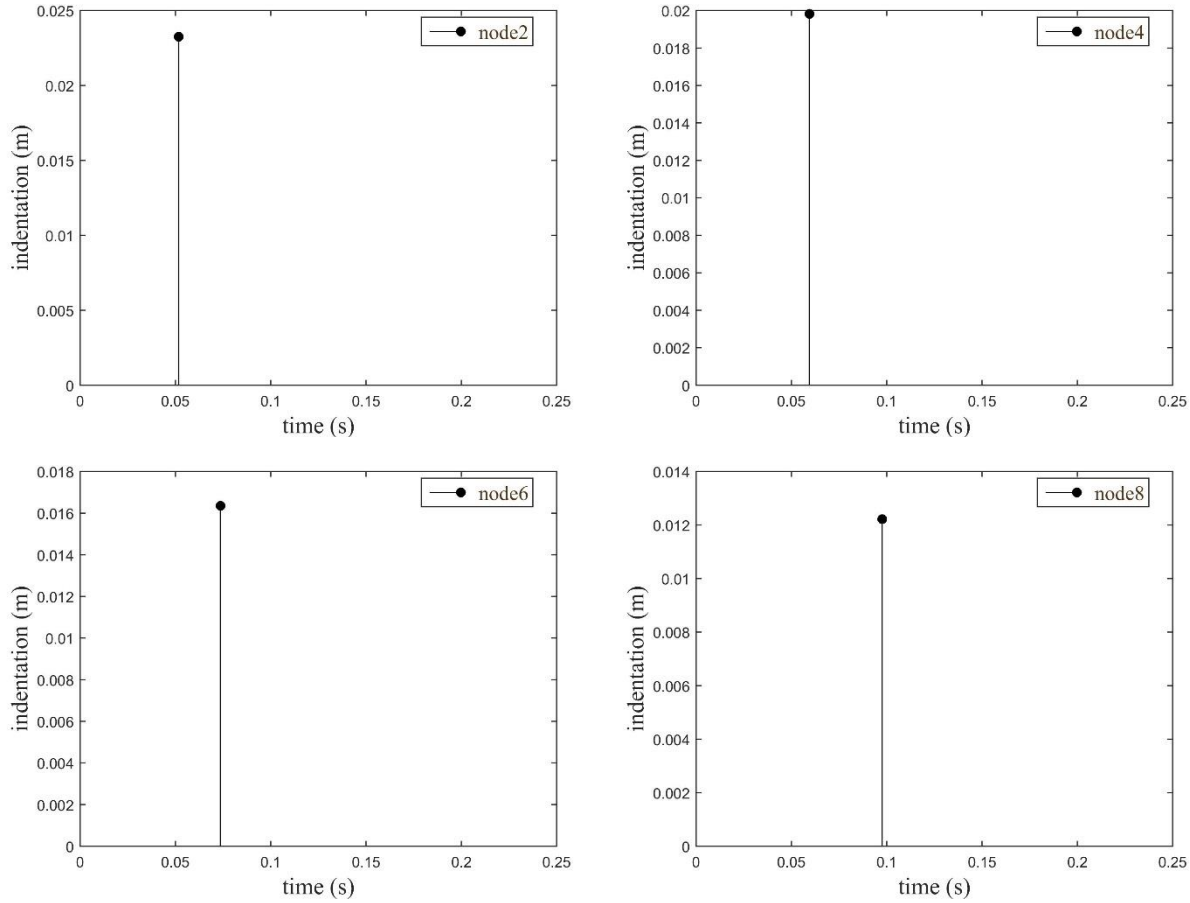

(b)

Figure 5.12 (continued)

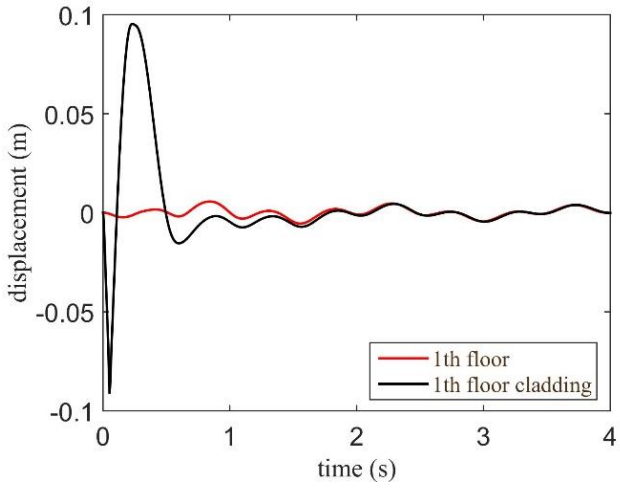

(a)

Figure 5.13 Relative response between cladding and main structure at (a) first floor (b) second floor (c) third floor (d) fourth floor

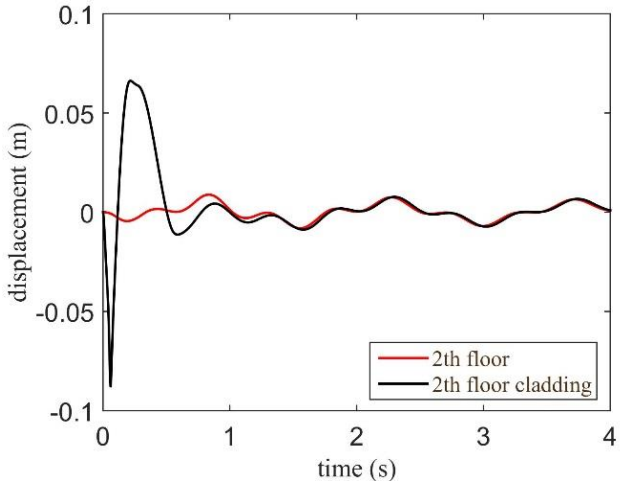

(b)

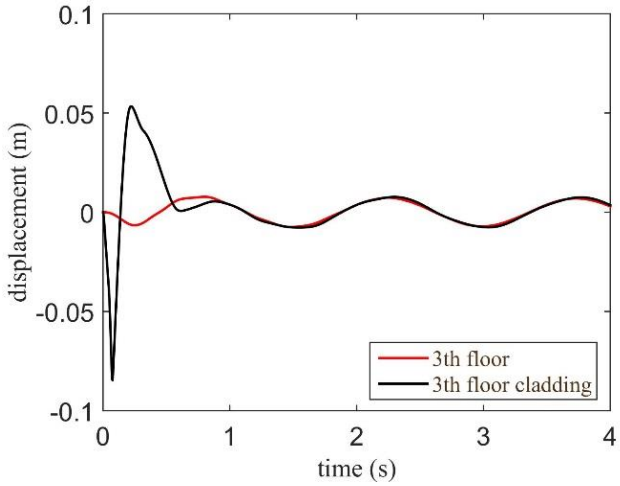

(c)

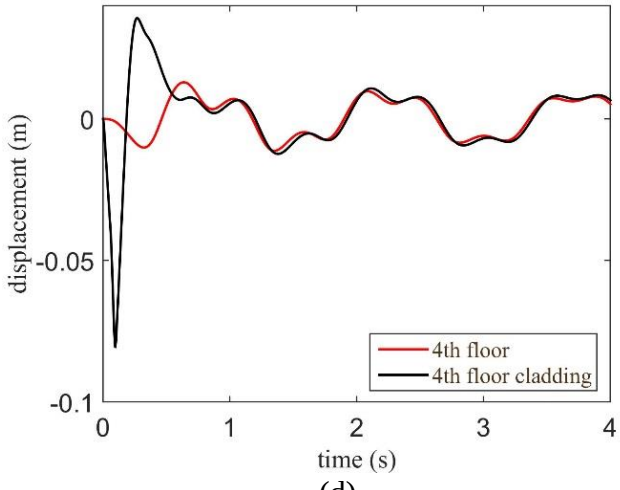

(d)

Figure 5.13 (continued)

CHAPTER 6. CONCLUSIONS

A novel semi-active cladding connection was proposed for improving the performance of the structural system versus multiple hazards. The purpose of the research was to investigate the performance of the device for blast mitigation in its passive mode, and to formulate performance-based design procedures enabling its holistic integration in the structural design procedure.

This thesis first introduced the principle of cladding components, where they are typically equipped with stiff connections to resist a given level of load. This results in the load being entirely transferred to the structure, unless plastic deformations were to occur at the cladding level. Unlike this strength-based approach, the principle of the device is based on leveraging motion between the cladding and the structural frame to dissipate blast energy through friction.

The idealization of the device and its interaction with the structure was presented. It was followed by a discussion of rubber bumpers used for mitigating the possible impact of the cladding on the structure, along with the selection of an idealized model. We also presented the friction model used in for the analytical model and numerical analysis.

After, a performance-based design procedure for the device was developed based on the idealized theory. The design procedure was focused on the sizing of dynamic parameters including the friction capacity and the stiffness of the connection itself along with the sizing of the rubber bumper. It assumed that the cladding element remained elastic during the blast, thus providing a conservative design approach by ignoring any potential energy dissipation from the cladding element itself. Transfer functions representing the amplification of the blast on the structural motion were analytically developed, and were used for establishing the performance-based design procedure. The procedure consists of 1) determining the prescribed performance

levels for a given design load; 2) designing the dynamic parameters of the damping mechanism; and 3) designing the impact rubber. Simulation results demonstrated that the proposed procedure generally leads to a conservative design. The methodology was formulated using a 2DOF model, and it was later demonstrated through simulation that the procedure could extend to MDOF systems. Lastly, a 4-story prototype building was selected to validate the proposed approach numerically. The building was modeled as a 12DOF system exposed to a representative blast load. Results showed the adequacy of the PBD procedure. It also demonstrated the mitigation capability of the semi-active device utilized in a passive mode.

Limitations

The higher errors in the approximation of the device's behavior arose from the friction and rubber dynamics. The friction dynamics is highly nonlinear in nature, and higher order models needs to be developed and analytically solved in order to provide more accurate H indices. The design procedure is therefore limited to systems with limited friction capacities. Also, some of the rubber dynamics was ignored, include the effects of very large (relative) deformations. It follows that the procedure is limited to low relative deformations of the impact rubber itself.

Future Work

Future work includes the laboratory validation and verification of the PBD procedure, characterization of the proposed semi-active connection, and development of PBD procedures for wind and seismic loads leverage a feedback mechanism (semi-active capacity).

REFERENCES

[1] Connor, Jerome, and Simon Laflamme. *Structural motion engineering*. Springer, 2014.

[2] Augusti, Giuliano, and Marcello Ciampoli. "Performance-based design in risk assessment and reduction." *Probabilistic Engineering Mechanics* 23.4 (2008): 496-508.

[3] Agrawal, Anil K., and Jann N. Yang. "Semiactive control strategies for buildings subject to near-field earthquakes." *SPIE's 7th Annual International Symposium on Smart Structures and Materials*. International Society for Optics and Photonics, 2000.

[4] Yang, Jann N., and Anil K. Agrawal. "Semi-active hybrid control systems for nonlinear buildings against near-field earthquakes." *Engineering Structures*24.3 (2002): 271-280.

[5] He, W. L., A. K. Agrawal, and J. N. Yang. "Novel semiactive friction controller for linear structures against earthquakes." *Journal of Structural Engineering* 129.7 (2003): 941-950.

[6] Primer, A. "Curtain Wall Systems." (2013).

[7] Pálsson, Hafsteinn, and Barry J. Goodno. "Influence of Interstory Drift on Cladding Panels and Connections." *Ninth World Conference on Earthquake Engineering*. 1988.

[8] Goodno, B. J., et al. "Use of advanced cladding systems for passive control of building response in earthquakes." *Proceedings, 10th World Conference on Earthquake Engineering, July*. 1992.

[9] Petrini, Francesco, and Alessandro Palmeri. "Performance-Based Design of bridge structures subjected to multiple hazards: a review." *6th International Conference on Bridge Maintenance, Safety and Management*. 2012.

[10] Alderson, Mrs A. S., and A. F. L. Wong. "BLAST RESISTANT GFRP CLADDING PANELS."

[11] Hinman, Eve, and PE Hinman Consulting Engineers. "Blast safety of the building envelope." *Whole Building Design Guide* (2011).

[12] Jogn F. Duntemann, and Wiss, Janney, Elstner Associates, Inc. "Building Envelope Design Guide-Cast-in-place Concrete wall systems." *Whole Building Design Guide* (2009).

[13] Paul E. Gaudette, and Wiss, Janney, Elstner Associates, Inc. "Building Envelope Design Guide-Precast Concrete wall systems." *Whole Building Design Guide* (2009).

[14] Mehta, Madan, Walter Scarborough, and Diane Armpriest. *Building construction: Principles, materials, and systems*. Ohio: Pearson Prentice Hall, 2008.

[15] Ballast, David Kent. *Architect's handbook of construction detailing*. John Wiley & Sons, 2009.

[16] Moriarty, Collin W., and Chuck Oswald. "Blast-resistant architectural precast concrete cladding for government buildings." *PCI Journal* 59.3 (2014).

[17] Cheng, Franklin Y., and Y. Y. Wang. *Post-earthquake rehabilitation and reconstruction*. Elsevier, 1996.pp345-354

[18] Montgomery, Robert M., and James A. Ward. "Facility Damage and Personnel Injury From Explosive Blast." *Research Triangle Institute, Technical Report No. RT/5180/26-08F April* (1993).

[19] Kinney, Gilbert F., and Kenneth J. Graham. *Explosive shocks in air*. Springer Science & Business Media, 1985.

[20] Glasstone, Samuel. *The effects of nuclear weapons*. US Department of Defense, 1977.

[21] Mays, Geoffrey. *Blast effects on buildings: Design of buildings to optimize resistance to blast loading*. Thomas Telford, 1995.

[22] Alderson, Mrs A. S., and A. F. L. Wong. "BLAST RESISTANT GFRP CLADDING PANELS."

[23] Ngo, T., et al. "Blast loading and blast effects on structures–an overview."*Electronic Journal of Structural Engineering* 7 (2007): 76-91.

[24] Zhang, R., and B. M. Phillips. "Numerical Study on the Benefits of Base Isolation for Blast Loading."

[25] Mendis, P. and T. Ngo. *Vulnerability assessment of concrete tall buildings subjected to extreme loading conditions*. in *Proceedings of the CIB-CTBUH international conference on tall buildings*. 2003

[26] Gantes, Charis J., and Nikos G. Pnevmatikos. "Elastic–plastic response spectra for exponential blast loading." *International Journal of Impact Engineering* 30.3 (2004): 323-343

[27] Larcher, Martin. "Pressure-time functions for the description of air blast waves."*JRC Technical Note* 46829 (2008).

[28] Draganić. H and Sigmund. V, "*Blast loading on structures*." Tehnicki vjesnik/Technical Gazette 19 (3).

[29] Dusenberry, Donald O., ed. *Handbook for blast-resistant design of buildings*. J. Wiley, 2010.

[30] Blast Protection of Buildings (ASCE/SEI59-11), 2011, pp49-53

[31] Schmidt, Jon A. "Structural design for external terrorist bomb attacks."*Structure* 3 (2003): 21-23.

[32] Mills, C. A. "The design of concrete structure to resist explosions and weapon effects." *Proceedings of the 1st Int. Conference on concrete for hazard protections*. 1987.

[33] Castellano, A., et al, "*Structures to Resist the Effects of Accidental Explosions*." T.Army, Tm 5-1300

[34] Force, Air. "US Air Force Installation Force Protection Guide." (2004).

[35] Polycarpou, Panayiotis C., Petros Komodromos, and Anastasis C. Polycarpou. "A nonlinear impact model for simulating the use of rubber shock absorbers for mitigating the effects of structural pounding during earthquakes." *Earthquake Engineering & Structural Dynamics* 42.1 (2013): 81-100.

[36] Komodromos, Petros, et al. "Response of seismically isolated buildings considering poundings." *Earthquake Engineering & Structural Dynamics* 36.12 (2007): 1605-16

[37] Kawashima, Kazuhiko, and Gaku Shoji. "Effect of restrainers to mitigate pounding between adjacent decks subjected to a strong ground motion."*Proceeding of the 12th World Conference on Earthquake Engineering*. 2000.

[38] Pounding and unseating damage mitigation on bridge structures subjected to spatially varying ground motions using restrainers and rubber bumpers.

[39] Anagnostopoulos, Stavros A. "Pounding of buildings in series during earthquakes. " *Earthquake Engineering and Structural Dynamics* 16.3 (1988): 443-456.

[40] Jankowski, Robert. "Analytical expression between the impact damping ratio and the coefficient of restitution in the non-linear viscoelastic model of structural pounding." *Earthquake engineering & structural dynamics* 35.4 (2006): 517-524.

[41] Jankowski, Robert. "Non-linear viscoelastic modelling of earthquake-induced structural pounding." *Earthquake engineering & structural dynamics* 34.6 (2005): 595-611.

[42] Muthukumar, Susendar, and Reginald DesRoches. "A Hertz contact model with non-linear damping for pounding simulation." *Earthquake Engineering and Structural Dynamics* 35.7 (2006): 811-828.

[43] Berger, E. J. "Friction modeling for dynamic system simulation." *Applied Mechanics Reviews* 55.6 (2002): 535-577.

[44] Pinelli, Jean-Paul, James I. Craig, and Barry J. Goodno. "Energy-based seismic design of ductile cladding systems." *Journal of Structural Engineering* 121.3 (1995): 567-578.

[45] Moncarz, Piotr D., and Helmut Krawinkler. *Theory and application of experimental model analysis in earthquake engineering*. Vol. 50. Stanford University, 1981.

[46] Mlakar, Sr, Paul F., et al. "The Oklahoma City bombing: analysis of blast damage to the Murrah Building." *Journal of Performance of Constructed Facilities* 12.3 (1998): 113-119.

[47] Longinow, Anatol, and Kim R. Mniszewski. "Protecting buildings against vehicle bomb attacks." *Practice Periodical on Structural Design and Construction* 1.1 (1996): 51-54.

[48] Chopra, Anil K. *Dynamics of structures*. Vol. 3. New Jersey: Prentice Hall, 2012

[49] Bounds, William L., ed. *Design of blast-resistant buildings in petrochemical facilities*. ASCE Publications, 2010.

[50] Downey, Austin, et al. "High capacity variable friction damper based on band brake technology." *Engineering Structures* 113 (2016): 287-298.

[51] Lstiburek, Joseph. *Moisture control handbook: principles and practices for residential and small commercial buildings*. John Wiley & Sons, 1996.

[52] Portis, Alan M., and Hugh D. Young. "Elektronen Und Felder (EF)." *Physik Im Experiment* (1978): 81-109. Web

[53] "GFRC Blast Hazard Mitigation Cladding." *GFRC Information*. N.p., 30 Jan. 2013. Web. 20 Apr. 2016.

[54] "Fire & Blast Walls and Cladding." *ProTek® Cladding*. N.p., n.d. Web. 20 Apr. 2016.

[55] "Blast Relief Cladding." *Blast Relief Cladding*. N.p., n.d. Web. 20 Apr. 2016.

[56] "Storefront and Entrances." *Blast Hazard Mitigation*. N.p., n.d. Web. 20 Apr. 2016.

[57] 4-010-01, Unified facilities criteria (UFC), 9. February 2012, and Including Change 1, 1 October 2013. *EL L* (n.d.): n. pag. Web.

[58] "Blast Rated Buildings – Steel vs Concrete." *MB Industries*. N.p., 06 Nov. 2009. Web. 20 Apr. 2016.

[59] "Lloyd D. George United States Courthouse." • *Clark Pacific • California's Leader in Precast Concrete • Architectural Precast Panels, Precast Cladding, Precast Parking Structures, Precast Panels, California Precast*. N.p., n.d. Web. 21 Apr. 2016.

[60] "San Diego Federal Courthouse." • *Clark Pacific • California's Leader in Precast Concrete • Architectural Precast Panels, Precast Cladding, Precast Parking Structures, Precast Panels, California Precast*. N.p., n.d. Web. 21 Apr. 2016.

[61] "Michael D. Antonovich Antelope Valley Courthouse." • *Clark Pacific • California's Leader in Precast Concrete • Architectural Precast Panels, Precast Cladding, Precast Parking Structures, Precast Panels, California Precast*. N.p., n.d. Web. 21 Apr. 2016

[62] "Fresno Federal Courthouse." • *Clark Pacific • California's Leader in Precast Concrete • Architectural Precast Panels, Precast Cladding, Precast Parking Structures, Precast Panels, California Precast*. N.p., n.d. Web. 21 Apr. 2016.

[63] "Blast Considerations. " *PCI| DN-14*. Precast/Prestressed Concrete Institute,n.d Web 25 Aug 2016.

[64] Zhang, Ruiyang, and Brian M. Phillips. "Performance and Protection of Base-Isolated Structures under Blast Loading." *Journal of Engineering Mechanics* 142.1 (2015): 04015063.

[65] Lam, Nelson, Priyan Mendis, and Tuan Ngo. "Response spectrum solutions for blast loading." *Electronic Journal of Structural Engineering* 4 (2004): 28-44.

[66] Ander, Gregg D. "Windows and Glazing." *Whole Building Design Guide* (2008).

[67] Lin, Lorraine H., et al. "Survey of window retrofit solutions for blast mitigation." *Journal of performance of constructed facilities* 18.2 (2004): 86-94.

[68] Block, Valerie. "Bomb Blast Resistant Glazing: Testing and Standards."

[69] Norville, H. Scott, and Edward J. Conrath. "Considerations for blast-resistant glazing design." *Journal of Architectural Engineering* 7.3 (2001): 80-86.

[70] Block, Valerie. "Bomb Blast Resistant Glazing: Testing and Standards."

[71] American Society of Civil Engineers. *Minimum design loads for buildings and other structures*. Vol. 7. Amer Society of Civil Engineers, 2010.

[72] "A.T.-Blast." *Www.ara.com*. N.p., n.d. Web. 05 July 2016.

[73] PINELLI, J–P., et al. "Testing of energy dissipating cladding connections." *Earthquake engineering & structural dynamics* 25.2 (1996): 129-147.

[74] Youssef, Maged. "Vibration Structure System: A Building Technology for Resisting Dangers."

[75] Harle, Shrikant M. "Review on the performance of glass fiber reinforced concrete." *International Journal of Civil Engineering Research* 5.3 (2014): 281-284.

[76] Koccaz, Zeynep, Fatih Sutcu, and Necdet Torunbalci. "Architectural and structural design for blast resistant buildings." *The 14th world conference on earthquake engineering October*. 2008.

[77] Punch, S. "Blast Design of Steel Structures to Prevent Progressive Collapse." *Structural Engineers Association Convention Proceedings*. 1999.

[78] Hill, J. A., et al. "The structural Engineer's Response to Explosion Damage." *The Institution of Structural Engineer's Report, SETO Ltd, London* (1995).

[79] Oswald, Chuck. "Energy Absorbing Connections for Blast Loading. " *PEC*. Protection Engineering Consultant, n.d. Web. 25 Jan 2017.

[80] Reston, Va. "Courtesy Structural Design for Physical Security: State of the Practice", *Structural Engineering Institute of American Society of Civil Engineers*, 1999.

[81] Nagesh, S. N., et al. "Characterization of brake pads by variation in composition of friction materials." *Procedia Materials Science* 5 (2014): 295-302

[82] Blau, P. J. "Compositions, Functions and Testing of Friction Brake Materials and their Additives. Being a report by Oak Ridge National Laboratory for US Dept. of Energy." (2001).

[83] Pan, Y. G., and A. J. Watson. "Interaction between concrete cladding panels and fixings under blast loading." *Cement and Concrete Composites* 18.5 (1996): 323-332.

APPENDIX. H FUNCTIONS WITH DIFFERENT PARAMETERS

H_2 function with structural damping $\xi = 3\%$ and $\rho_{space} = \frac{l_c - l_r}{u_{st}}$: (a) $\rho_{space} = 1\%$, (b) $\rho_{space} = 2\%$, (c) $\rho_{space} = 3\%$, (d) $\rho_{space} = 4\%$, (e) $\rho_{space} = 5\%$, (f) $\rho_{space} = 6\%$

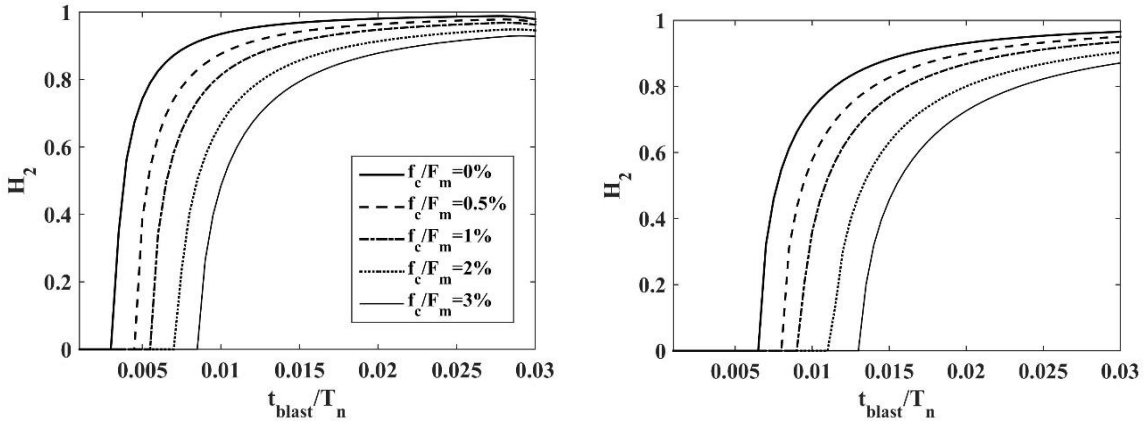

(a) (b)

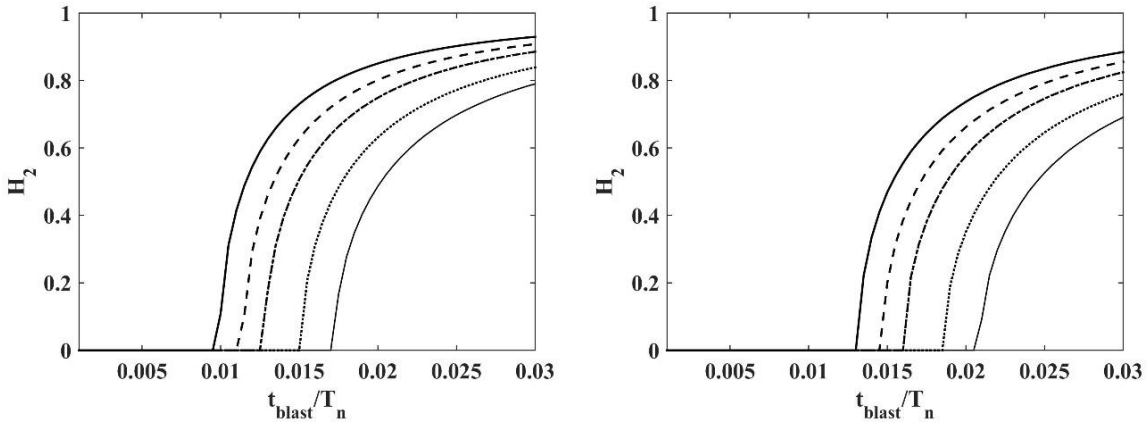

(c) (d)

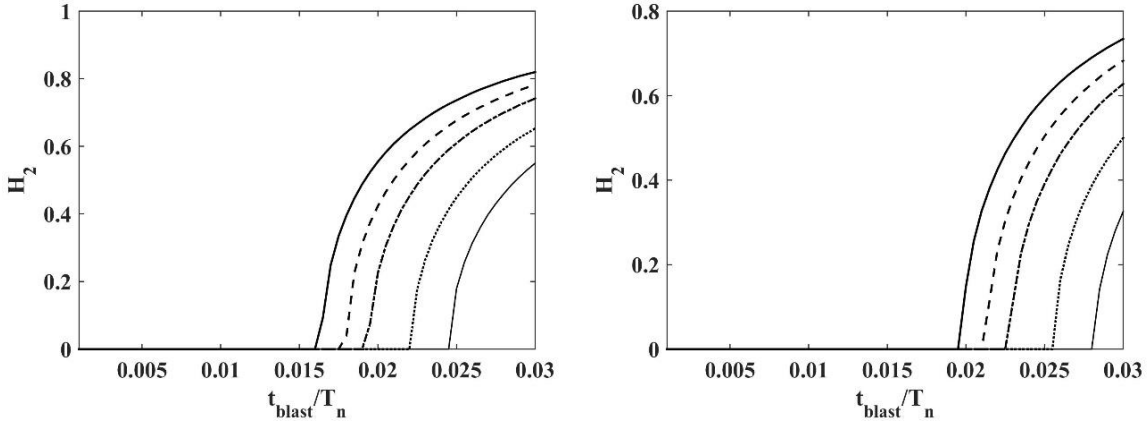

(e) (f)

H_2 function with structural damping $\xi = 5\%$ and $\rho_{space} = \frac{l_c - l_r}{u_{st}}$: (a) $\rho_{space} = 1\%$, (b) $\rho_{space} = 2\%$, (c) $\rho_{space} = 3\%$, (d) $\rho_{space} = 4\%$, (e) $\rho_{space} = 5\%$, (f) $\rho_{space} = 6\%$

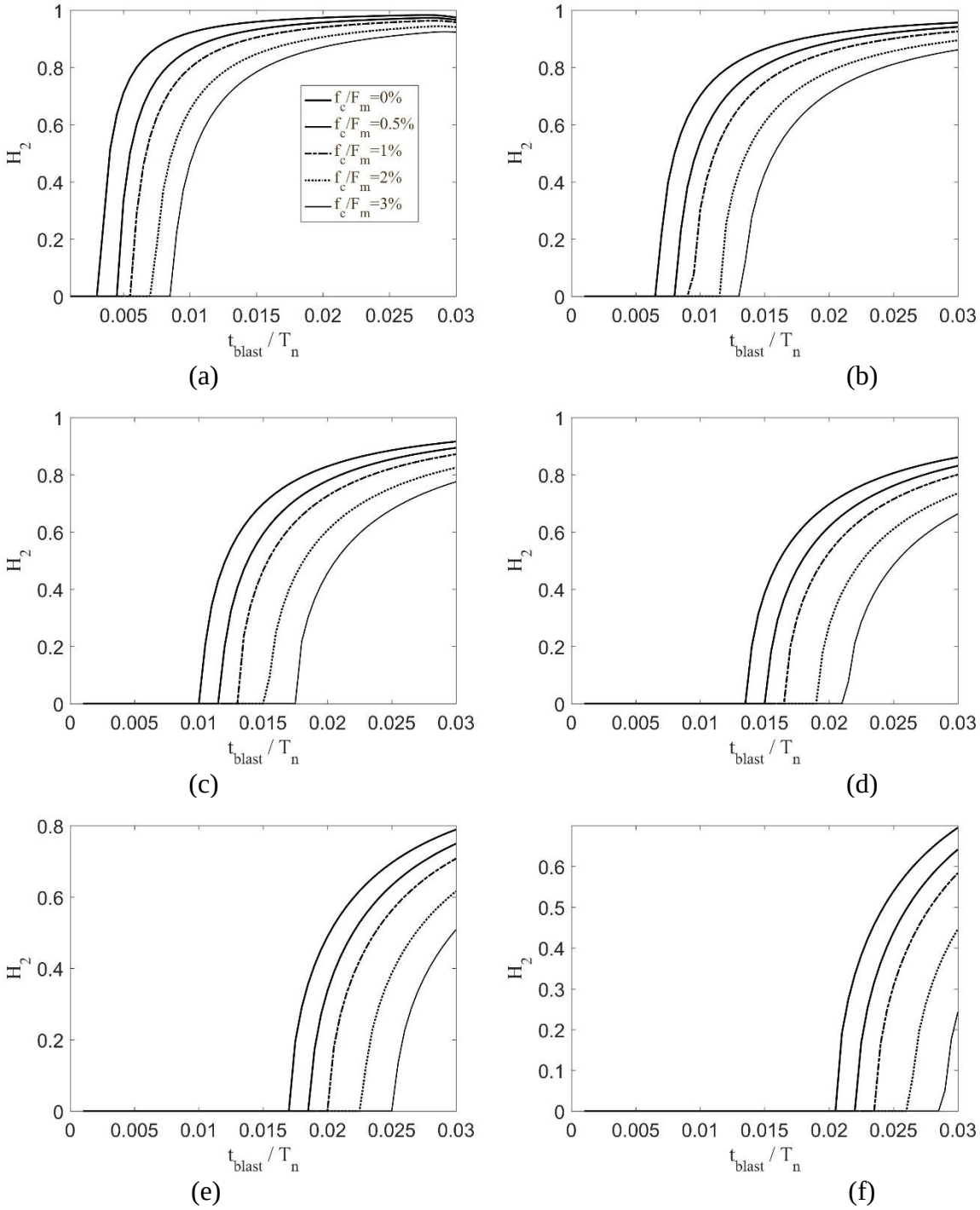

H_2 function with structural damping $\xi = 10\%$ and $\rho_{space} = \frac{l_c - l_r}{u_{st}}$: (a) $\rho_{space} = 1\%$, (b) $\rho_{space} = 2\%$, (c) $\rho_{space} = 3\%$, (d) $\rho_{space} = 4\%$, (e) $\rho_{space} = 5\%$, (f) $\rho_{space} = 6\%$

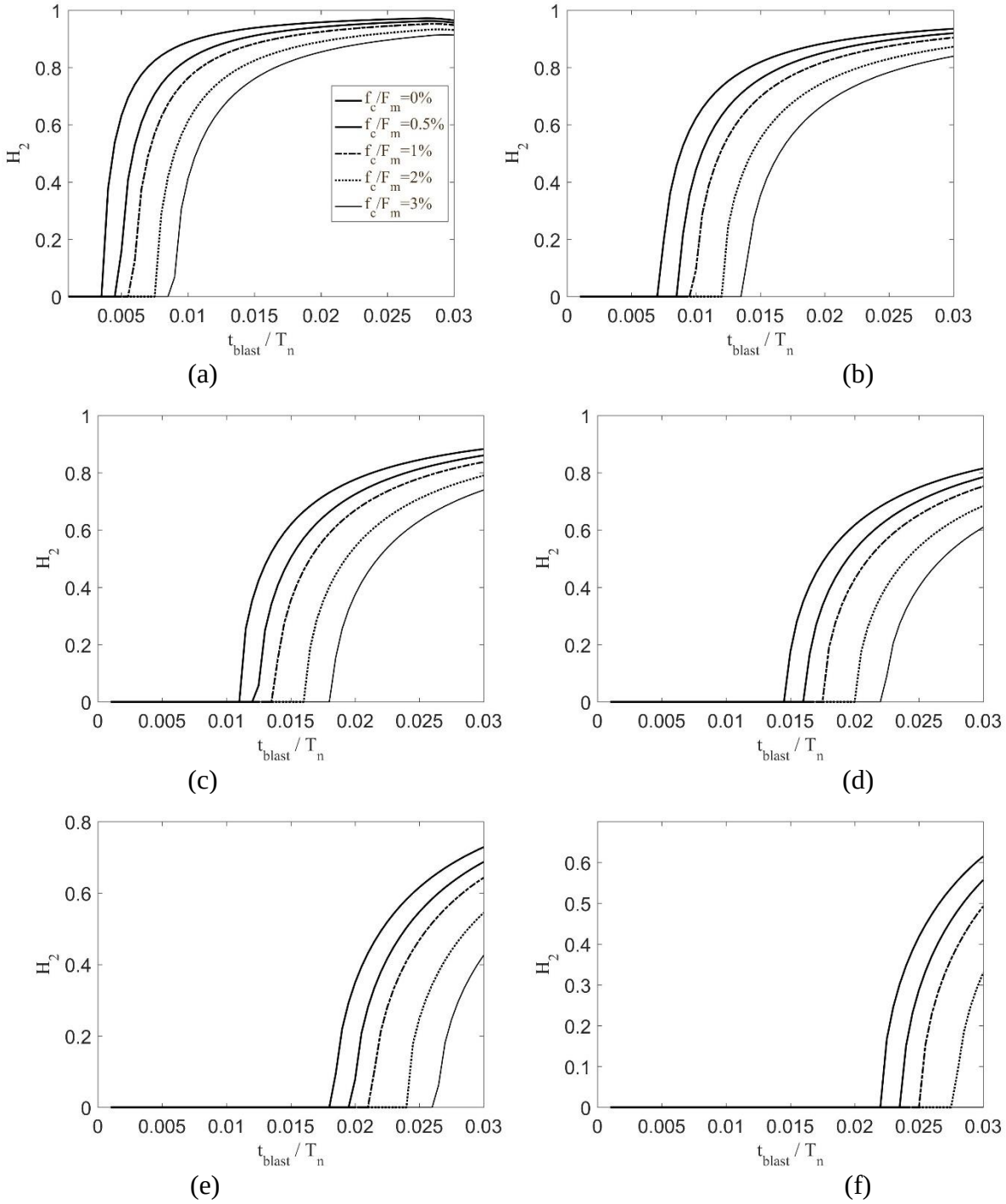

H_3 functions with structural damping $\xi = 2\%$ and assuming $\rho_{space} = 2\%$,: (a) $f_c/F_m = 0\%$, (b) $f_c/F_m = 0.5\%$, (c) $f_c/F_m = 1\%$, (d) $f_c/F_m = 2\%$, (e) $f_c/F_m = 3\%$

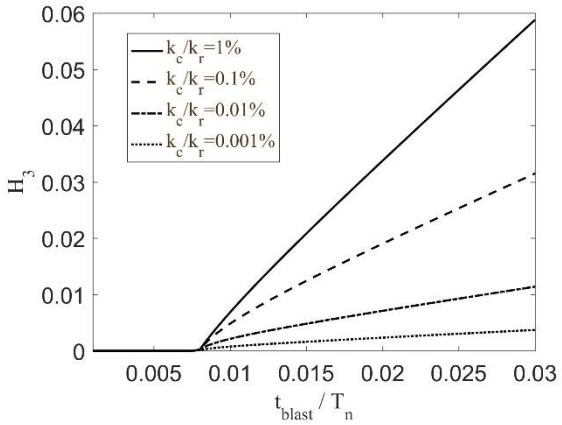

(a)

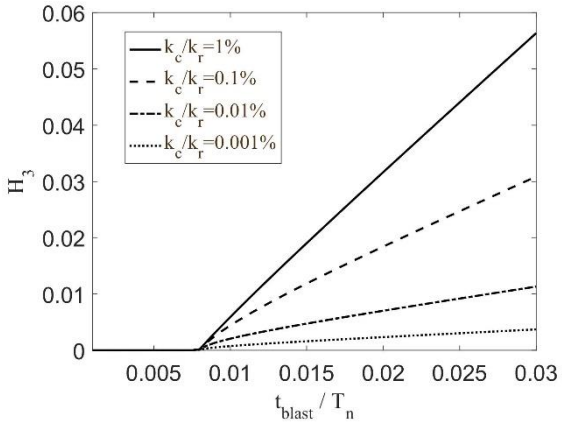

(b)

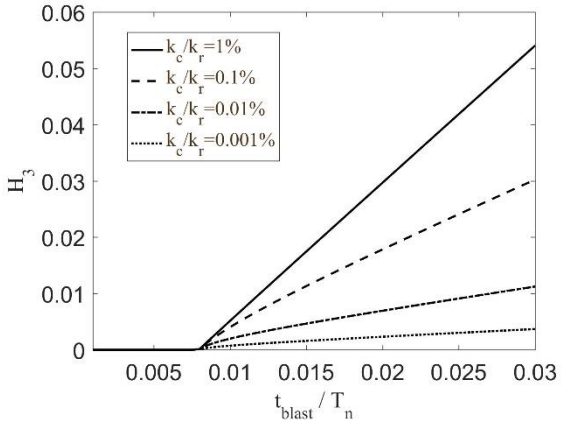

(c)

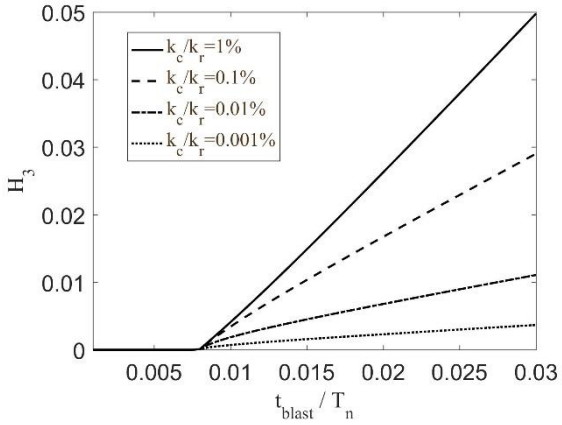

(d)

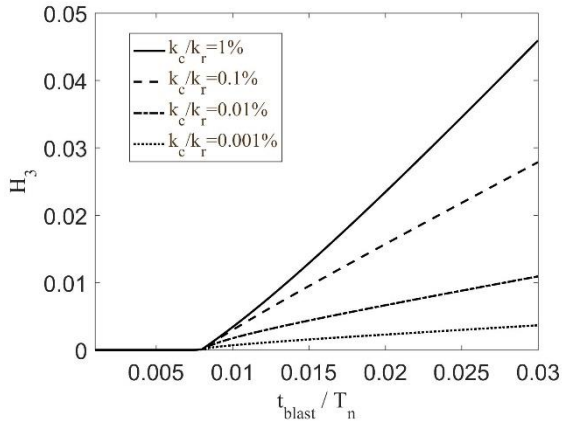

(e)

H_3 functions with structural damping $\xi = 2\%$ and assuming $\rho_{space} = 3\%$,: (a) $f_c/F_m = 0\%$, (b) $f_c/F_m = 0.5\%$, (c) $f_c/F_m = 1\%$, (d) $f_c/F_m = 2\%$, (e) $f_c/F_m = 3\%$.

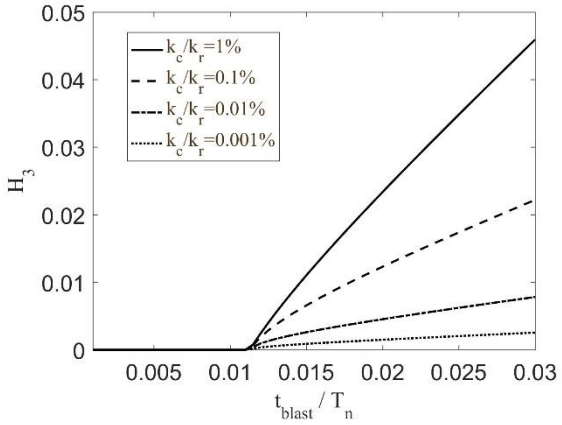

(a)

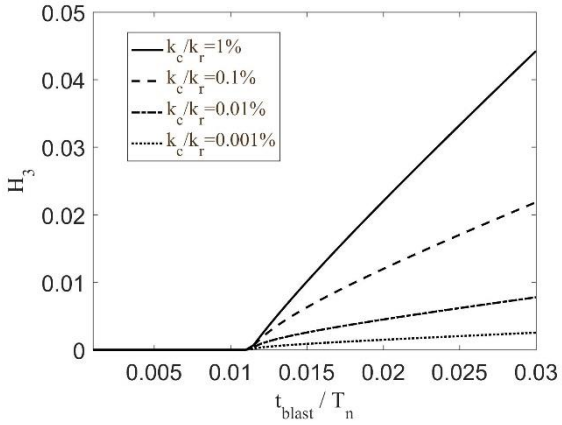

(b)

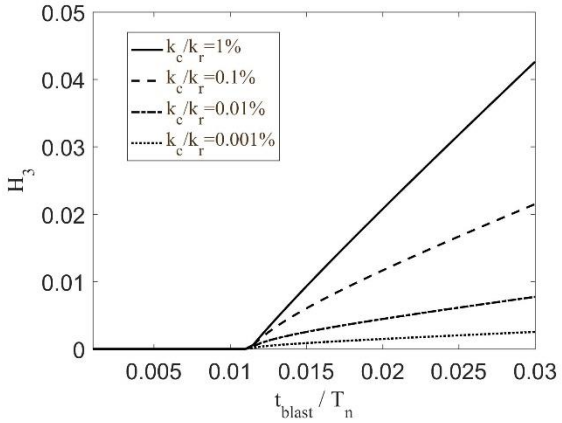

(c)

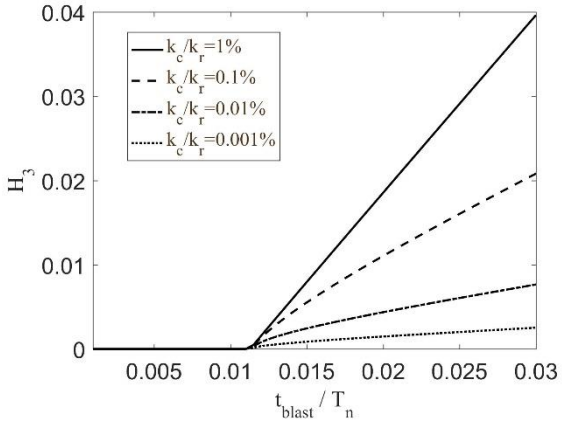

(d)

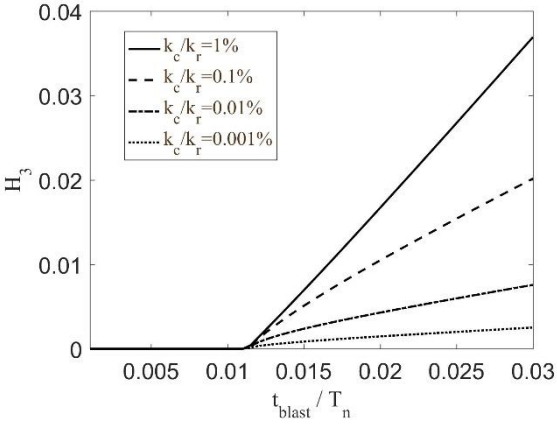

(e)

H_3 functions with structural damping $\xi = 2\%$ and assuming $\rho_{space} = 4\%$,: (a) $f_c/F_m = 0\%$, (b) $f_c/F_m = 0.5\%$, (c) $f_c/F_m = 1\%$, (d) $f_c/F_m = 2\%$, (e) $f_c/F_m = 3\%$.

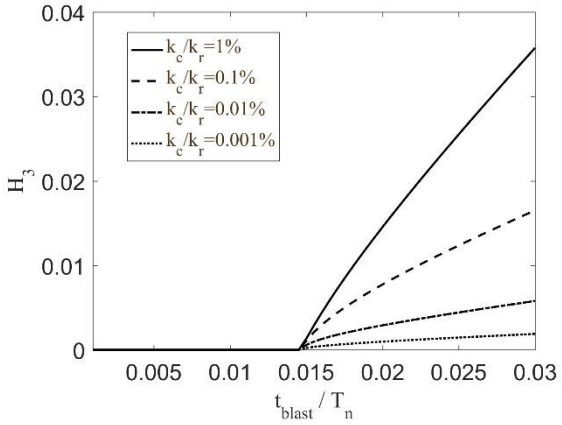

(a)

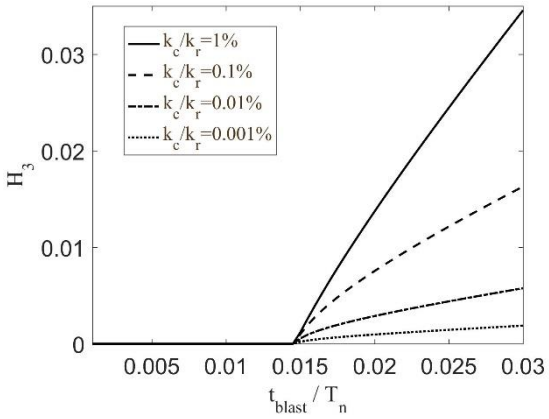

(b)

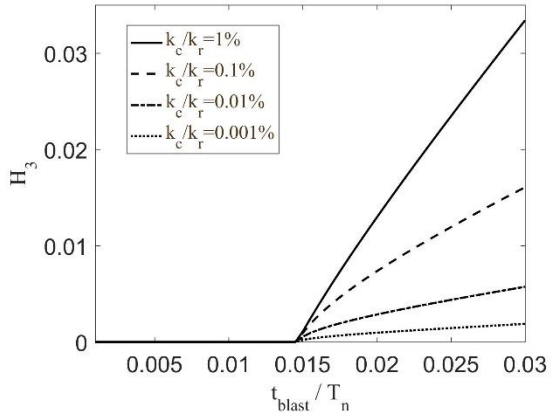

(c)

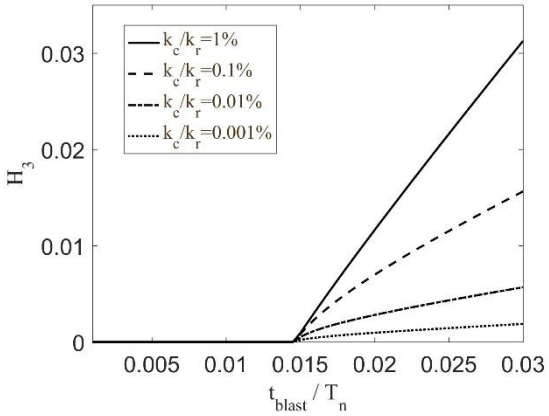

(d)

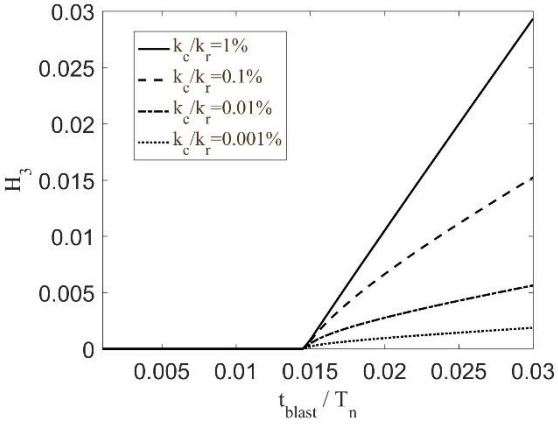

(e)

H_3 functions with structural damping $\xi = 2\%$ and assuming $\rho_{space} = 5\%$,: (a) $f_c/F_m = 0\%$, (b) $f_c/F_m = 0.5\%$, (c) $f_c/F_m = 1\%$, (d) $f_c/F_m = 2\%$, (e) $f_c/F_m = 3\%$.

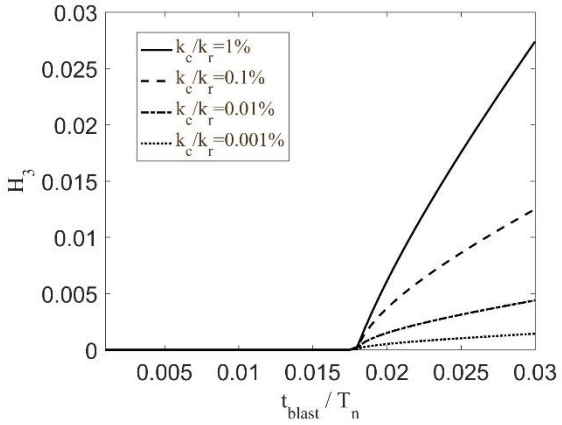

(a)

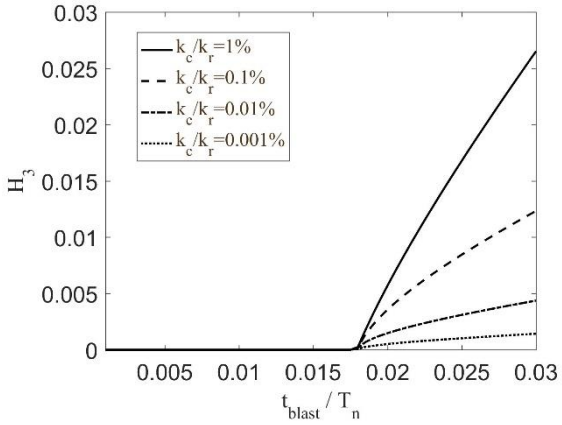

(b)

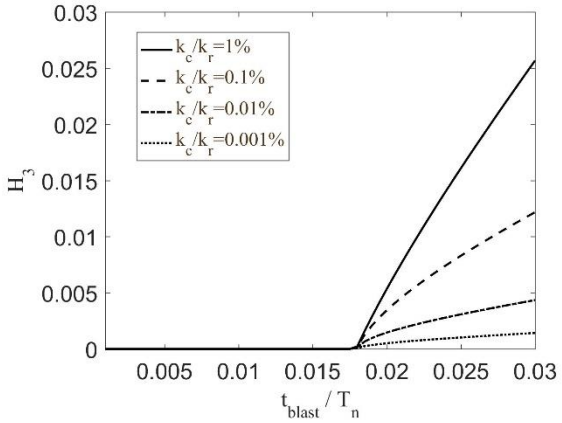

(c)

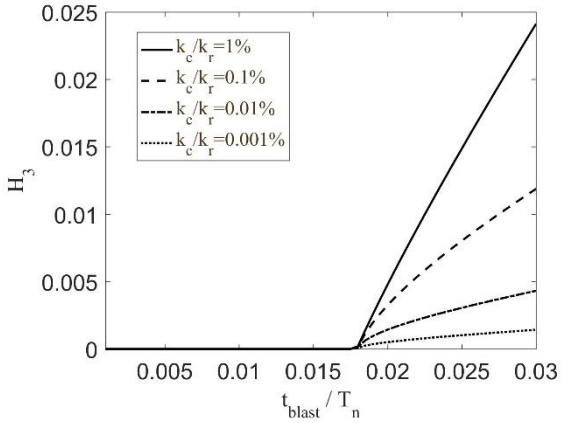

(d)

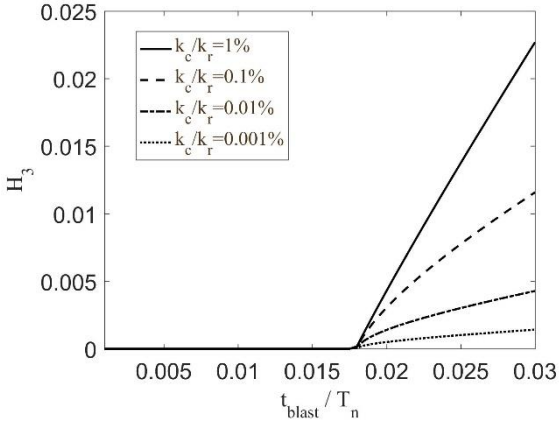

(e)

H_3 functions with structural damping $\xi = 2\%$ and assuming $\rho_{space} = 6\%$,: (a) $f_c/F_m = 0\%$, (b) $f_c/F_m = 0.5\%$, (c) $f_c/F_m = 1\%$, (d) $f_c/F_m = 2\%$, (e) $f_c/F_m = 3\%$

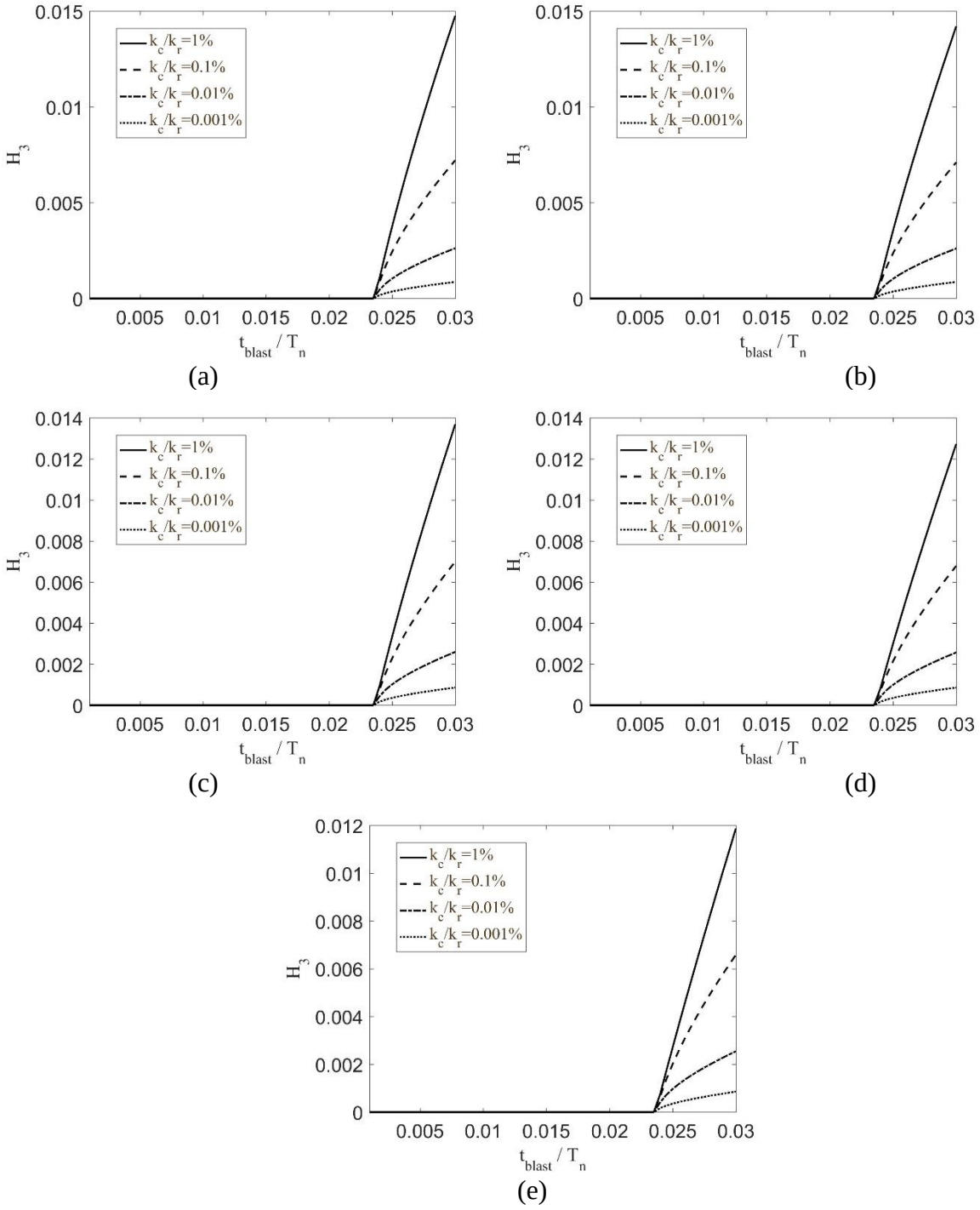

H_3 functions with structural damping $\xi = 3\%$ and assuming $\rho_{space} = 1\%$,: (a) $f_c/F_m = 0\%$, (b) $f_c/F_m = 0.5\%$, (c) $f_c/F_m = 1\%$, (d) $f_c/F_m = 2\%$, (e) $f_c/F_m = 3\%$.

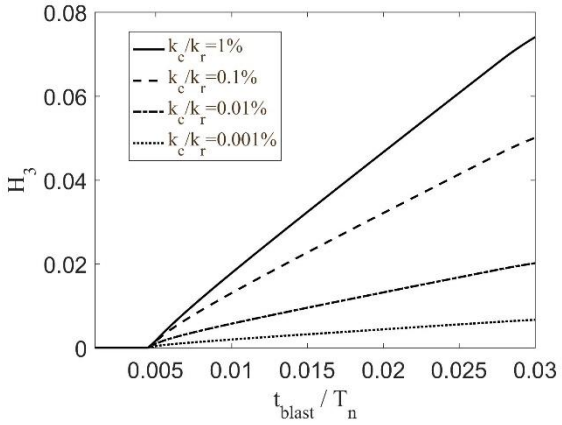

(a)

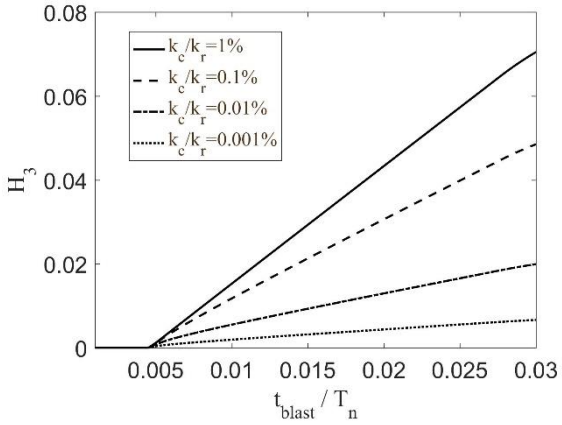

(b)

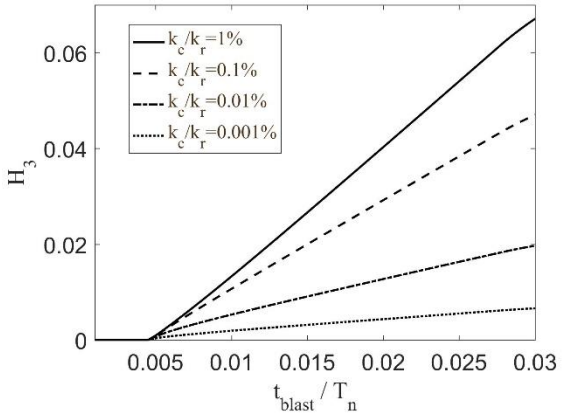

(c)

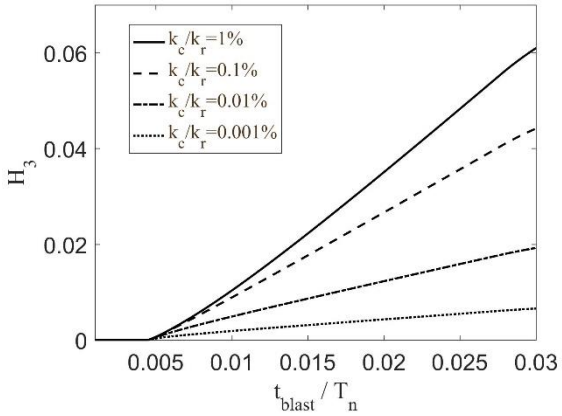

(d)

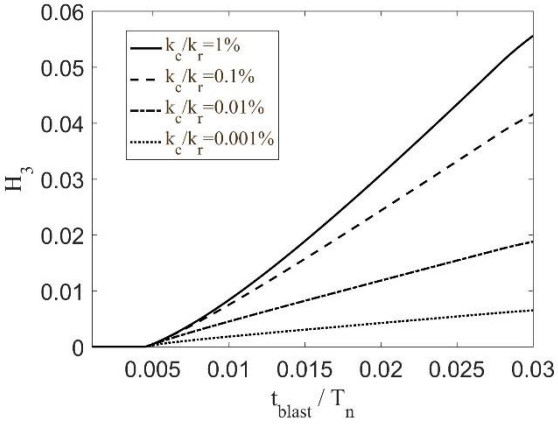

(e)

H_3 functions with structural damping $\xi = 3\%$ and assuming $\rho_{space} = 2\%$,: (a) $f_c/F_m = 0\%$, (b) $f_c/F_m = 0.5\%$, (c) $f_c/F_m = 1\%$, (d) $f_c/F_m = 2\%$, (e) $f_c/F_m = 3\%$

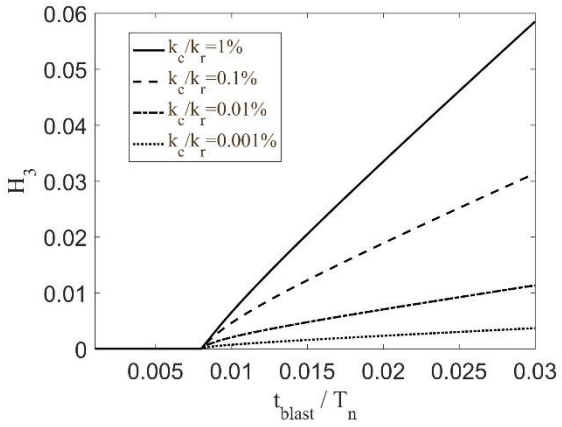

(a)

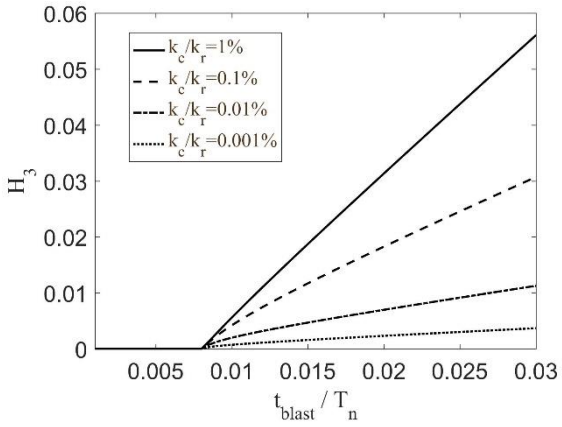

(b)

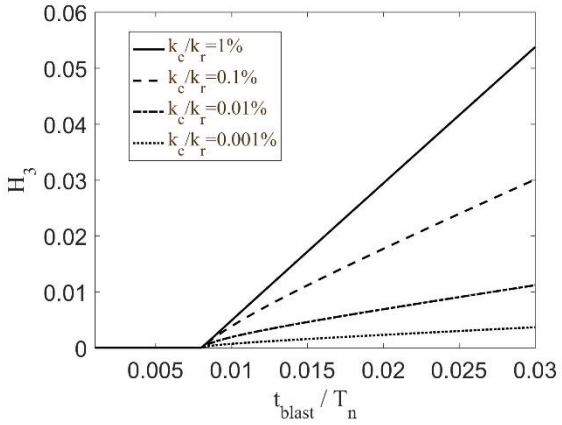

(c)

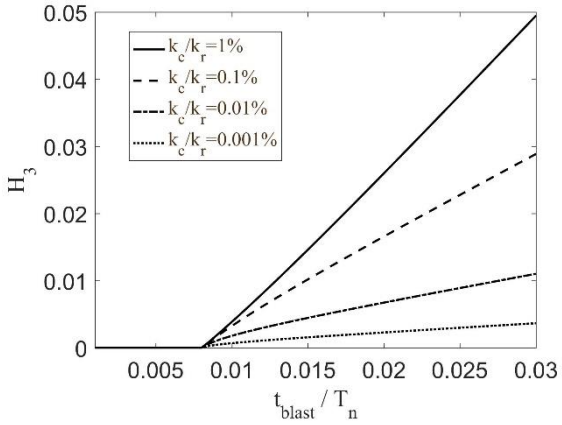

(d)

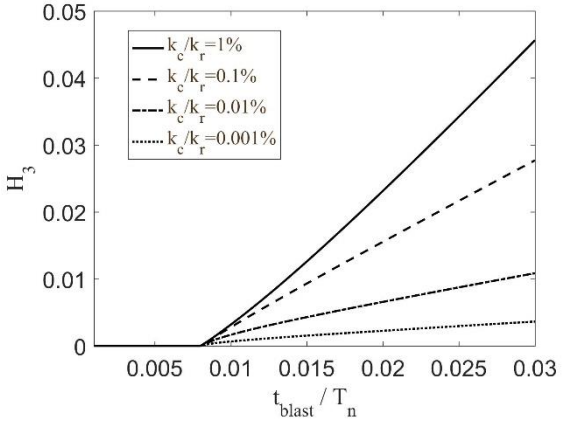

(e)

H_3 functions with structural damping $\xi = 3\%$ and assuming $\rho_{space} = 3\%$,: (a) $f_c/F_m = 0\%$, (b) $f_c/F_m = 0.5\%$, (c) $f_c/F_m = 1\%$, (d) $f_c/F_m = 2\%$, (e) $f_c/F_m = 3\%$

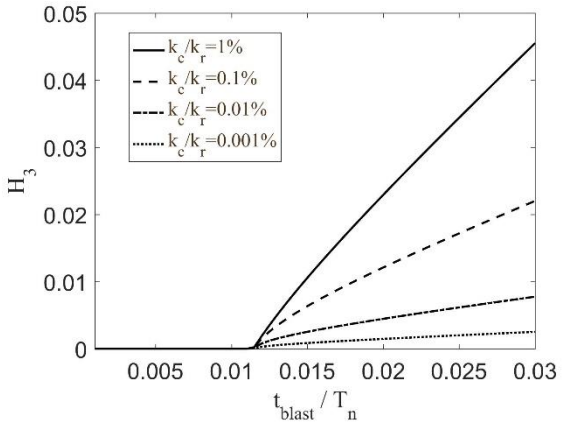

(a)

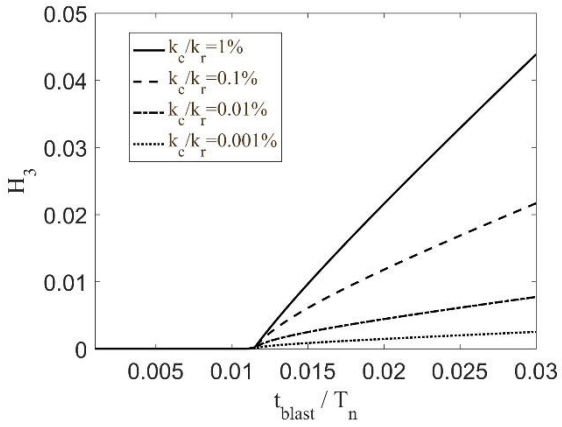

(b)

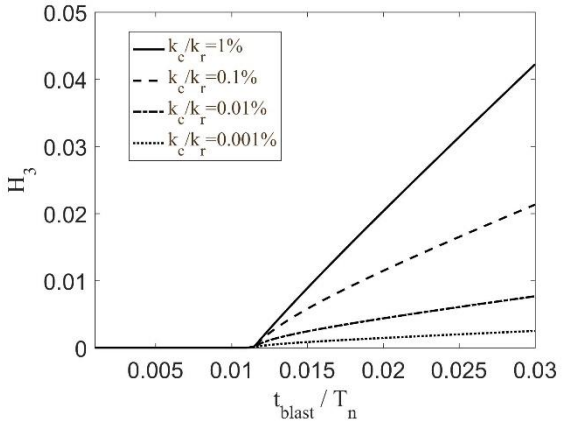

(c)

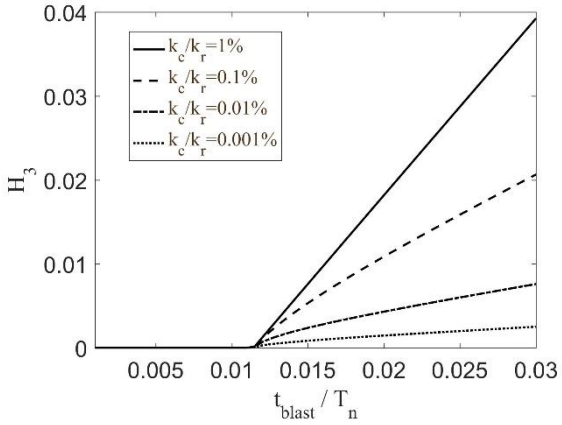

(d)

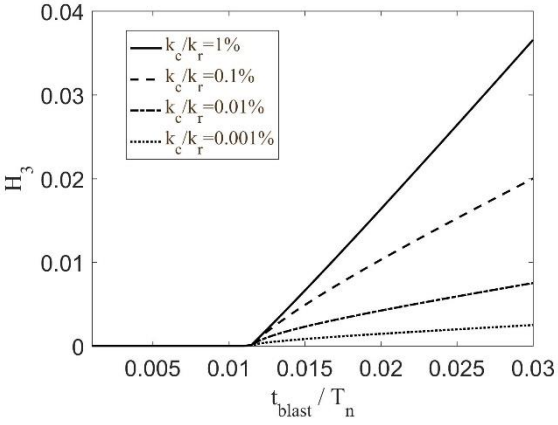

(e)

H_3 functions with structural damping $\xi = 3\%$ and assuming $\rho_{space} = 4\%$,: (a) $f_c/F_m = 0\%$, (b) $f_c/F_m = 0.5\%$, (c) $f_c/F_m = 1\%$, (d) $f_c/F_m = 2\%$, (e) $f_c/F_m = 3\%$

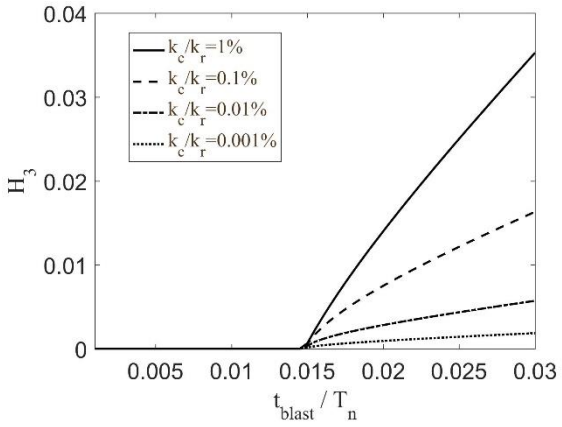

(a)

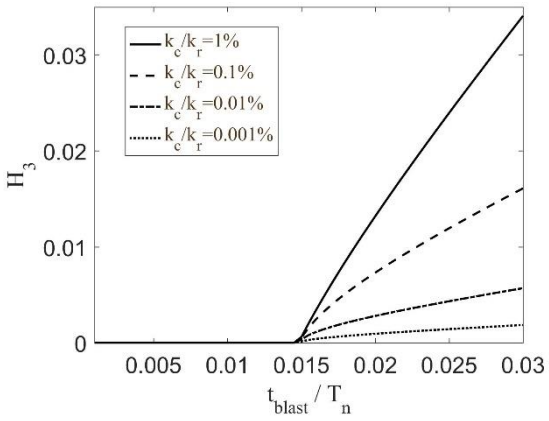

(b)

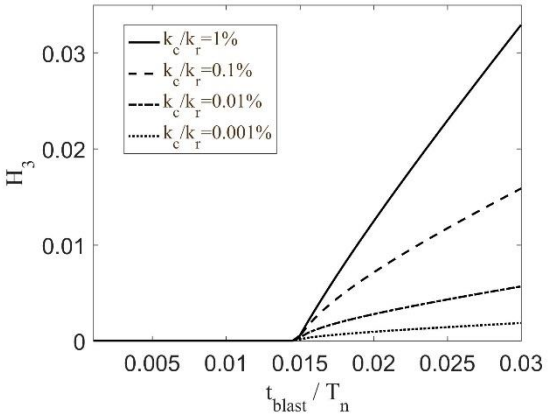

(c)

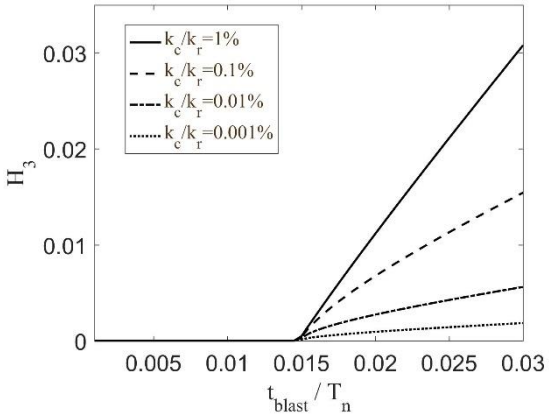

(d)

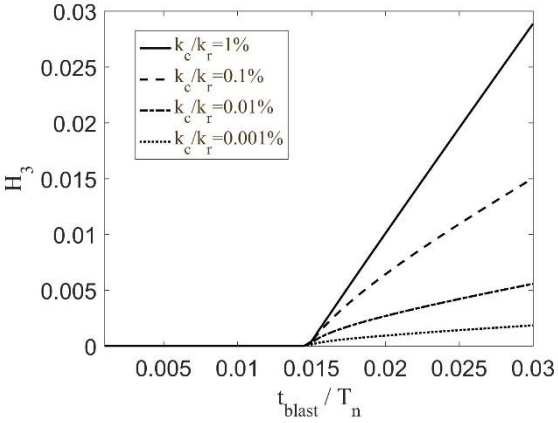

(e)

H_3 functions with structural damping $\xi = 3\%$ and assuming $\rho_{space} = 5\%$,: (a) $f_c/F_m = 0\%$, (b) $f_c/F_m = 0.5\%$, (c) $f_c/F_m = 1\%$, (d) $f_c/F_m = 2\%$, (e) $f_c/F_m = 3\%$

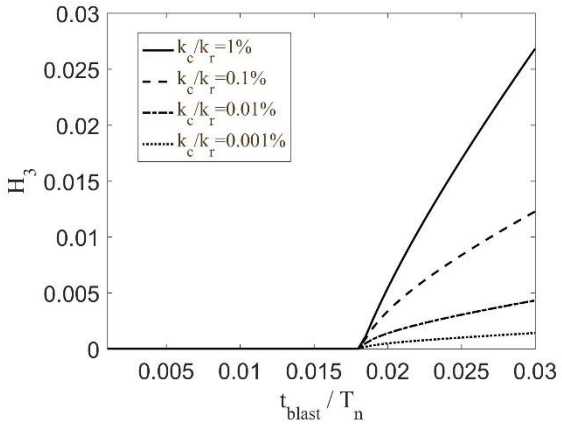

(a)

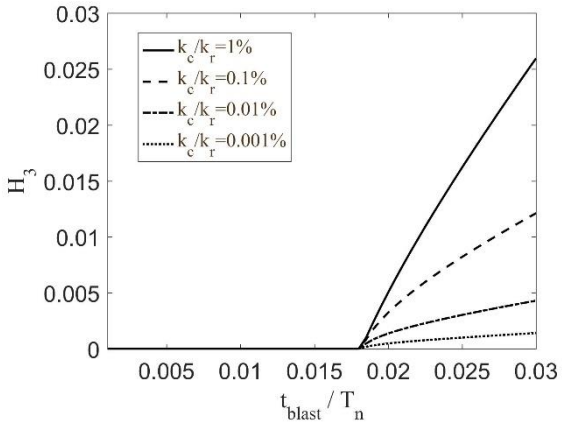

(b)

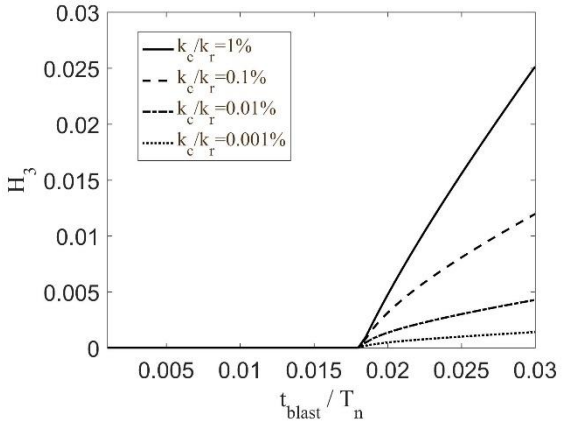

(c)

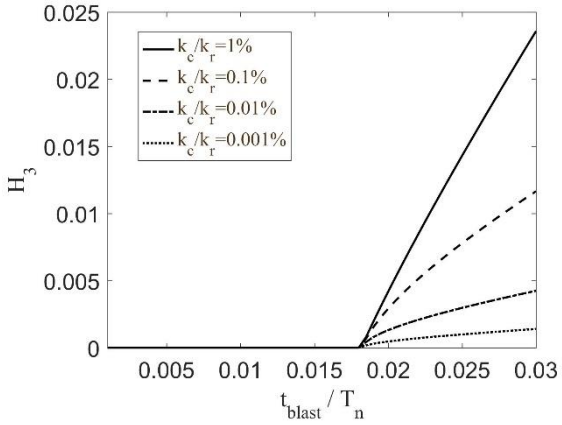

(d)

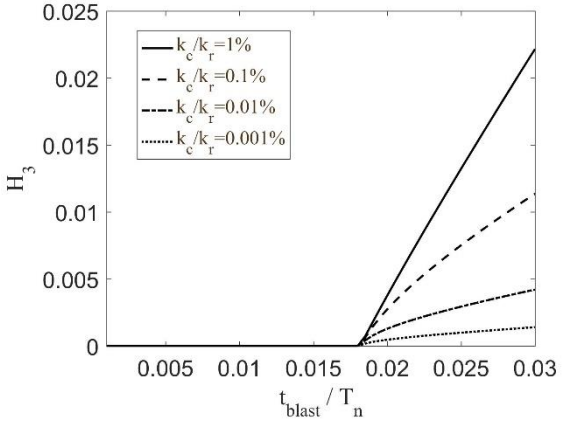

(e)

H_3 functions with structural damping $\xi = 3\%$ and assuming $\rho_{space} = 6\%$,: (a) $f_c/F_m = 0\%$, (b) $f_c/F_m = 0.5\%$, (c) $f_c/F_m = 1\%$, (d) $f_c/F_m = 2\%$, (e) $f_c/F_m = 3\%$

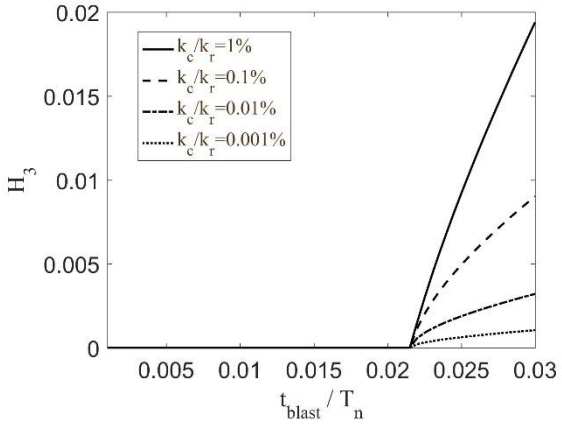

(a)

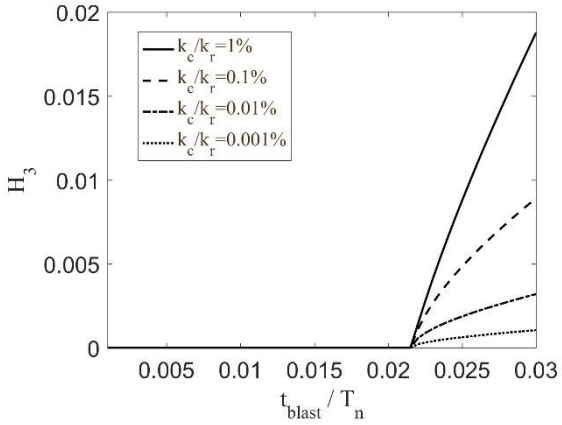

(b)

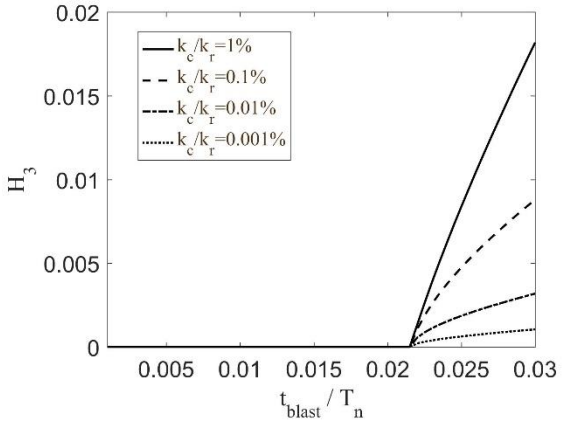

(c)

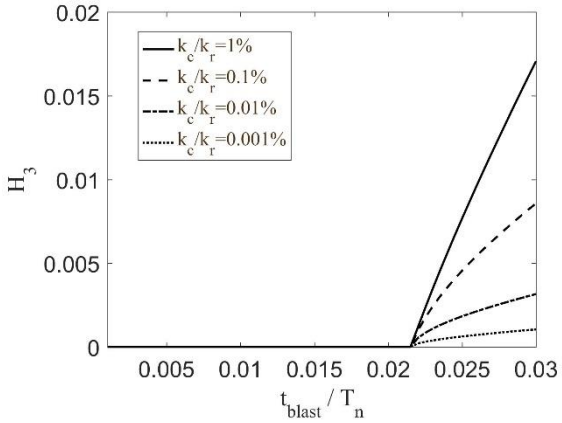

(d)

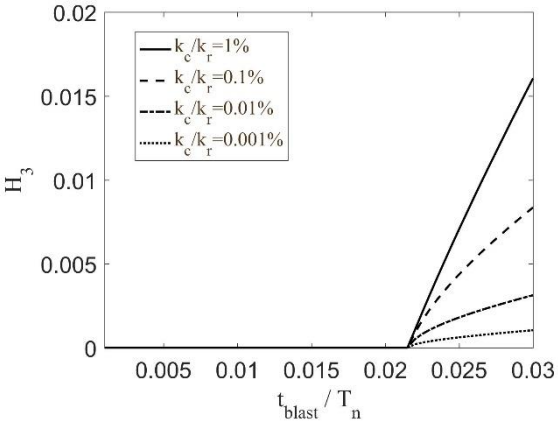

(e)